INGENIUS

José Trinidad Holguín Momaca, MSc, Centro de Investigación en Materiales Avanzados, México.

Juan Manuel Alvarado Orozco, PhD, Centro de Ingeniería y Desarrollo Industrial, México.

Arnaldo Jélvez Caamaño, PhD, Universidad del BIOBIO, Chile.

Javier Murillo, PhD, Centro Internacional Franco Argentino de Ciencias de la Información y de Sistemas, Argentina.

Lucas Daniel Terissi, PhD, Universidad Nacional de Rosario, Argentina.

Rene Vinicio Sanchez Loja, MSc, Universidad Politécnica Salesiana, Ecuador.

Freddy Leonardo Bueno Palomeque, MSc, Universidad Politécnica Salesiana, Ecuador.

Diego Cabrera Mendieta, MSc, Universidad Politécnica Salesiana, Ecuador.

Edwuin Jesus Carrasquero, PhD, Universidad Técnica de Machala, Ecuador.

Carlos Mauricio Carrillo Rosero, MSc, Universidad Técnica de Ambato, Ecuador.

Diego Carrion Galarza, MSc, Universidad Politécnica Salesiana, Ecuador.

Carmen Celi Sanchez, MSc, Universidad Politécnica Salesiana, Ecuador.

Diego Chacon Troya, MSc, Universidad Politécnica Salesiana, Ecuador.

Paul Chasi, MSc, Universidad Politécnica Salesiana, Ecuador.

Juan Chica, MSc, Universidad Politécnica Salesiana, Ecuador.

Diego Marcelo Cordero Guzmán, MSc, Universidad Católica de Cuenca, Ecuador.

Luis Javier Cruz, PhD, Universidad Pontificia Bolivariana, Medellin, Colombia.

Fabricio Esteban Espinoza Molina, MSc, Universidad Politécnica Salesiana, Ecuador.

Jorge Fajardo Seminario, MSc, Universidad Politécnica Salesiana, Ecuador.

Patricia Fernandez Morales, PhD, Universidad Pontificia Bolivariana, Medellin, Colombia.

Marcelo Flores Vazquez, MSc, Universidad Politécnica Salesiana, Ecuador.

Carlos Flores Vázquez, MSc, Universidad Católica de Cuenca, Ecuador.

Carlos Franco Cardona, PhD, Universidad Nacional de Colombia, Colombia.

Cristian García García, MSc, Universidad Politécnica Salesiana, Ecuador.

Teonila García Zapata, PhD, Universidad Nacional Mayor de San Marcos, Perú.

Luis Garzón Mñoz, PhD, Universidad Politécnica Salesiana, Ecuador.

Natalia Gonzalez Alvarez, MSc, Universidad Politécnica Salesiana, Ecuador.

Ernesto Granado, PhD, Universidad Simón Bolívar, Venezuela.

Adriana del Pilar Guaman, MSc, Universidad Politécnica Salesiana, Ecuador.

Juan Inga Ortega, MSc, Universidad Politécnica Salesiana, Ecuador.

Esteban Inga Ortega, PhD, Universidad Politécnica Salesiana, Ecuador.

Paola Ingavélez, MSc, Universidad Politécnica Salesiana, Ecuador.

Cesar Isaza Roldan, PhD, Universidad Pontificia Bolivariana.

Nelson Jara Cobos, MSc, Universidad Politécnica Salesiana, Ecuador.

Ruben Jerves, MSc, Universidad Politécnica Salesiana, Ecuador.

Victor Ramon Leal, PhD, Investigador de PDVSA, Venezuela

Gabriel Leon, MSc, Universidad Politécnica Salesiana, Ecuador.

Edilberto Llanes, PhD, Universidad Internacional SEK, Ecuador.

Luis López, MSc, Universidad Politécnica Salesiana, Ecuador.

Carlos Mafla Yépez, MSc, Universidad Técnica del Norte, Ecuador.

Hader Martínez, PhD, Universidad Pontificia Bolivariana, Medellin, Colombia

Javier Martínez, PhD, Instituto Nacional de Eficiencia Energética y Energías Renovables, Ecuador.

Alex Mayorga, MSc, Universidad Técnica de Ambato, Ecuador.

Jimmy Molina, MSc, Universidad Técnica de Machala, Ecuador.

Andres Montero, PhD, Universidad de Cuenca, Ecuador.

Vicente Morales, MSc, Universidad Tecnica de Ambato, Ecuador.

Fabián Morales, MSc, Universidad Técnica de Ambato, Ecuador.

Diego Morales, MSc, Ministerio de Electricidad y Energías Renovables del Ecuador.

Yoandrys Morales Tamayo, PhD, Universidad Técnica de Cotopaxi, Cotopaxi

Olena Leonidivna Naidiuk, MSc, Universidad Politécnica Salesiana, Ecuador.

Oscar Naranjo, MSc, Universidad del Azuay, Ecuador.

Paul Narvaez, MSc, Universidad Politécnica Salesiana, Ecuador.

Hernán Navas Olmedo, MSc, Universidad Técnica de Cotopaxi, Ecuador.

Cesar Nieto, PhD, Universidad Pontificia Bolivariana, Medellin, Colombia

Fabio Obando, MSc, Universidad Politécnica Salesiana, Ecuador.

Luis Ortiz Fernandez, MSc, Universidade Federal de Rio Grande del Norte, Brasil

Pablo Parra, MSc, Universidad Politécnica Salesiana, Ecuador.

Paulo Peña Toro, PhD, Ministerio de Productividad, Ecuador.

Patsy Prieto Velez, MSc, Universidad Politécnica Salesiana, Ecuador.

Diego Quinde Falconi, MSc, Universidad Politécnica Salesiana, Ecuador.

Diana Quintana Espinoza, MSc, Universidad Politécnica Salesiana, Ecuador.

William Quitiaquez Sarzosa, MSc, Universidad Politécnica Salesiana, Ecuador.

Flavio Quizhpi Palomeque, MSc, Universidad Politécnica Salesiana, Ecuador.

Washington Ramirez Montalvan, MSc, Universidad Politécnica Salesiana, Ecuador.

Fran Reinoso Avecillas, MSc, Universidad Politécnica Salesiana, Ecuador.

Néstor Rivera Campoverde, MSc, Universidad Politécnica Salesiana, Ecuador.

Jorge Romero Contreras, MSc, Universidad de Carabobo, Venezuela

Fabian Saenz Enderica, MSc, Universidad de las Fuerzas Armadas, ESPE, Ecuador.

Luisa Salazar Gil, PhD, Universidad Simón Bolivar, Venezuela

Gustavo Salgado Enríquez, Msc, Universidad Central del Ecuador., Ecuador.

Juan Carlos Santillán Lima, MSc, Universidad Nacional de Chimborazo

Jonnathan Santos Benítez, MSc, Universidad Politécnica Salesiana, Ecuador.

Andrés Sarmiento Cajamarca, MSc, Universidad Federal de Santa Catarina, Brasil

Luis Serpa Andrade, MSc, Universidad Politécnica Salesiana, Ecuador.

Cristian Timbi Sisalima, MSc, Universidad Politécnica Salesiana, Ecuador.

Milton Tipan Simbaña, MSc, Universidad Politécnica Salesiana, Ecuador.

Paul Torres Jara, MSc, Universidad Politécnica Salesiana, Ecuador.

Rodrigo Tufiño Cárdenas, MSc, Universidad Politécnica Salesiana, Ecuador.

Fernando Urgiles Ortíz, MSc, Universidad Politécnica Salesiana, Ecuador.

Juan Valladolid Quitoisaca, MSc, Universidad Politécnica Salesiana, Ecuador.

Efrén Vázquez Silva, PhD, Universidad Politécnica Salesiana, Ecuador.

Julio Verdugo, MSc, Universidad Politécnica Salesiana, Ecuador.

Mary Vergara Paredes, PhD, Universidad de los Andes, Merida, Venezuela

Jennifer Yepez Alulema, MSc, Universidad Politécnica Salesiana, Ecuador.

Julio Zambrano Abad, MSc, Universidad Politécnica Salesiana, Ecuador.

Patricia Zapata Molina, MSc, Universidad Politécnica Salesiana, Ecuador.

The administration of the journal is done through the following parameters:

The journal uses the academic anti-plagiarism system

The articles have an identification code (Digital Object Identifier)

The editorial process is managed through the Open Journal System

It is an open access publication (Open Access) licensed Creative Commons

The politics copyright of use postprint,are published in the Self-Archive Policy Repository Sherpa/Romeo.

The articles of the present edition can be consulted in
http://revistas.ups.edu.ec/index.php/ingenius

INGENIUS Journal, is indexed in the following Databases and scientific information systems:

SELECTIVE DATABASES

REVIEWS EVALUATION PLATFORMS

SELECTIVE DIRECTORIES

SELECTIVE SERIAL LIBRARY

SCIENTIFIC LITERATURE SEARCHERS OPEN ACCESS

OTHER BIBLIOGRAPHICAL DATABASES

CATALOG OF INTERNATIONAL UNIVERSITY LIBRARIES

Dear readers:

The philosophy of Science is a product of the 20th century, but many authors contributed significantly to consolidate the very concept of science; I share with you some data that will allow us to strengthen acting as researchers.

One of the philosophers that has great importance until our times is Archimedes who was born in Syracuse - Sicily, (287-212 BC), he is considered an eccentric genius and many of his inventions are currently the foundation of many developments. scientific and technological.

In the second half of the 16th century (1564-1630) Galileo Galilei, who bases his actions on a very significant phrase: «It seems to me that those who only base themselves on arguments of authority to maintain their affirmations, without looking for reasons to support them, act in an absurd way. I wish I could freely question and answer freely without adulation. That's how the one that follows the truth behaves"; he always resorts to nature to confirm his conclusions previously deduced from a reasoning based on purely theoretical hypotheses, it is the beginning of the scientific method of investigation.

In that same century, another very influential astronomer and philosopher, Johannes Kepler (1571-1630), with the discovery of planetary movements, defined the so-called Kepler laws; he also made contributions in the field of optics, enunciated a first satisfactory approximation of the law of refraction and analyzed the geometric aspect of various optical systems.

In the seventeenth century Isaac Newton (1642-1727) made fundamental discoveries in the field of mathematics and optics, the contributions generated by this philosopher support the entire analysis of heat transfer that supports the development of technology for the use of energy. thermal energy.

Descartes (1596-1650) states: «In our search for the direct path to truth, we should not deal with objects for which we cannot achieve a certainty similar to those of the demonstrations of arithmetic and geometry», it is required to implement procedures that guarantee reliability of the measured data to give reliability to the proposed models.

Claude Bernard (1813-1878) maintains, among others, that observation is the pure and simple verification of natural phenomena as they appear to the senses, while experimentation is the verification of phenomena created by the experimenter.

The experimental method, as a scientific method, rests entirely on the experimental verification of a scientific hypothesis.

Popper (1985) states that the scientific method considers the formulation of innovative ideas and submitting them to the most reasonable, rigorous and effective possible refutations; determines the trial and error method that consists of proposing bold hypotheses and exposing them to the most severe criticism to try to determine a mistake if it exists.

Another current philosopher who has generated great contributions in the scientific method is Mario Bunge (2007), he explains that an efficient technology is based on hypotheses of well-confirmed mechanisms, for this processes are required that are part of a specific system which he calls materialism. systemic; he calls the system a complex object whose parts or components are held together by links of some kind, whether they are logical or material. The bridges that are generated between theory and fact can be described as the hypothetico-deductive method where, first, the observable consequences of the theory are deduced, then empirical data are obtained, these are confronted with predictions and, finally, The theory is evaluated, it indicates that it contains an important part of truth, but that it is also seriously flawed since the theories do not imply such observations without further ado and, consequently, the data cannot be contrasted directly with the relevant empirical data.

John Calle-Sigüencia, PhD

Editor in Chief

TABLE OF CONTENTS

Determination of the maximum compression pressure of a spark-ignition engine based on a recurrent artificial neural network

Determinación de la presión máxima de compresión de un motor de encendido provocado basado en una red neuronal artificial recurrente

Wilmer Contreras[1,*], Mauricio Arichávala[1], Cristian Jérez[1]

Abstract

This research presents an explanation of the applied methodology for the determination of the maximum compression pressure of a reciprocating internal combustion spark-ignition engine (SIE), which is based on a study that begins with the characterization of amper-age consumption curves of the starter motor. A proto-col for data acquisition and subsequent statistical anal-ysis is applied. The statistical values of the signal as energy, average, standard deviation, variance, kurtosis, asymmetry, maximum, minimum and crest factor are selected in function of a greater contribution of infor-mation for the characterization of the experiment; these values generate databases that are applied for the crea-tion and training of a recurrent artificial neural network (RANN) in which an absolute error of less than 2% is obtained. In a first instance, the test methodology is applied to an engine assembled in a didactic work-bench, after which the method is applied to engines in vehicles.

Keywords: diagnosis, compression pressure, RANN, SIE, Elman Network, recurrent layer.

Resumen

En la presente investigación se realiza la explicación de la metodología aplicada a la determinación de la presión máxima de compresión de un motor de combustión interna alternativo de encendido provocado (MEP), el cual se basa en un estudio que parte de la caracterización de las curvas del consumo de amperaje del motor de arranque. Se aplica un protocolo de adquisición de datos y su posterior análisis estadístico. Los valores estadísticos de la señal como energía, promedio, desviación estándar, varianza, kurtosis, asimetría, máximo, mínimo y factor de cresta son seleccionados en función al mayor aporte de información para la caracterización del experimento; estos valores generan bases de datos las cuales son aplicadas para la creación y entrenamiento de una red neuronal artificial recurrente (RNAR) en la cual se obtiene un error absoluto menor al 2 %. En una primera instancia se aplica la metodología de pruebas en un motor ensamblado en un banco didáctico y luego se procede a la aplicación del método en motores aplicados en vehículos.

Palabras clave: diagnóstico, presión de compresión, RNAR, MEP, red Elman, capa recurrente.

[1,*]Transport Engineering Research Group (GIIT), Automotive Mechanical Engineering Major, Universidad Politécnica Salesiana, Cuenca – Ecuador. Author for correspondence ✉: rcontreras@ups.edu.ec
  http://orcid.org/0000-0003-2300-9457,   http://orcid.org/0000-0002-3111-7848,
  http://orcid.org/0000-0003-1474-5014.

1. Introduction

Nowadays, the repair and diagnosis processes applied in the area of automotive transport range from artisanal schemes to those reaching a high technical level [1]. The daily increase in number of circulating vehicles demands specialized services, with a subsequent reduction in failure detection and repair times. This has led to the development of research through vibration analysis [2], in order to identify parameters of critical operation, experimental analysis of the acoustic emissions of reciprocating engines [3], non-intrusive determination of engine cylinder capacity [4].

Due to the complexity of the variables that intervene in the diagnosis of internal combustion engines, the application of computational mathematics is necessary.

The use of neural network techniques is considered to be a great contribution in the analysis of the parameters of internal combustion engines, according to Saraswati and Chand; cylinder pressure can be reconstructed with the use of a recurrent neural network (RNN) [5]. Likewise, in 2012 Cay and Cicek indicated that specific fuel consumption can be predicted based on parameters such as: engine braking, effective power, effective average pressure, and the temperature of the engine's exhaust gas. For this, an ANN model based on the standard backpropagation algorithm was used, with average errors of less than 3.8% [6].

According to Czarnigowski, it is possible to determine the spark advance value by using inverse neural network modeling of the effective torque, thus achieving idle speed stabilization [7].

The research of Wu, Huang and Chang proposes a fault diagnosis system of the ICE, based on the pressure of the intake manifold, by using Discrete Wavelet Transform (DWT) and RAN application. This type of diagnosis reduces the conventional defect of relying too much on the experience of technicians [8]. A very similar study was proposed by Shatnawi and Al-khassaweneh, where the sound signal emitted by the ICE is the source of information to discover faults, by means of an extension neuronal network (ENN), which improves performance compared to a RAN [9].

Efforts to predict future engine states are also of great interest in the technological development of engines, as demonstrated by a study developed by the University of Michigan, where RANs are used to predict combustion behavior of an ignition engine by homogeneous charge compression ignition (HCCI) during its transient operation [10].

With the same purpose of predicting the performance and exhaust emissions under different EGR strategies, researchers Roy, Banerjee and Bose present a study that uses RAN, obtaining, as a result, correlation coefficients within the range of 0.987–0.999 and an absolute error in the range of 1.1–4.57% [11]. For the purpose of optimizing RANs, parallel strategies can be used, such as the smooth variable structure filter (SVSF) used to train RANs efficiently, consequently known as SVSF-based RAN, which is used again for the detection and classification of engine faults using vibration data in the crankshaft angle domain [12].

Likewise, through the use of RANs, an automated diagnostic system for ignition failures in the ICE has been developed, which consists of three stages: detection, location and identification of failure severity [13].

Researchers Chen and Randall trained a RAN for time domain analysis that uses the parametric characteristics of acoustic emissions (AE), to detect damage to the valves of the ICE [14].

It should be noted that there are very few intelligent systems at the general level focused on the diagnosis of mechanical faults involving pressure compression of the EPI, with expert systems such as DELTA, by General Electric Company [15], used for the repair of diesel and electric locomotives. Another example is STEAMER [15], developed by the Navy Research Perssoner Development Center, designed to teach the operation of a steam propulsion plant such as those used in steam-powered vessels, and finally we can mention Project Eolo CN-235, developed by the Spanish company Construcciones Aeronáuticas S.A., an interactive teaching system for pilots and aircraft maintenance technicians, model CN-235.

At a commercial and academic level there are different softwares such as Autodata, which has technical specifications sheets and estimated repair times, fault codes, repair routines of different brands and models of cars, allowing technical personnel to perform any type of repair with the disadvantage of the subjectivity of the operators in decision-making based on trial and error in their professional experience, which maintains an incipient diagnostic system that in many cases could cause erroneous and deficient repairs to the automobile [1].

This bibliographic review leads to the investigation for the generation of methodologies put forth in order to determine the maximum compression pressure in the combustion chamber in spark-generated ignition engines, in a way that is minimally intrusive and quickly realizable.

2. Materials and methods

This section explores the main topics related to the selection of less invasive parameters, engine instrumentation, soft-ware design, data collection, validation of samples, and the creation and training of a RANN.

2.1. Selection of less invasive parameters

The main objective is to avoid the manipulation and disas-sembly of elements that would otherwise be nec-

Contreras et al. / Determination of the maximum compression pressure of a spark-ignition engine based on a recurrent artificial neural network

11

essary to access the spark plugs and install a leak tester or a compres-someter, for which the following options are considered: the measurement of the mass flow parameter of engine air, in-stalling a pressure gauge in the intake manifold [16], meas-uring the current consumption of the starter engine, measur-ing the battery's voltage drop. All these options involve the condition of the starter engine for a determined time period.

2.2. Engine instrumentation

The previous section outlines the measurement parameters for the development of the experiment, after which we see that a MAF type hot wire sensor can be used to perform the measurement of mass flow air intake, a MAP type sensor can be used for pressure measurement in the intake mani-fold, a clamp meter can be used for the measurement of the consumption current of the starter engine, a voltage divider connected directly to the battery terminals can be used for the determination of the voltage drop, all of which is shown in Table 1 and Figure 1.

Table 1. Engine instrumentation.

Parameters	Sensors
Mass flow of air	MAF
Intake pressure	MAP
Current	Clamp meter
Voltage	Divided voltage

To identify a cylinder that shows a significant difference in its compression value, an inductive clamp is applied to register the spark that corresponds to cylinder 1 and, ac-cording to ignition order, the cylinder with the greatest var-iation is located. The signal of the CMP sensor is registered to identify each of the cylinders in the engine on the test workbench.

Figure 1. Engine instrumentation.

For the application of the MAF sensor, several couplings are needed that depend on the diameter of the

intake manifold, so this option is discarded as it also requires the disassembly of several conduits from the intake manifold. For the MAP application, a tap on the intake manifold must be identified which allows the sensor to be connected, which in some vehicles is non-existent. Therefore, conduits must be disconnected and can generate mechanical failures if they are not reinstalled correctly, and so this option is discarded.

Energy consumption of the starter engine can be measured with the installation of a clamp meter, for which no further requirements are needed, only the identification of the cable and the subsequent installa-tion; voltage measurement is achieved direct-ly through the application of clamps on the battery terminals, in-dicated in Figure 2, without this option representing major complications.
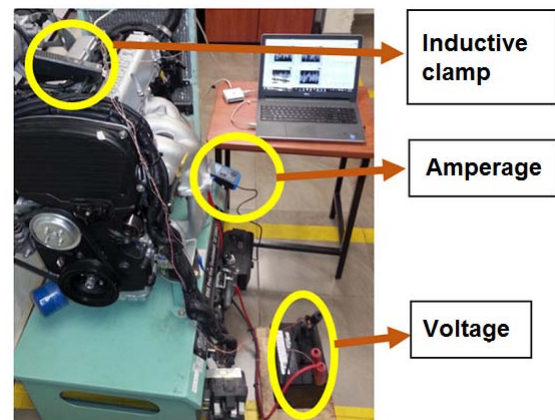
Figure 2. Measurement of battery amperage and voltage.

Table 2 summarizes the characteristics of the motor being tested and of the applied current clamp.

Table 2. Equipment

Graphic	Characteristics
SIE	Hyundai 4 cylinders DOHC Electronic fuel injection (MFI) VT = 1997 cc ignited by spark / Unleaded petrol (RON 95) Rc = 10.0 : 1 MAP – DIS
Hantek CC – 650	AC/DC Current Clamp Bandwidth 400 Hz 1 mV / 10 mA 650 A AC/DC frecuency range: Up to 400 Hz Effective Measurement range: 20 mA to 650 A DC

2.3. Software design

Once it is determined that amperage consumption, together with the measurement of the voltage drop, is the least invasive parameter, the LabView software, which is compatible with a Ni 6009 card, is used for the acquisition of data at a rate of 1 kHz, meeting the Nyquist criterion for signal analysis.

The software also performs the extraction of characteristic parameters and descriptive statistics of each test performed and, in addition, it generates a database which will subsequently be applied in the creation and training of a recurrent artificial neural network.

Figures: 3a, 3b and 3c present a sequence and part of the programming applied for the acquisition and development of the software and its graphic environment.

2.4. Data collection

The graphs resulting from the sampling of the studied engine, with differences in compression pressure (the engine is in starting condition), are shown below.

Figure 4 shows the compression pressure curve as a function of the oscillogram of the starter engine's am-perage consumption curve, in which the engine is in standard conditions, that is, all its cylinders present a standard compression pressure of about 125 PSI.
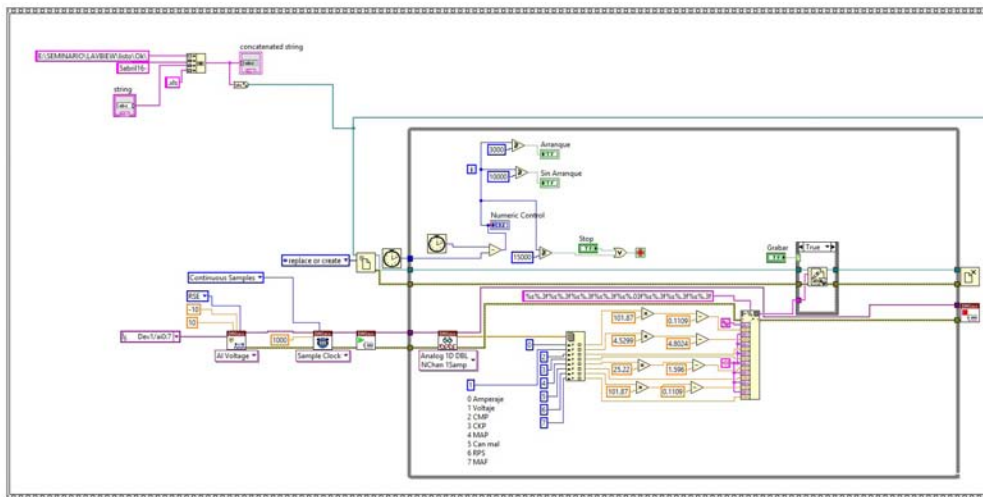
Figure 3a. Signal acquisition.
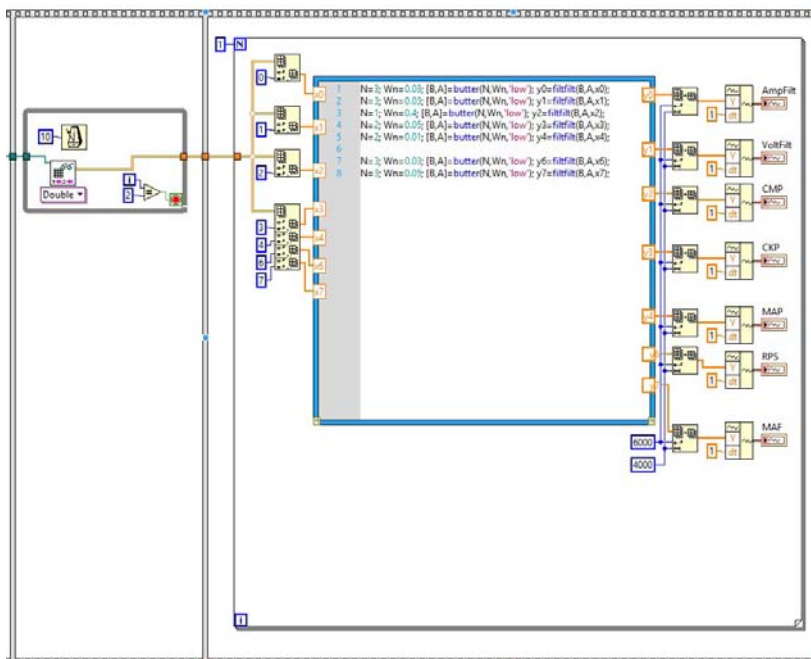
Figure 3b. Signal filtering, development and extraction.

Contreras et al. / Determination of the maximum compression pressure of a spark-ignition engine based on a recurrent artificial neural network

13
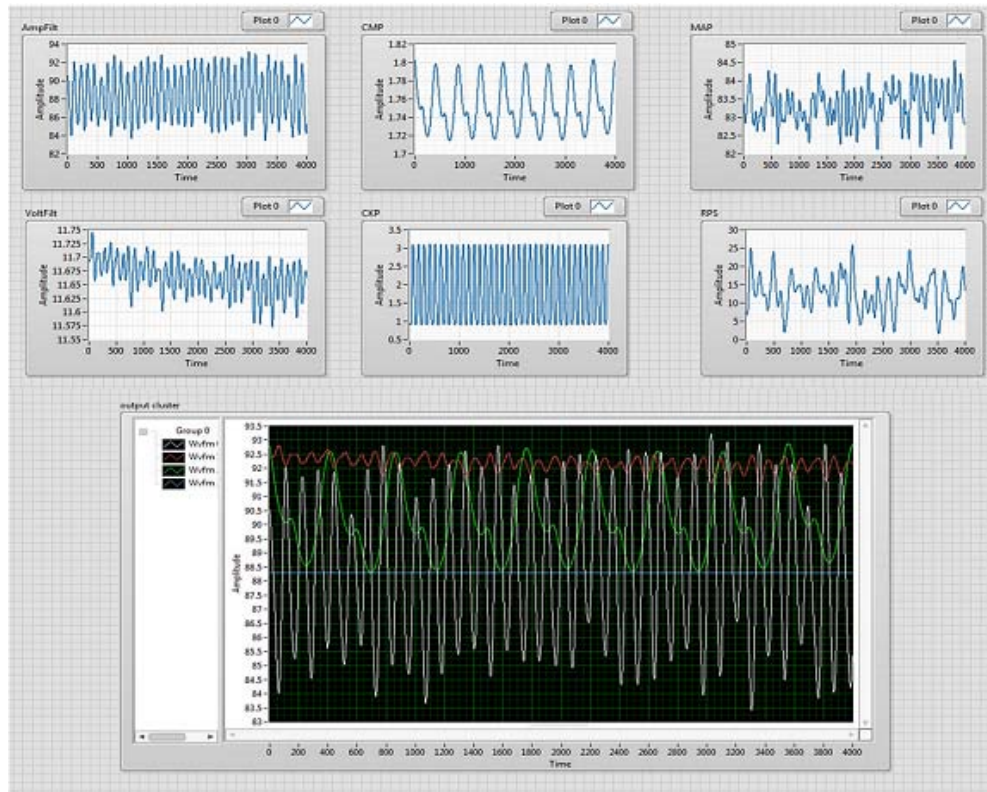
Figure 3c. Visualization of the signals and their graphic environment.
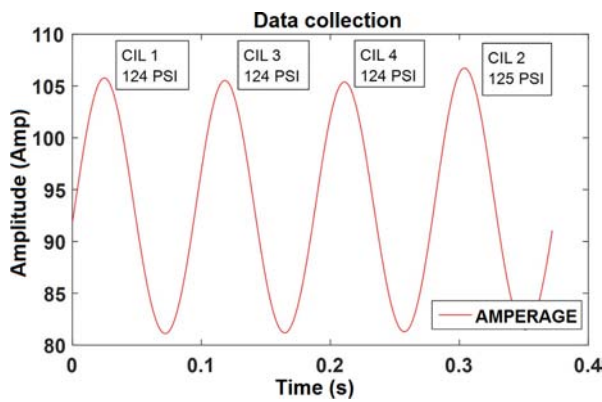
Figure 4. Engine data collection without major compression variation.

Figure 5. Engine data collection with compression variation in cylinder 1.

In Figures 5, 6, 7 and 8, the compression pressure curve is plotted according to the oscillogram of the starter engine's amperage consumption curve, in which the engine presents compression variations in each cylinder. This means that the cylinder corresponding to the ignition order has a compression pressure of 90 PSI, while the 3 remaining cylinders maintain their standard pressure. In addition, the signal curve of the CMP sensor can be identified.

Figure 6. Engine data collection with compression variation in cylinder 3.
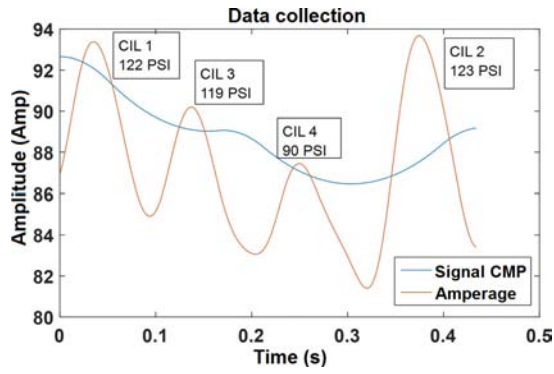
Figure 7. Engine data collection with compression variation in cylinder 4.

Figure 8. Engine data collection with compression variation in cylinder 2.

Next, in Figures 9, 10, 11 and 12 a bar diagram is applied, in which each bar represents the value of the compression pressure as a function of the amperage consumption of the starter engine when the engine presents compression pressure variations in each cylinder, that is, the cylinder corresponding to the 1-2-3-4 order has a compression pressure of 90 PSI, while the other 3 remaining cylinders maintain their standard pressure.
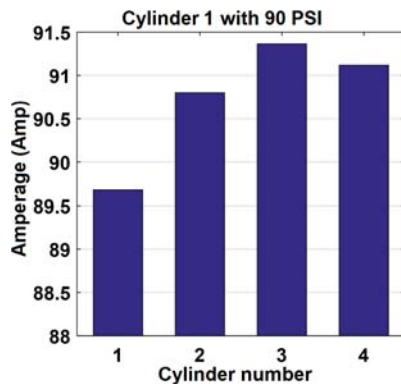
Figure 9. Engine with compression variation in cylinder 1.

Figure 10. Figure 10. Engine with compression variation in cyl-inder 2.

Figure 11. Engine with compression variation in cylinder 3.
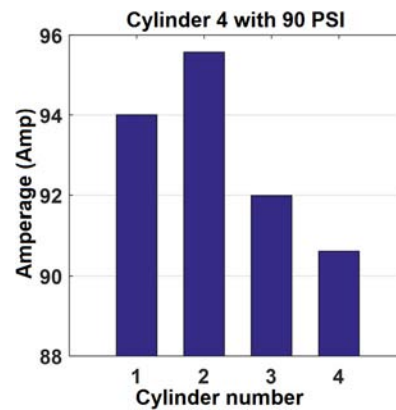
Figure 12. Engine with compression variation in cylinder 4.

2.5. Sample validation

The samples taken by the software designed in the LabView virtual platform are analyzed statistically through an ANOVA, which yields the following results.

Contreras et al. / Determination of the maximum compression pressure of a spark-ignition engine based on a recurrent artificial neural network

15
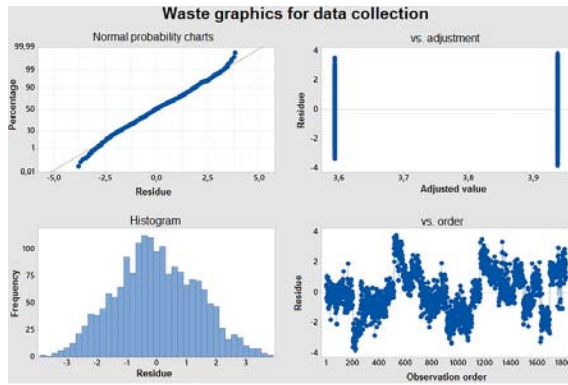
Figure 13. ANOVA of samples.

The scatter plot in the graph showing residual vs. percentage shown in Figure 13 tends to be a straight line which affirms the normality of the data and which, furthermore, is confirmed by the distribution of values in the form of the Gaussian bell in the histo-gram. The assumption of constant variance is validated because, in the graph for adjusted value vs residual value, no point accumulation pattern is observed. Ad-ditionally, this corroborates that the samples were ran-domized, since the point values in the observation order vs. residue graph show no regions of accumula-tion in the upper or lower part of zero. Rather, they fluctuate in a random pattern around the zero line.

In summary, the data collection is correct and the ANOVA results corroborate this fact.

To determine the most significant characteristic sta-tistical values, a unidirectional ANOVA is applied to the variables under study in order to analyze the p-value results, with the lowest value revealing the great-est significance of the variables. Next, Table 3 lists the statistical values in order of significance based on the lowest value of ρ.

Table 3. Equipment

Statistical values	*p-valúe*
Amp peak	0,000
Energy	0,000
Max	0,000
Mean	0,000
Standard Deviation	0,000
Variance	0,000
RMS	0,000
Asymmetry	0,000
F. Crest	0,001
Kurtosis	0,003

2.6. Elman type neuronal network

An Elman-type neural network is applied, based on a pre-experimental run in which trainings were carried out with different types of networks, including «feed-forward», «cascade-forward», «elman-forward». The one showing lesser errors was selected. Having made the previous observation, it is indicated that the input parameters are characteristic values resulting from the analysis of the amperage consumption curve of the starter engine; these are presented in Figure 14.
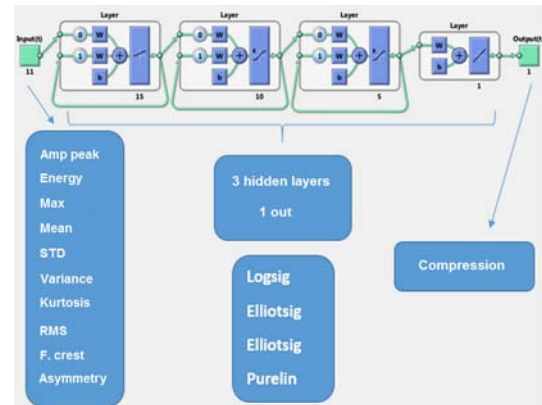
Figure 14. Elman-type neural network

Three hidden layers are applied, each with 15, 10 and 5 neurons per layer, due to the lower computa-tional expense, since increasing layers and neurons does not reduce error and the execution time increases. Moving forward, the activation functions between the input neuron and the first neuron are of the Logsig type, followed in the two layers by an Elliotsig func-tion, and finally between the layer and the output neu-ron a Purelin type function.

The output neuron indicates the value of the com-pression result, this according to the computational analysis generated by the Elman-type RANN.

The network training is done with the Levenberg-Marquardt function (trainlm), which is shown in Fig-ure 15.

Figure 16 indicates the gradient in the reduction of the squared error or MSE and the number of Epochs created for training the RANN.

3. Results and discussion

In order to compare the correct operation of the creat-ed and trained RANN according to the proposed pro-cess, several tests of various compression values are performed. In this section, two specific compressions are presented, with values ranging near 120 PSI in the case of engines operating correctly; another case is where the values are around 90 PSI, which indi-cates an imbal-ance fault in the engine's generalized combustion.
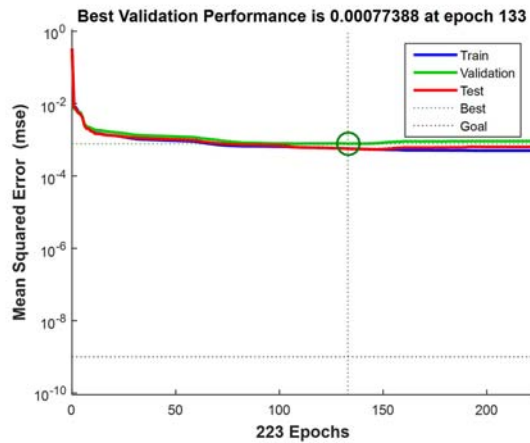
Figure 15. Elman-type network training.
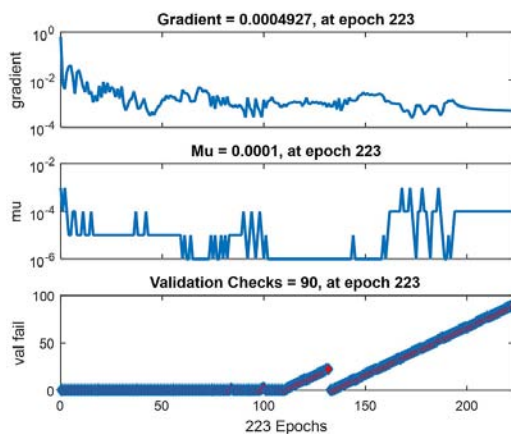
Figure 16. Evolution of Elman-type network training.

Figure 17 shows the result of the values obtained by the RANN for 120 PSI compression sockets, where the average value of the resulting error and the real value is 0.0895% of the absolute value.
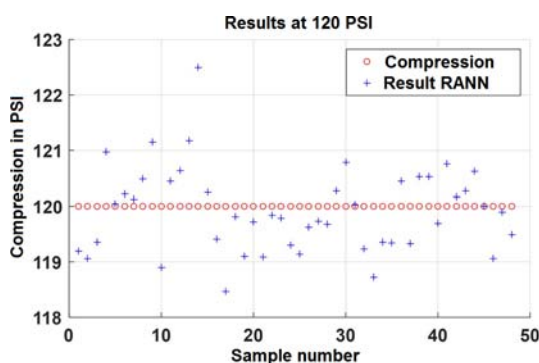
Figure 17. Compression results at 120 PSI.

Figure 18 shows the result of the values obtained by the RANN for 90 PSI compression sockets, where the average value of the resulting error and the real value is 0.2591% of the absolute value.
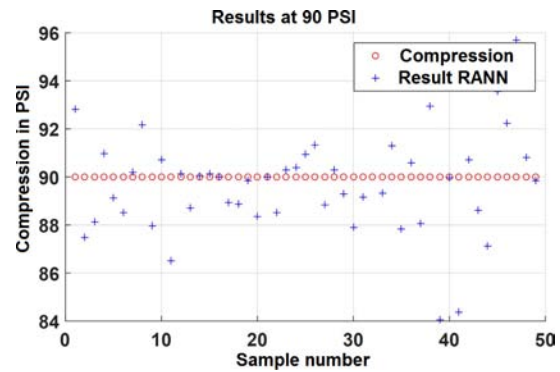
Figure 18. Compression results at 90 PSI.

4. Conclusions

This work demonstrates that the application of recurrent artificial neural networks (RANN) in the determination of the compression of an SIE constitutes a clearly viable alternative; in addition, it has the advantage of being minimally invasive with error ranges of less than 1%, and with the possibility of determin-ing the compression value with a high degree of probability.

Another fundamental aspect to take into account is that the compression measurement process is applied very frequently in the evaluation of vehicles for sales. Therefore, this methodology is presented as a highly appropriate technique to be integrated into a diagnostic system with the computational speed that neural net-works offer.

After the elaboration of this study, in which an Elman-type neuronal network structure is applied, it has been observed that this is the most appropriate given the dynamic nature of the patterns obtained by the analysis of the starter engine's energy consumption.

References

[1] R. F. Covarrubias and A. G. F. Covarrubias, "Desarrollo de un sistema experto para el diagnostico de fallas automotrices." *Revista Iberoamericana de Tecnología en Educación y Educación en Tecnología (TE&ET)*, no. 11, pp. 83–91, 2013. [Online]. Available: https://goo.gl/Uz5g5y

[2] O. Criollo and H. Matute, "Diagnóstico de fallos en la combustión para motores de combustión interna alternativos diésel por análisis de vibraciones." Tesis de Grado, Universidad Politécnica Salesiana, 2014. [Online]. Available: https://goo.gl/24c27G

[3] J. García, "Diseño de una sala de pruebas para motores alternativos de combustión interna." in *Trabajo final de carrera, Universidad Politécnica de Cataluña*, 03 2007. [Online]. Available: https://goo.gl/xJv1ym

Contreras et al. / Determination of the maximum compression pressure of a spark-ignition engine based on a recurrent artificial neural network

17

[4] W. Contreras and J. Fajardo, "Diseño y construcción de un sistema prototipo para determinar la cilindrada total de un motor ciclo otto por un método no invasivo mediante labview," Master's thesis, Escuela Politécnica Nacional, 2012. [Online]. Available: https://goo.gl/SdZ6ec

[5] S. Saraswati and S. Chand, "Reconstruction of cylinder pressure for si engine using recurrent neural network." *Neural Computing & Applications*, vol. 19, no. 6, pp. 935–944, 2010. [Online]. Available: https://doi.org/10.1007/s00521-010-0420-6

[6] Y. Çay, A. Çiçek, F. Kara, and S. Saˇgiroğlu, "Prediction of engine performance for an alternative fuel using artificial neural network," *Applied Thermal Engineering*, vol. 37, no. Supplement C, pp. 217–225, 2012. [Online]. Available: https://doi.org/10.1016/j.applthermaleng.2011.11.019

[7] J. Czarnigowski, "A neural network model-based observer for idle speed control of ignition in si engine," *Engineering Applications of Artificial Intelligence*, vol. 23, no. 1, pp. 1–7, 2010. [Online]. Available: https://doi.org/10.1016/j.engappai.2009.09.008

[8] J.-D. Wu, C.-K. Huang, Y.-W. Chang, and Y.-J. Shiao, "Fault diagnosis for internal combustion engines using intake manifold pressure and artificial neural network," *Expert Systems with Applications*, vol. 37, no. 2, pp. 949–958, 2010. [Online]. Available: https://doi.org/10.1016/j.eswa.2009.05.082

[9] Y. Shatnawi and M. Al-khassaweneh, "Fault diagnosis in internal combustion engines using extension neural network," *IEEE Transactions on Industrial Electronics*, vol. 61, no. 3, pp. 1434–1443, March 2014. [Online]. Available: https://doi.org/10.1109/TIE.2013.2261033

[10] V. M. Janakiraman, X. Nguyen, and D. Assanis, "Nonlinear identification of a gasoline hcci engine using neural networks coupled with principal component analysis," *Applied Soft Computing*, vol. 13, no. 5, pp. 2375–2389, 2013. [Online]. Available: https://doi.org/10.1016/j.asoc.2013.01.006

[11] S. Roy, R. Banerjee, and P. K. Bose, "Performance and exhaust emissions prediction of a crdi assisted single cylinder diesel engine coupled with egr using artificial neural network," *Applied Energy*, vol. 119, Supplement C, pp. 330–340, 2014. [Online]. Available: https://doi.org/10.1016/j.apenergy.2014.01.044

[12] R. Ahmed, M. E. Sayed, S. A. Gadsden, J. Tjong, and S. Habibi, "Automotive internal-combustion-engine fault detection and classification using artificial neural network techniques," *IEEE Transactions on Vehicular Technology*, vol. 64, no. 1, pp. 21–33, Jan 2015. [Online]. Available: https://doi.org/10.1109/TVT.2014.2317736

[13] J. Chen and R. B. Randall, "Improved automated diagnosis of misfire in internal combustion engines based on simulation models," *Mechanical Systems and Signal Processing*, vol. 64-65, Supplement C, pp. 58–83, 2015. [Online]. Available: https://doi.org/10.1016/j.ymssp.2015.02.027

[14] S. M. Jafari, H. Mehdigholi, and M. Behzad, "Valve fault diagnosis in internal combustion engines using acoustic emission and artificial neural network," *Shock and Vibration*, vol. 2014, pp. 1–9, 2014. [Online]. Available: http://dx.doi.org/10.1155/2014/823514

[15] J. Giarratano and G. Riley, *Sistemas expertos, principios y programación.*, T. Ed, Ed., 2004.

[16] M. Khajavi, S. Nasiri, and A. Eslami, "Combined fault detection and classification of internal combustion engine using neural network," *Journal of Vibroengineering*, vol. 16, no. 8, pp. 3912–3921, 2014. [Online]. Available: https://goo.gl/aWc9oW
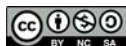
CHARACTERIZATION OF AN AXIAL FLOW GENERATOR FOR APPLICATIONS IN WIND ENERGY

CARACTERIZACIÓN DE UN GENERADOR DE FLUJO AXIAL PARA APLICACIONES EN ENERGÍA EÓLICA

Mauricio Carrillo-Rosero[1,*], Cristian Claudio-Medina[1], Alex Mayorga-Pardo[1]

Abstract

The use of unconventional energy resources in recent years has developed mainly with the intention of reducing the use of fossil fuels to obtain electricity. When talking about electricity generation at medium and small scale, the global trend while taking advantage of wind energy, is the use of permanent magnet generators. Axial flow generators are the most often available: the main feature of these generators is their ability to deliver electrical power at low revolutions, with an acceptable efficiency. In this research project two types of axial flow generators were characterized; one with coils in series and another with coils in parallel, with the intention of evaluating the performance of each one. The design starts from the determination of the magnetic flux, number of revolutions, number of poles, number of coils, output voltage and electrical losses, to then carry out the contrast through the data acquisition of amperage and voltage with respect to the theoretical calculation; the purpose is to establish the efficiency of each of the configurations. It was established that the series generator has characteristics that make it a configuration that has an efficiency greater than that of the generator in parallel.

Keywords: Generators, flow, axial, energy, wind, efficiency.

Resumen

El aprovechamiento de los recursos energéticos no convencionales en los últimos años se ha desarrollado principalmente con la intención de disminuir el uso de combustibles. A mediana y pequeña escala la tendencia mundial, cuando se habla de generación eléctrica utilizando la energía eólica, es el uso de generadores de imanes permanentes. Los generadores de flujo axial son lo que se encuentran con mayor frecuencia a disposición. La principal característica de estos generadores es su capacidad de entregar energía eléctrica a bajas revoluciones, con una eficiencia aceptable. En este proyecto de investigación se caracterizaron dos tipos de generadores de flujo axial; uno con bobinas en serie y otro con bobinas en paralelo, con la intención de valorar el rendimiento de cada uno. El diseño parte de la determinación del flujo magnético, número de revoluciones, número de polos, número de bobinas, voltaje de salida y pérdidas eléctricas, para luego realizar el contraste a través de la toma de datos de amperaje y voltaje con respecto al cálculo teórico; la finalidad es establecer la eficiencia que presentan cada una de las configuraciones. Se estableció que el generador en serie posee características que lo convierten en una configuración que tiene una eficiencia mayor que la del generador en paralelo.

Palabras clave: generadores, flujo axial, imanes permanentes, energía eólica, eficiencia.

[1,*]Faculty of Civil and Mechanical Engineering, Universidad Técnica de Ambato – Ecuador. Author for correspondence ✉: cmcarrillo@uta.edu.ec. ⬡ http://orcid.org/0000-0001-6578-9362,
⬡ http://orcid.org/0000-0001-7091-3516, ⬡http://orcid.org/0000-0001-8875-8470.

1. Introduction

The growing demand for fossil fuels, together with the reduction of their reserves, has unleashed a continuous increase in prices that affects the world economy. In addition, the use of these fuels produces gases, such as carbon dioxide (CO_2), whose greenhouse effect causes an increase in the temperature of the planet's surface [1].

According to the WWEA in its September 2016 newsletter, at the end of 2014 the installed capacity of small-scale wind registered more than 830 MW worldwide. This represents a growth rate of 10.9% in relation to 2013, when 749 MW were registered. The year 2013 was 10.3% higher than the total of 678 MW installed in 2012.

China accounts for 41% of global capacity, the United States 30% and the United King-dom 15%. At the end of 2014, a cumulative total of at least 945 000 small wind turbines were installed worldwide. This represents an increase of 8.3% (7.4% in 2013) compared to the previous year, when 872 000 units were registered [2]. It is estimated that the capacity in the mini-wind industry by 2020 could sup-ply 50 000 MW worldwide [1].

To help reduce costs and minimize maintenance as much as possible, many wind turbine developers employ direct-drive (without gearbox) permanent magnet generators (PMG) as long as they have a mechanically simple generator design. Several permanent magnet generator topologies can be used [3].

A suitable design for a generator with central stator axial flow is based on two rotor pieces that are lateral-ly fixed to the axis of the machine. This configuration of two air gaps has the advantage of canceling the lon-gitudinal forces on the stator. In addition, this topology minimizes the dispersion inductance [4].

The goal of this project is to characterize PMG axi-al flow in two configurations of coils, one in series and the other in parallel using iron-boron-neodymium magnets, to determine the efficiency of each of them.

1.1. Design features of an axial flow generator

It consists of a pair of thin iron disks that revolve around an axis perpendicular to it, and in whose contour a set of magnets is placed, which in turn creates a magnetic field parallel to the axis of rotation as shown in Figure 1. The axial arrangement for cutting the magnetic field is parallel to the winding. This kind of arrangement allows an excitation of the electrons without friction and magnetic opposition. The cut made is of 180° producing fewer losses than with radial generation [5].
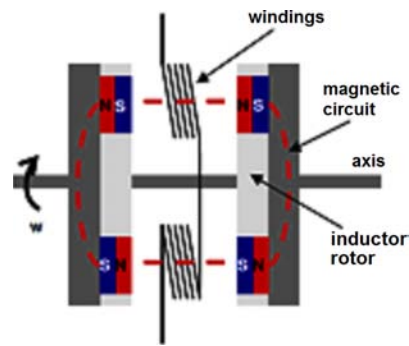
Figure 1. Transverse view of an axial generator.

1.2. Coils with an air core

The conductor is rolled up on a hollow support which is then removed, resulting in something that looks similar to a spring. It is utilized in elevated frequencies. A variant of the previous coil is called a solenoid, which differs in the insulation of the coils and the presence of a support that does not necessarily have to be cylindrical. It is utilized when several turns are required. These coils can have intermediate sockets. In such cases, they can be considered as two or more coils on the same support and connected in a series.

Each coil produces a voltage depending on how they are connected, which can be of two types: in series and in parallel. The series connection consists of joining the end of the first coil with the beginning of the next so that the voltages are added. On the other hand, in parallel connections the ends are connected to each other and the resulting voltage is the same as that of a coil, with the difference that twice the current can be obtained. It is inevitable that the output voltage of each coil will be slightly different in parallel configu-rations, which leads to the generation of eddy currents that waste energy [6].

Figure 2 shows the connection of three coils in se-ries for each phase, and a stator composed of nine coils in total, therefore it is a three-phase generator. A remarkable advantage of this generator is that the recti-fier only requires three cables [6].
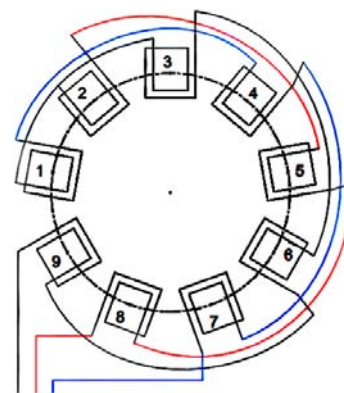
Figure 2. Wiring diagram of coils in series.

Figure 3 shows ten cables, each connected in parallel to its respective coil; the number of output cables de-termines the location of the rectifier, since if there are too many cables the movement of the generator at the end of the tower is limited, which implies that the rec-tifier must be located next to the generator and this causes maintenance problems. The number of phases is not a problem for rectification since the bridge con-nections can be varied to rectify up to two phases for each one [6].
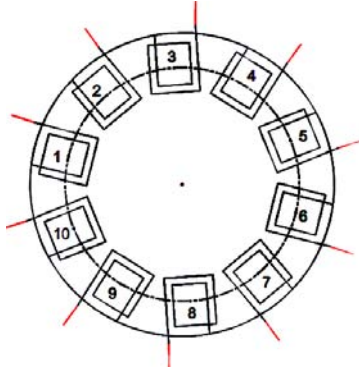
Figure 3. Connection diagram of parallel coils.

1.3. Permanent magnets

The basic compound in the permanent magnets used in this research is Neodymium-Ironboron (NdFeB), which has low resistance to corrosion due to its coating with thin layers of nickel and chromium to isolate the base material from the environment, overcoming the disadvantage of demagnetization at lower temperatures like other com-pounds [7]. Magnets with a high degree of magnetiza-tion are required, which make it possible to place sev-eral magnets in each rotor [8, 9]. In addition, the polar-ization direction must be relevant to this purpose; hence, neodymium grade 40 (N40) magnets were se-lected.

2. Materials and methods

Figure 4 shows the scheme for determining the magnetic flux density through Equation 1, applicable to rectangular magnets [10].
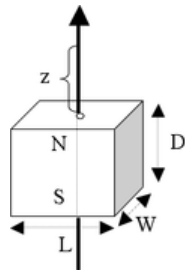
Figure 4. Scheme for the application of the flow density formu-la.

The magnetic flux density is determined as:

$$B = \frac{Br}{\pi}\left[tan^{-1}\left(\frac{LW}{2z\sqrt{4z^2 + L^2 + W^2}} \right) \\ - tan^{-1}\left(\frac{LW}{2(D+z)\sqrt{4(D+z)^2 + L^2 + W^2}} \right) \right] \quad (1)$$

Br = Remanence field independent of the geometry of the magnet (1.26 T, which is obtained from the magnet's physical data).

z = Distance on the axis of symmetry of a polar surface (10.5 mm which is half the distance to which the magnets are separated in each rotor).

L = Length of the parallelepiped (46 mm).

D = Thickness of the parallelepiped (10 mm).

W = Width of the parallelepiped (30 mm).

Substituting the data in the equation we have:

$$B = 0,137\ T$$

To check the calculated data, simulations were performed in the FEMM software as shown in Figure 5.
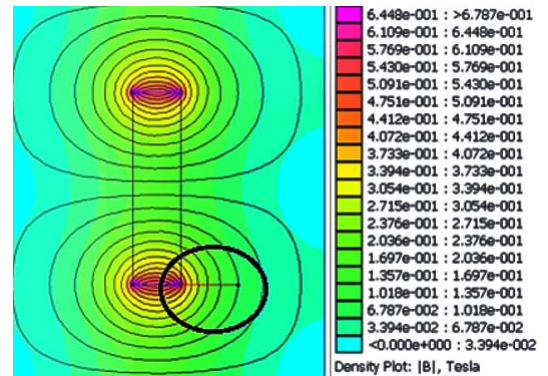
Figure 5. Simulation of the flux density of a magnet side view.

In the software, 0.1357 T is obtained, which is very close to the calculated value and is used for the design. When adding a low carbon steel plate, Figure 6 shows that the flow values practically doubled due to the effects of magnetic concentration and isolation of steel.
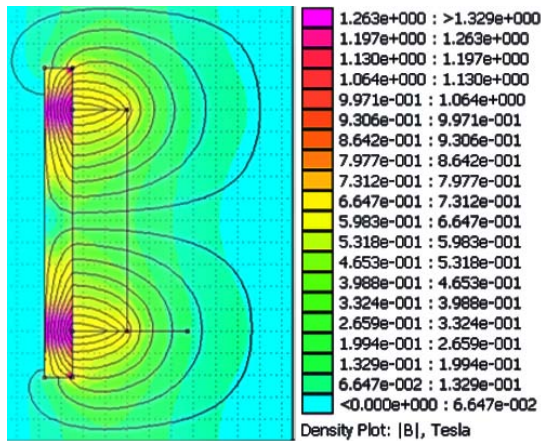
Figure 6. Simulation of the flux density of a magnet glued to a steel plate, side view.

Finally, the two-plate system with facing magnets is analyzed as shown in Figure 7, to obtain the total flow.
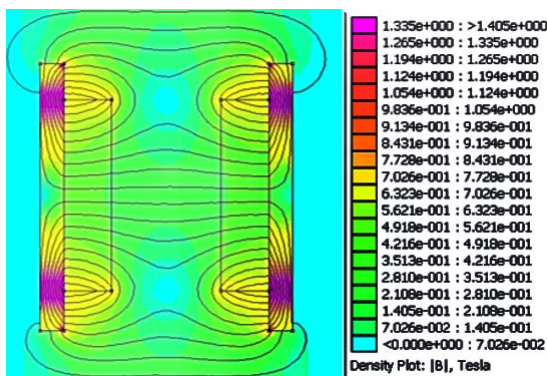
Figure 7. Simulation of the flux density of two plates with facing magnets, side view.

The flux between the plates is 0.5621 T (approximately half of the remaining flux), which confirms the proposed rule [6]: «If there are magnets in both disks and the gap between them is roughly equal to the combined length of the magnets, B will be half of the remaining flux».

2.1. Determination of the number of revolutions for operation

To determine this value, it is necessary to obtain the peak speed ratio, which is the index of the rotational speed of the blades in relation to wind speed, as indicated in equation (2).

$$\lambda = \frac{\omega r}{v} \qquad (2)$$

Where:

λ = Peak speed ratio (a recommended value of 7 will be used for all calculations).

ω = angular velocity (rad/s).

r = Blade radius (m) (a value of 1.5 is used for all calcula-tions).

v = Wind speed (m/s).

Equation (3) [11] is used to determine the speed in r.p.m.

$$N = \frac{30\lambda v}{r\pi} \qquad (3)$$

2.2. Determination of the number of poles

According to [12] the number of poles is calculated with equation (4) where f stands for electric frequen-cy:

$$p = \frac{4 \cdot f \cdot r \cdot \pi}{\lambda \cdot v} \qquad (4)$$

Using equation (4), Table 1 is obtained, setting a maximum frequency of 60 Hz available in the electric network.

From Table 1 we conclude that the higher the frequency, the more poles are needed. In addition, if the wind speed is low, a greater number of poles is necessary to obtain the required frequency. Taking into ac-count the recommendation in [6], a number of 24 poles (12 in each rotor) is chosen, which guarantees an adequate distribution of the magnets in the rotors. The value of operation frequency does not have to be high since direct current that lacks frequency is obtained in the rectification.

Table 1. Physical data of magnets

V. of 2 m/s		V. of 4 m/s		V. of 6 m/s	
Freq. (Hz)	# of poles	Freq. (Hz)	# of poles	Freq. (Hz)	# of poles
10	13,46	10	6,73	10	4,49
20	26,93	20	13,46	20	8,98
30	40,39	30	20,2	30	13,46
40	53,86	40	26,93	40	17,95
50	67,32	50	33,66	50	22,44
60	80,78	60	40,39	60	26,93
V. of 8 m/s		V. of 10 m/s		V. of 12 m/s	
Freq. (Hz)	# of poles	Freq. (Hz)	# of poles	Freq. (Hz)	# of poles
10	3,37	10	2,69	10	2,24
20	6,73	20	5,39	20	4,49
30	10,1	30	8,08	30	6,73
40	13,46	40	10,77	40	8,98
50	16,83	50	13,46	50	11,22
60	20,2	60	16,16	60	13,46

2.3. Determination of the number of coils

According to [6] the number of coils is a function of the available poles:

$$N_B = \frac{3N_p}{4} \tag{5}$$

Where:

N_B = Number of coils.

N_P = Number of rotor poles.

The ratio is: 3 coils for each 4 pairs of poles, applying equation (5) a number of 9 coils is obtained; this distribution guarantees that 3 magnets are synchronized with 3 coils at the same time [11], allowing the induced electromotive force (emf) to add up.

In order to make the comparison between generators with different coil connections, the decision to test another generator with 10 coils all connected in parallel was made. This arrangement is proposed by [6] and guarantees that a battery can be charged with this generator.

2.4. Number of turns per coil

The dimensions of the coil are determined by the measurements of the magnet, since the coil must provide a hollow section for the passage of the magnetic field. As the coils have an air core with support, an inductance of 1 mH is considered for this dimensioning.

$$n = \sqrt{\frac{lL}{\mu A}} \tag{6}$$

Where:

n = Number of turns.

l = Coil length (0.013 m).

L = Inductance (1 mH).

μ = Permeability of the core ($4\pi \times 10^{-7}$ Hm^{-1}).

A = Cross section area ($1{,}2 \times 10^{-3}$ m^2).

For reasons of space and packaging, AWG 14 wire with a diameter of 1.63 mm has been used for the construction of the coils [6].

Table 2 shows the necessary parameters for the construction of the stator.

Table 2. Stator parameters

	Number of poles (p)	Number of colis (Nc)	Number of turns per coil (n)
Generators in series	24	9	93
Generators in parallel	24	10	67

2.5. Coil distribution

The built stator must allow the screws connecting the rotors to pass through, leaving the central part empty and circular in shape. For this, [6] recommends the use of an «island» that is nothing more than a circular sec-tion of wood as shown in Figure 8. The diameter of the island (DIS) is 13 cm.

Figure 8. Location of coils.

The finished stator can be seen in Figure 9, the foot of the coils is located 1 cm from the hole. From these measurements, the magnets are placed on steel discs so that their perimeter coincides with the internal spaces of the coils.

Figure 9. Stator

2.6. Distribution of magnets

The 12 magnets are distributed symmetrically in each rotor disk, where their diameter is in function of the diameter of the island as shown in Figure 10, the distance to the foot of the coils, and the width of the coils (AB). Therefore, the diameter at the foot of the mag-nets (DIM) expressed in centimeters is:

$$D_{IM} = D_{IS} + 2 \cdot A_B + 2 \qquad (7)$$

Figure 10. Location of magnets

2.7. Determination of electrical losses

- **Losses due to resistance in the series generator coils:**

The resistance measured in two phases or 6 coils is 2.2Ω, therefore the resistance per coil is 0.37Ω. To deter-mine the resistance in the stator according to [6] it is considered that 2 phases are always working and it follows that the resistance in the stator is:

$$R_E = 2 \cdot N_B \cdot R_B \qquad (8)$$

Where:

R_E = Resistance in the stator.

R_B = Resistance per coil.

Resulting in a stator resistance of 2.22Ω.

- **Losses due to resistance in the parallel generator:**

The resistance per coil is 0.26Ω and, due to its configu-ration, this is the resistance of the stator because only one coil works at a time.

- **Losses due to resistance in the coils:**

The resistance of the coil turns prevents the current from flowing completely free, since every material has some electrical resistance. This can help determine if the materials are good or bad conductors, which is evaluated by means of equation:

$$P_B = I^2 \cdot R_E \qquad (9)$$

Where:

P_B = Loss power in the coils.

I = Intensity of current circulating in the windings.

- **Losses in the rectifier:**

After the energy collection at the ends of the coils, the following step is the rectification process, from alternating to direct. The rectification method chosen for this application is full wave, with rectifier bridges. Three bridges were used for the series generator, and five for the parallel generator. The intention is to take full advantage of the alternating current generated. Each phase is distributed for four diodes which reduc-es the heating and, therefore, its wear. The only disad-vantage of this arrangement is the voltage drop of 1.4 volts for the two generators.

$$P_R = I \cdot V \qquad (10)$$

Finally, the total electrical losses (P_E) are:

$$P_E = P_B + P_R \qquad (11)$$

$$P_E = I^2 \cdot R_E + I \cdot V \qquad (12)$$

The greater the losses, the lower the efficiency, but in order to determine this, generation trends must be analyzed.

2.8. Determination of efficiencies

The output power (P_S) is obtained from the measured voltage and amperage, the efficiency (η) is determined by the net power output and losses. The generator must provide the net power value plus the losses, therefore:

$$\eta = \frac{P_S}{P_S + P_E} \qquad (13)$$

3. Results and Discussion

The voltage and current intensity data were obtained by operating each of the generators at different angular velocity values (in r.p.m.), rotating the rotors in the mandrel of a lathe as shown in Figure 11. To load the generator, a rheostat was used with different resistance values connected to its output.

Figure 11. Assembly of the generator on the lathe.

Through this arrangement the voltage and amperage data were obtained simultaneously with the help of two multimeters connected as seen in Figure 12.
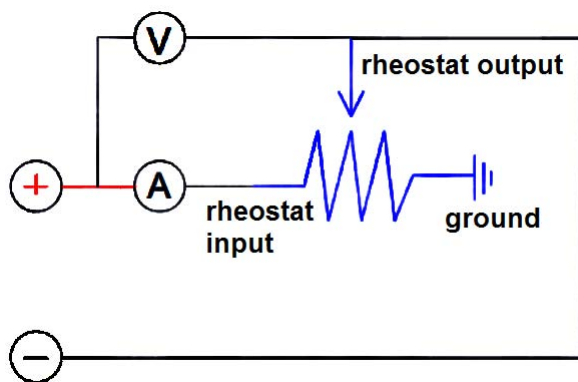
Figure 12. Connection scheme

With the obtained data, graphs are made taking into account that all the values are in function of the angu-lar velocity, since the generation variations depend on it.

Figures 13 to 15 show the graphs with the data of the parallel coil generator:
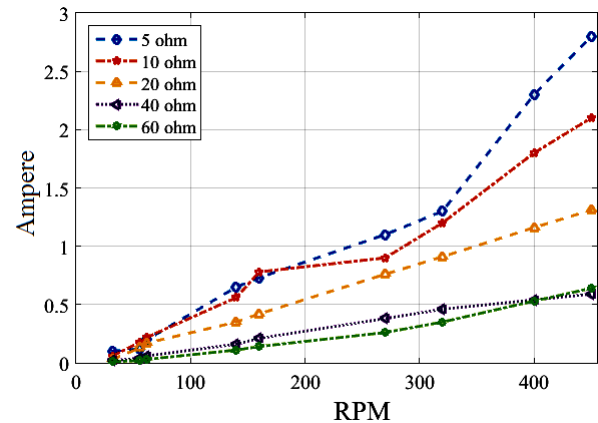
Figure 13. Current intensity at different values of resistance.

The variation of intensity is proportional to the an-gular velocity as shown in Figure 13, which shows that with a higher resistance of the load and a greater angu-lar velocity, the amperage decreases.
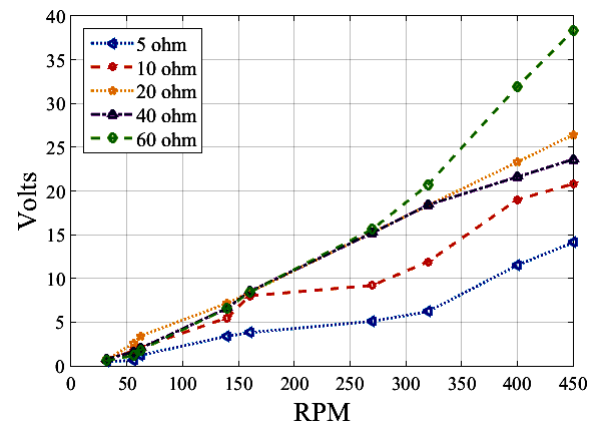
Figure 14. Electromotive force at different resistance values.

Since the voltage is proportional to the current according to Ohm's law, an increase in voltage is observed in Figure 14 as the value of the resistance in-creases, being more significant at high angular velocities.

Figure 15 shows the behavior of the generator power versus its angular velocity. Up to 250 r.p.m. there is no significant increase in power. When the speed of the rotors increases, the power increases. This increment is more evident at low resistance.
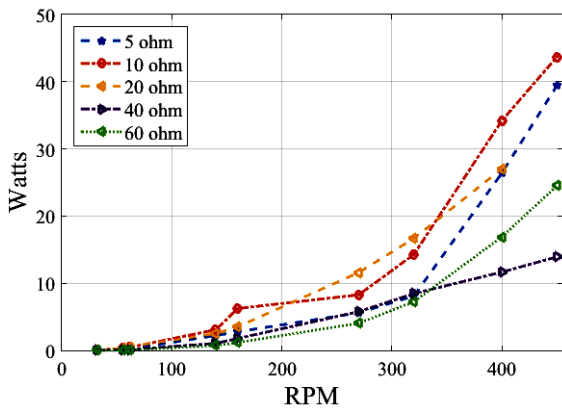
Figure 15. Powers at different resistance values.

Figures 16 to 18 show the graphs with the serial coil generator data.

The behavior of the amperage is increasing in all cases as shown in Figure 16 and it should be noted that the lower the resistance the greater the amperage.
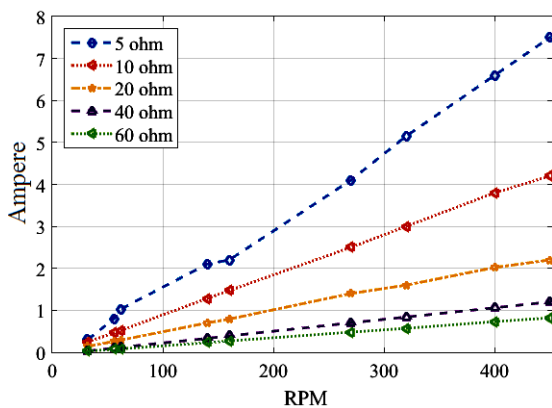
Figure 16. Amperages at different resistance values.

Figure 17 shows that there are important variations in the voltage values. If you take 100% growth, both in resistance and in angular speed, the voltage has a 120% growth at the same load.
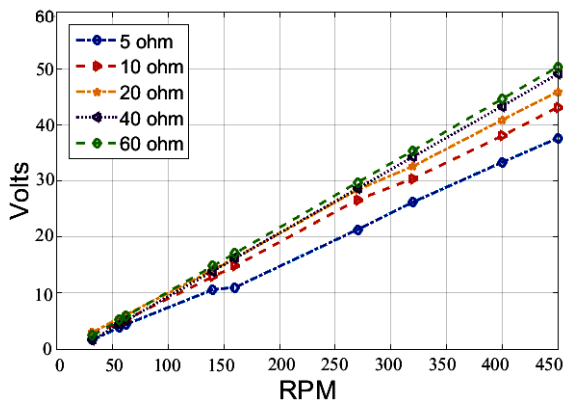
Figure 17. Voltages at different resistance values.

This is a very favorable feature for this generator because, although its amperage changes remarkably as seen in Figure 16, the behavior of the voltage is linear.

The increase in resistance prevents the free passage of current as can be seen in Figure 18.
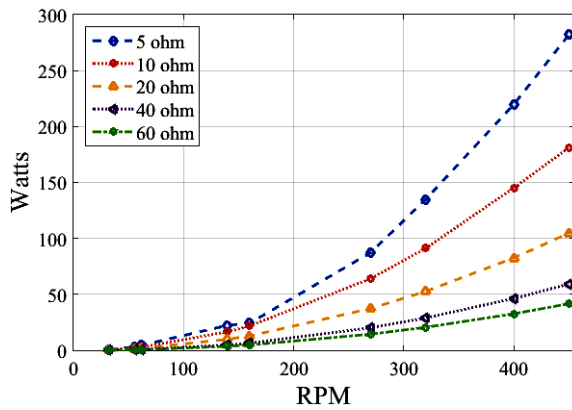
Figure 18. Powers at different resistance values.

This causes the power to be lower at high load de-spite the increase of angular speed in the generator.

In Figures 19 to 22 the theoretical and experimental characteristics of the series and parallel generators are compared. The value chosen for the resistance is 5Ω, which generates sufficient amperage or current, as well as the voltage at angular speeds common in the use of wind microgenerators. In addition, it is necessary to overcome the resistance caused by a charge controller, the wiring and the batteries to be charged.

Although the parallel coil generator has one more coil than the series generator, the difference in voltages can be clearly seen in Figure 19.
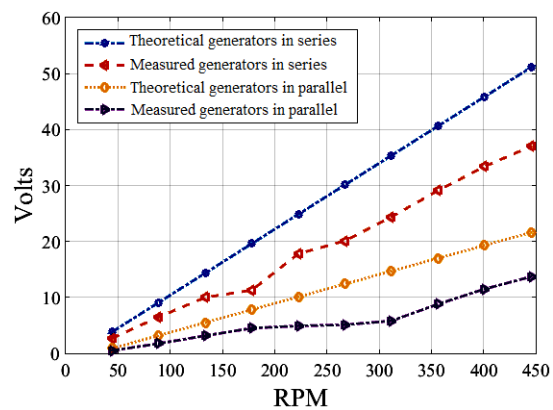
Figure 19. Comparisons of theoretical and measured voltages.

This is because, in the series generator, the three coils act as one because of their connection, with the difference that three pairs of magnets act at the same time. This causes the voltage to be much higher than in the case of the parallel coil generator, where only one coil acts at a time with a pair of magnets.

As can be seen in Figure 20 the series generator ex-ceeds the parallel generator in providing greater amperage. This allows the battery to be charged quickly for energy storage, or their number could be increased.
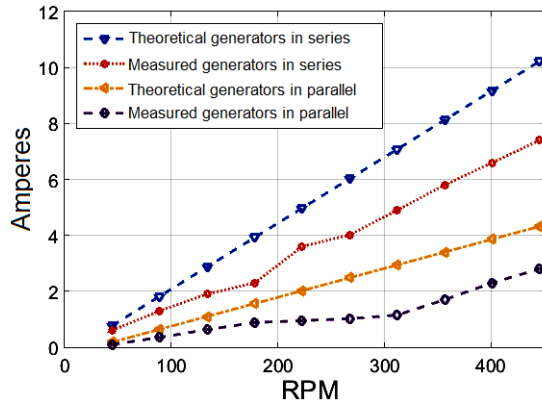
Figure 20. Comparisons of theoretical and measured amperage.

The powers determined in Figure 21 are no more than the reflection of the voltage and amperage values, therefore, they are directly proportional.

In the case of power, the measured values tend to behave quadratically.
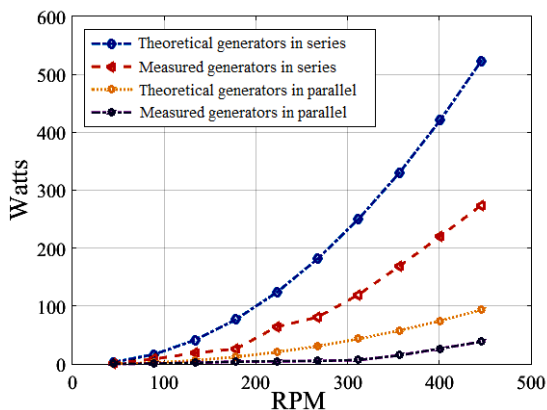
Figure 21. Comparisons of theoretical and measured powers.

The amperage and voltage obtained in both tests of the series coil generator are greater and imply that its power is also greater.

Regarding the efficiency of the generators, Figure 22 shows that although the parallel generator is exceeded in voltage and amperage by the series generator, it is more efficient.
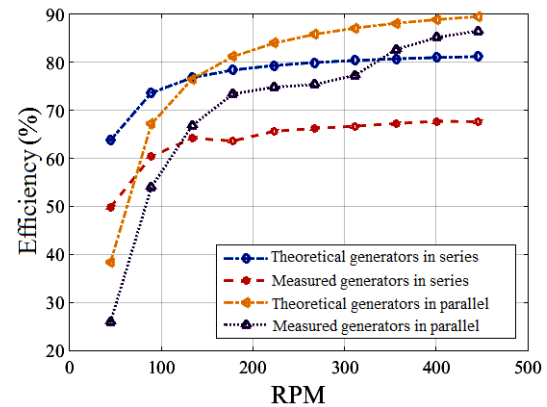
Figure 22. Comparisons of theoretical and measured efficiency.

This fact is reasonable since, in the series generator, the resistances per phase add up, causing more losses; the parallel generator only has one resistance per phase.

These qualities must be considered in their selection, taking energy requirements into account. If high voltages and amperages and a reasonable efficiency are needed, a series generator must be selected; but if what is sought is greater stability of voltage and am-perage at low revolutions with greater efficiency, the parallel generator is the appropriate choice.

4. Conclusions

The main parameters for the dimensioning of an axial flow generator are the selection of magnets, determination of the field density, number of poles, number of coils, number of turns per coil, wire gauge for the coils, and symmetric distribution of magnets and coils.

The dimensions of the discs for the rotors and the stator measurements are determined by the arrangement of the coils: the larger they are and the greater their number, the larger the discs and therefore the stator.

This study shows that the best configuration for the connection of coils is in series, as in enables the best use of the distribution of magnets, and has the quality of adding the f_{em} of each group of coils. However, the series generator has higher losses, which indicates that it will have more heating problems than the parallel generator.

Axial flow generators provide very good voltages and amperage at low revs. This highlights the benefits that these generators have for applications in wind energy despite the fact that there is a low or limited wind potential.

If you compare the theoretical results with the experimental ones, the axial flow generators are adequate for small-scale electricity generation. If a three-phase generator is tested in a place where the average wind

speed is between 4 to 8 m/s, with rotor speeds of 220 to 450 rpm, the amperage reached ranges from 3 to 7 amps. In addition, if during the day there are 4 to 8 hours with this wind speed, this results in 18 to 24 ampere-hours in the day, which represents a quarter of the total amperage of a common 100 Ah battery.

References

[1] I. Arraña, E. Marino, P. Bertinat, J. Salerno, J. Chemes, M. Barone, and J. Saenz, "Estado del arte en el desarrollo de pequeños generadores eólicos," *Avances en Energías Renovables y Medio Ambiente*, vol. 16, pp. 41–48, 2012. [Online]. Available: https://goo.gl/kQEezZ

[2] WWEA, "Reporte anual de la energía eólica en el mundo 2010," in *10a Conferencia Mundial sobre Energía Eólica y exhibición de Energías Renovables*, 2011. [Online]. Available: https://goo.gl/z7wYsP

[3] J. R. Bumby and R. Martin, "Axial-flux permanent-magnet air-cored generator for small-scale wind turbines," *IEE Proceedings - Electric Power Applications*, vol. 152, no. 5, pp. 1065–1075, Sept 2005. [Online]. Available: https://doi.org/10.1049/ip-epa:20050094

[4] W. Rogel and R. Alejandro, "Diseño de un generador de flujo axial con imanes permanentes para aplicaciones eólicas," *Revista Facultad de Ingeniería*, pp. 3–12, 2000. [Online]. Available: https://goo.gl/WwuQfq

[5] A. Carvajal and L. Muñoz, "Ecoductos energéticos: Explotación de la energía cinética del gas para generación de energía eléctrica." Tesis de Grado, Universidad Nacional Abierta y a Distancia, Colombia, 2012. [Online]. Available: https://goo.gl/bw6JpJ

[6] H. Piggott, "Manual para la autoconstrucción de generadores eólicos." Bajatec manuales, 2009, pp. 24–60.

[7] R. Muñoz, "Generalidades sobre imanes permanentes y su caracterización." Instituto Nacional de Tecnología Industrial, 2008. [Online]. Available: https://goo.gl/U4wrrX

[8] L. Herrera, A. Alarcón, and E. RivasTrujillo, "Diseño de un generador de flujo axial usando el método de elementos finitos," *Redes de Ingeniería*, vol. 4, no. 2, pp. 6–15, 2013. [Online]. Available: https://goo.gl/wD7ywj

[9] C. Brad, I. Vadan, and I. Berinde, "Design and analysis of an axial magnetic flux wind generator," in *2017 International Conference on Modern Power Systems (MPS)*, June 2017, pp. 1–7. [Online]. Available: https://doi.org/10.1109/MPS.2017.7974377

[10] Supermagnete. (2016) Bloques magnéticos. [Online]. Available: https://goo.gl/S3N7E5

[11] P. Wannakarn, T. Tanmaneeprasert, N. Rugthaicharoencheep, and S. Nedphograw, "Design and construction of axial flux permanent magnet generator for wind turbine generated dc voltage at rated power 1500 w," in *2011 4th International Conference on Electric Utility Deregulation and Restructuring and Power Technologies (DRPT)*, July 2011, pp. 763–766. [Online]. Available: https://doi.org/10.1109/DRPT.2011.5993994

[12] J. Murillo, "Diseño de un alternador de flujo axial con imanes permanentes," *Escuela Universitaria de Ingeniería Técnica Industrial*, 2012. [Online]. Available: https://goo.gl/pbqSEz
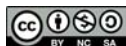
Energetic, exergetic and economic analysis of a cogeneration system: Case for a sugarcane plant of São Paulo

Análisis energético, exergético y económico de un sistema de cogeneración: Caso para una planta azucarera de San Pablo

Omar R. Llerena P.[1]

Abstract

Due to many advantages that cogeneration systems present, they have become a widely used technology for energy generation. In these processes, the efficiency is relatively high and the emissions of greenhouse gases are low. In this paper a technical and economic study of a cogeneration system for a sugar plant in São Paulo is carried out. For this propose the 1st and 2nd laws of thermodynamics are applied for the technical analysis. The cost of the electrical energy and steam produced are determined in the economic analysis. In the sizing of the plant, four gas turbines are analyzed that are in thermal parity with the process. The results show that the plant has a production capacity of 148MW of electricity and 147MW of steam. On the one hand the energy analysis reveals that the efficiency of the plant is 67%, while the exergetic analysis shows that this efficiency is 56%. The results of the economic analysis indicate that the prices of electricity and steam produced are 0.105 and 0.068 US $ / kWh, respectively.

Keywords: Cogeneration, economic analysis, energetic analysis, exergetic analysis.

Resumen

Los sistemas de cogeneración, debido a las numerosas ventajas que presentan, se han convertido en una tecnología bastante utilizada para la generación de energía. En estos procesos, la eficiencia es relativamente alta y las emisiones de gases de efecto invernadero son bajas. En este trabajo se realiza un estudio técnico y económico de un sistema de cogeneración para una planta azucarera en San Pablo. La primera y segunda ley de la termodinámica son aplicadas para el análisis técnico. Los costos de producción de la energía eléctrica y vapor producido son determinados en el análisis económico. En el dimensionamiento se analizan cuatro turbinas de gas que están en paridad térmica con el proceso. Los resultados muestran que la planta tiene una capacidad para producir 148 MW de electricidad y 147 MW de vapor. Por un lado el análisis energético revela que la eficiencia de la planta es de 67 %, mientras que el análisis exergético muestra que esta eficiencia es de 56 %. Los resultados del análisis económico expresan que los precios de la electricidad y vapor producido son de 0,105 y 0,068 US$/kWh, respectivamente.

Palabras clave: Cogeneración, análisis económico, análisis energético, análisis exergético.

[1]Grupo de Optimización de Sistemas Energéticos (GOSE), Universidad Estatal de San Pablo – Brasil.
Autor para correspondencia ✉: ollerenap@yahoo.com. ⓘ http://orcid.org/0000-0003-2115-4036

1. Introduction

Cogeneration is the process of combined energy production from a single source of fuel. For example, the production of thermal and electrical energy from natural gas [1]. This term is not new; industrial plants used the concept of cogeneration in the early 1880s when steam was the main source of energy. However, at present, this type of processes still play an important role in the production of energy, since their low in-vestment, operation and maintenance costs, as well as their greater efficiency and lower environmental im-pact, make them more attractive [2–4].

The combined cycle (CC) is one of the most common cogeneration systems. This cycle works in two stages: the first one works at high temperature (gas turbine) and the second stage of the cycle at a lower temperature (it uses the thermal energy of the exhaust gases of the gas turbine to produce steam) [5]. CCs have received much recognition in the last decades. Therefore, several plants have been installed and some existing units have been reactivated [6]. This fact means that technical and economic analyzes are used more frequently in order to optimize the performance of these plants.

On the other hand, the first and second law of thermodynamics are important tools to improve the efficiency of this type of process and reduce irreversibility. In the same way, an economic analysis is also considered to be a powerful tool for the study and optimization of energy systems. This analysis is applicable in investment decisions [7]. According to Silvei-ra and Tuna [8], the goal of an economic analysis is to evaluate the cost of energy produced by the cogenera-tion system (electricity and steam). In these contexts, several studies have been reported in specialized literature. Kordlar and Mahmoudi [9] present an exergo economic analysis and the optimization of a new co-generation system that produces energy and cooling. On the other hand, Gambini and Vellini [10], as well as Gvozdenac et al. [11] show an analysis of high ef-ficiency cogeneration systems.

Kanbur et al. [12] present a thermodynamic evaluation of a microcogeneration system. The results show that exergy and energy efficiencies are between two and three times higher than in the case of conventional energy generation. In his work, Sun [13] determined energy efficiency and analyzed the economic viability of an engine driven cogeneration system. In this case, the system provided electricity and cooling/heating for buildings. Here, the results show that the primary energy savings of the cogeneration system is greater than 37% compared to the conventional system.

For their part, Abusoglu and Kanoglu [14] applied the first and second laws of thermodynamics to cogeneration systems with diesel engines. In this study, the results show that the overall thermal efficiency of the plant is 44.2% and the exergy efficiency is 40.7%.

As shown in the specialized literature, there are several studies for the technical and economic evaluation of cogeneration systems to date. The present work differs from the articles studied in the literature; An energy, exergy and economic analysis is made to a particular cogeneration system, with the purpose of applying it to a sugar mill in São Paulo. The thermal demand of the process (main parameter for sizing), the type of gas turbine and the methodology used for the analyzes make this an original work.

This article is structured as follows: Section 2 presents the case study. The methodology adopted for the energetic, exergetic and economic analysis is described step by step in Section 3. The results and discussions are shown in Section 4 and, finally, the conclusions are presented in Section 5.

2. Description of the system

2.1. Description of the sugar plant

In the sugar industry, the main cogeneration system uses steam turbines in three basic configurations: back pressure turbines, combination of backpressure tur-bines with condensation turbines, and extraction-condensation turbines [15]. The present work analyzes a plant that implements two of the configurations men-tioned above (counterpressure and condensation-extraction turbines), an existing plant in São Paulo, Brazil (see Figure 1).
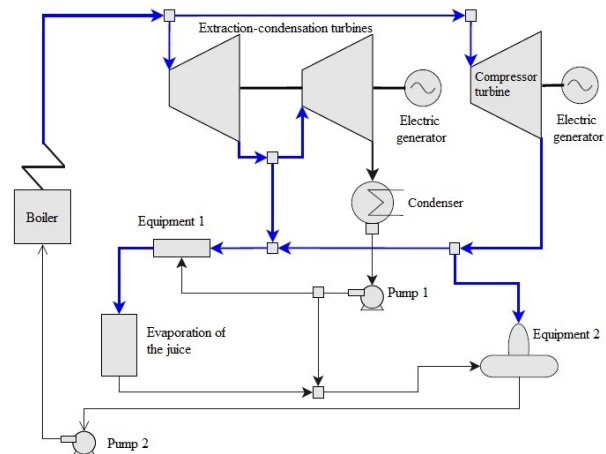
Figure 1. Existing sugar plant in São Paulo, Brazil.

The conventional boiler of this plant has a capacity to produce 160 t/h of steam at 68.6 bar, and 530 °C. 125 t/h of this steam is consumed by an extraction-condensation turbine coupled to a 32 MW generator. In this section, an extraction of 97 t/h of steam at a pressure of 2.45 bar is carried out for the cane juice evaporation process. The remaining steam (35 t/h) is

Llerena / Energetic, exergetic and economic analysis of a cogeneration system: Case for a sugarcane plant of São Paulo

31

directed to the backpressure turbine which is coupled to a 12 MW generator.

Additionally, the plant analyzed in this paper has the capacity to process 1 500 000 tons of sugarcane, corresponding to 240 harvest days. It mills 286 t/h of cane and generates 75.2 t/h of bagasse. The latter is used as fuel in conventional boilers to generate the necessary steam for the plant [15].

2.2. Description of the proposed system

The proposed cogeneration system has to satisfy the same thermal demands (160 t/h of steam) and generate at least 4 times more electrical energy. To accomplish this goal, the possibility of changing the conventional steam boiler (see Figure 1) for a gas turbine and a re-covery boiler is analyzed in this paper, as shown in Figure 2.
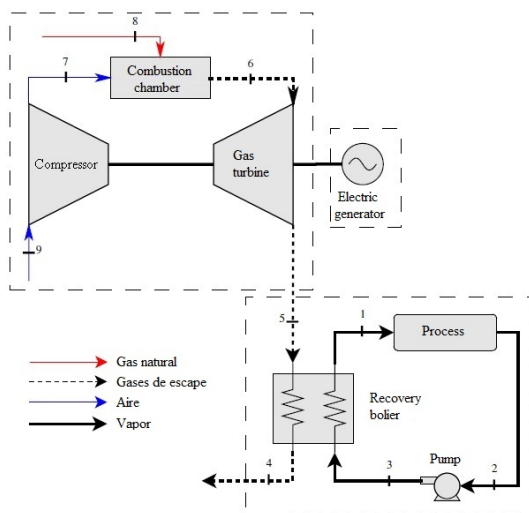
Figure 2. Scheme for the proposed cogeneration system.

As noted in Figure 2, the system is composed of a gas turbine, a combustion chamber (CC), a compressor, a recovery boiler (CR), a generator, a pump and the process. The latter includes almost all the equipment in the plant in Figure 1, the only element that remains outside is the conventional boiler.

We opted for a combined cycle system using natural gas in order to determine the feasibility of installing this process specifically in this sugar industry. If the installation of the CC is feasible, future studies will include the analysis of the gasification of the 75.2 t/h of cane bagasse generated by the plant to produce synthesis gas and substitute the use of natural gas.

3. Materials and methods

3.1. Selection of the gas turbine

The first stage in the design of this cogeneration process is the selection of the gas turbine. This turbine

is selected in parity to the thermal demand of the pro-cess. Thus, the selection is made based on the temperature and the flow of the exhaust gases. The latter is determined by Equation 1 [16]:

$$\dot{m}_5 = \frac{\dot{m}_1(h_1 - h_3)}{\eta_{CR} Cp_G (T_5 - T_4)} \tag{1}$$

Where:

$\dot{m}_5$ = exhaust gas flow (kg/s)
$\dot{m}_1$ = vapor flow in the CR (kg/s)
h_3 = enthalpy of steam in CR (kJ/kg)
h_1 = enthalpy of water (kJ/kg)
η_{CR} = performance of the CR (-)
Cp_G = specific heat at constant pressure of the exhaust gases (kJ/kg·K)
T_5 = exhaust gas temperature in the CR (°C)
T_4 = exhaust gas temperature at the CR CR outlet (°C)

3.1.1. Calculation thereof Cp_G

To apply Equation 1, it is necessary to calculate Cp_G, which is determined by Equation 2 [17]:

$$Cp_G = \frac{\sum Cp_i \cdot n_i}{\sum \dot{m}_i} \tag{2}$$

For the calculation of Cp_i we have Equation 3.

$$Cp_i = a + bT + cT^2 + dT^3 \tag{3}$$

Where:

Cp_G = specific heat at constant pressure of the exhaust gases (kJ/kg·K)
Cp_i = specific heat at constant pressure of component i of exhaust gases (kJ/kg·K)
$\dot{m}_i$ = exhaust gas flow (kg/s)
$\dot{n}_i$ = molar flow of component i of the exhaust gases (kmol/s)

Parameters a, b, c, and d are obtained in Çengel and Boles [17] and are the factors to calculate the spe-cific heat at constant pressure of an ideal gas.

3.1.2. Calculation of the mass of exhaust gases

For this calculation, the composition of the natural gas (Table 1) that will be used is first defined.

Table 1. Chemical composition of natural gas [18]

Composite	Formula	% Vol	% Molar
Methane	CH_4	95	1
Ethane	C_2H_6	3,2	0,0337
Propane	C_3H_8	0,2	0,0021
Butane	C_4H_{10}	0,03	0,0003
Nitrogen	N_2	1	0,0105
Carbon dioxide	CO_2	0,55	0,0058
Oxygen	O_2	0,02	0,0002

With the composition of natural gas, Equation 4 is established:

$$CH_4 + 0,0337C_2H_6 + 0,0021C_3H_5 + 0,0003\ldots$$
$$+0,0105N + 0,0058CO_2 + 0,0002O_2\ldots$$
$$+(1+x)a_{th}(O_2 + 3,76N_2) \rightarrow aCO_2 + bH_2O\ldots \quad (4)$$
$$+xa_{th}O_2 + dN_2$$
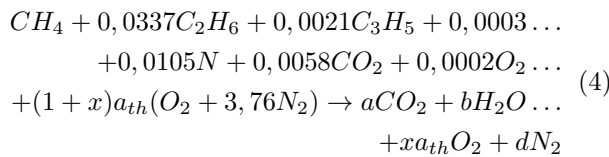
After the solution of Equation 4, the fuel mass and air mass are calculated.

Equation 5 is used for fuel mass:

$$\dot{m}_{comb} = m_{molar}CH_4 + 0,0337m_{molar}C_2H_6\ldots$$
$$+0,0021m_{molar}C_3H_5 + 0,0003m_{molar}C_4H_{10}\ldots$$
$$+0,0105m_{molar}N_2 + 0,0058m_{molar}CO_2\ldots \quad (5)$$
$$+0,0002m_{molar}O_2$$

Equation 6 is used for air mass:

$$\dot{m}_{ar} = (1+x)a_{th}(m_{molar}O_2 + 3,76m_{molar}N_2) \quad (6)$$

Equation 7 is used to calculate the combustible air ratio:

$$AC = \frac{\dot{m}_{ar}}{\dot{m}_{comb}} \quad (7)$$

Where:
 $\dot{m}_{ar}$ = air flow (kg/s)
 $\dot{m}_{comb}$ = fuel flow (kg/s)

Thus the compensated equation of the reaction is ob-tained and represented in 8:

$$CH_4 + 0,0337C_2H_6 + 0,0021C_3H_5 + 0,0003\ldots$$
$$C_4H_{10} + 0,0105N + 0,0058CO_2 + 0,0002O_2\ldots$$
$$+(1+x)a_{th}(O_2 + 3,76N_2) \rightarrow 1,0807CO_2\ldots \quad (8)$$
$$+2,1111H_2O + 4,3220O_2 + 24,2710N_2$$
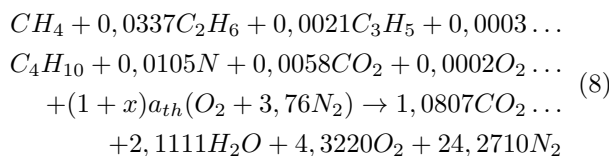
From Equation 8 we obtain the mass of the exhaust gases, which is calculated with Equation 9:

$$\dot{m}_{escape} = 1,0807m_{molar}CO_2 + 2,1111m_{molar}\ldots$$
$$H_2O + 4,3220m_{molar}O_2 + 24,2710m_{molar}N_2 \quad (9)$$

Now, equations 2 and 3 can be applied to obtain Cp_G. Figure 3 shows Cp_G obtained for a range of temperatures.
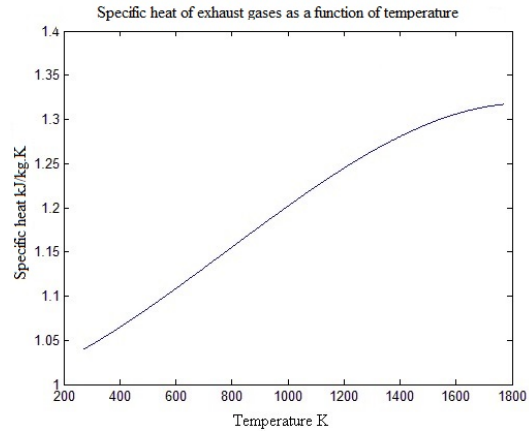
Figure 3. Specific heat of the exhaust gases as a function of temperature.

Finally, with the Cp_G Equation 1 can be applied. Table 2 shows the turbines selected and Figure 4 shows the location of each turbine according to the flow of exhaust gases.

Table 2. Selected turbines [19]

Code	Power (MW)	Efficiency	Exhaust gases (kg/s)	Gas temperature (°C)
V94.2	157	34,4	514,54	540
PG7241	171	36,5	455,9	599,44
SGT6	208	38,1	508,18	577,77
7EA	184	38,1	451,36	604,44
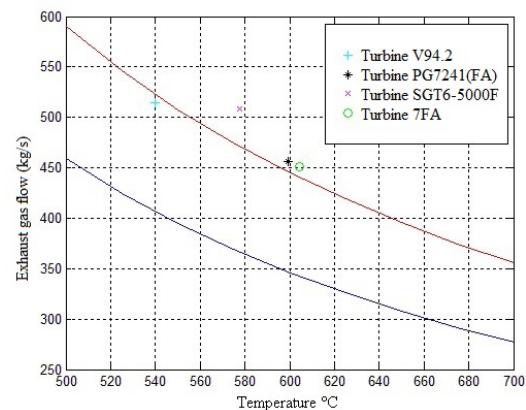
Figure 4. Turbines selected according to the temperature and flow of exhaust gases.

As can be seen in Figure 4, the V94.2 turbine is discarded because it does not meet the plant's thermal needs. The SGT6 turbine is discarded because it has an excess of exhaust gas flow. Turbines PG7241 and 7FA are the ones in thermal parity with the process. So, with the consideration that this system must generate at least 4 times more energy than the conventional sugar plant, the PG7241 turbine is finally selected.

The PG7241 turbine data is presented in Table 2 in the following conditions (Ambient Temperature =15 °C and altitude of 0 m). Therefore, turbine data must be corrected for the local conditions of the plant (Ambi-ent Temperature = 25 °C altitude of 530 m), this step is important to carry out since the environmental condi-tions directly influence the performance of the turbine.

3.1.3. Calculation of Pinch-Point

The temperature of the exhaust gases at the outlet of the recovery boiler must be corrected with the Pinch-Point method according to the criteria presented in Figure 5. This shows that in order to avoid a thermodynamic impropriety, one must have a minimum temperature difference for the cooling profile. According to Sue and Chuang, [20] this value can be between 10 °C and 30 °C.
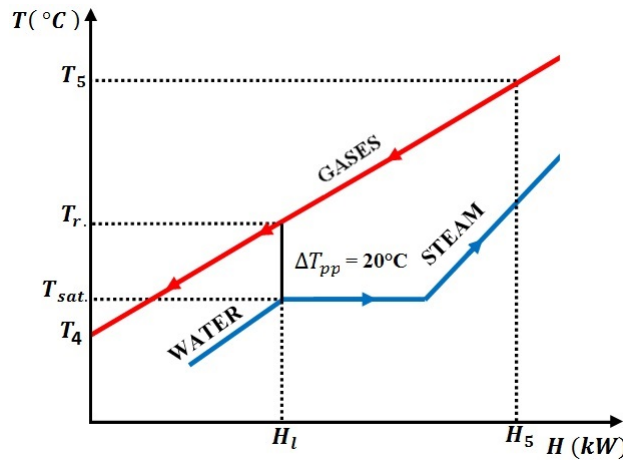
Figure 5. Pinch-Point.

The temperature at the dew point is determined with Equation 10:

$$T_r = T_{sat} + \Delta pp \tag{10}$$

For the temperature of the exhaust gases at the CR outlet, the following equations are used:

$$T_4 = T_5 - \left[\frac{T_5 - T_r}{H_5 - H_i} \cdot H_5 \right] \tag{11}$$

$$H_5 = \dot{m}_5 \cdot Cp_G(T_5) \cdot T_5 \tag{12}$$

$$H_l = \dot{m}_1 \cdot h_l \tag{13}$$

Where:
  h_l = enthalpy of the saturated liquid at the recovery boiler's operating pressure (kJ/kg)

3.2. Thermodynamic analysis

The technical analyses carried out in the cogeneration system are based on the 1st and 2nd law of thermodynamics, that is, energy and exergy analysis, respectively.

3.2.1. Energy analysis

Brayton cycle volume control

To calculate the flow of natural gas, we have Equation 14:

$$Heat\ rate \cdot P_{generador} = PCI_{gas\ natural} \cdot \dot{m}_8 \tag{14}$$

The LHV of natural gas is 48 300 (kJ/kg) [21].

The air flow at the compressor inlet is calculated with the following equations:

$$\dot{m}_9 = \dot{m}_5 - \dot{m}_8 \tag{15}$$

$$\dot{m}_9 = \dot{m}_7 \tag{16}$$

Compressor control volume

The pressure at the compressor outlet depends on the inlet pressure and the pressure ratio. This pressure is calculated with Equation 17:

$$Rp = \frac{P_7}{P_9} \tag{17}$$

The relative pressure at point 7 is calculated with Equation 18:

$$Pr_7 = Pr_9 \frac{P_7}{P_9} \tag{18}$$

The enthalpy of point 7 is calculated with Equation 19:

$$h_7 = \frac{h_{7s} - h_9}{\eta_{comp}} + h_9 \tag{19}$$

By the law of conservation of energy, we have:

$$\dot{m}_6 \cdot h_6 = \dot{m}_7 \cdot h_7 + PCI_{gas\ natural} \cdot \dot{m}_8 \tag{20}$$

Control volume of the gas turbine

The following equations are used to analyze the gas turbine:

$$Pr_5 = Pr_6 \left(\frac{P_5}{P_6} \right) \tag{21}$$

$$\eta_{isentrópica} = \frac{h_6 - h_5}{h_6 - h_{5s}} \qquad (22)$$

Energy efficiency

For the calculation of the efficiency of the gas turbine we have Equation 23:

$$\eta_{turbina} = \frac{P_{turbina}}{PCI_{gas\ natural} \cdot \dot{m}_8} \qquad (23)$$

Where:

$\dot{m}_8$ = natural gas flow (kg/s)

$PCI_{gas\ natural}$ = lower heating value of natural gas (kJ/kg)

$P_{turbina}$ = power in the turbine (kW)

$\eta_{turbina}$ = turbine efficiency (-)

To calculate the total efficiency of the cogeneration system, we have Equation 24:

$$\eta_{sistema} = \frac{P_{turbina} + [(h_1 - h_3) \cdot \dot{m}_1] - P_{bomba}}{PCI_{gas\ natural} \cdot \dot{m}_8} \qquad (24)$$

Where:

h_1 = enthalpy in point 1 (kJ/kg)

h_3 = enthalpy in point 3 (kJ/kg)

$\dot{m}_1$ = flujo de vapor (kg/s)

P_{bomba} = power consumed in the pump (kW)

$P_{turbina}$ = power in the turbine (kW)

$\eta_{sistema}$ = system efficiency (-)

3.2.2. Exergetic analysis

The exergy analysis consists of the qualitative evaluation of the losses through the concept of exergy via the application of the second law of thermodynamics. A basic procedure to perform this analysis is to deter-mine the input and output values of exergy for all the components of the system and the reason for its varia-tion in the entirety of the process [16].

Compressor control volume

In the compressor, point 9 is air at ambient temperature and pressure, and point 7 is compressed air (see Figure 2).

Equation 25 is applied to find the entropy difference between the compressor's input and output:

$$(s_7 - s_9) = (s_7^0 - s_9^0) - Rln\left(\frac{P_7}{P_9}\right) \qquad (25)$$

Where:

s = entropy in the different points of the process (kJ/kg K)

P = pressure in the different points of the process (kPa)

The exergy difference in the compressor is calculated with Equation 26:

$$\Delta\psi_{compressor} = (h_7 - h_9) - T_0(s_7 - s_9) \qquad (26)$$

Exergy at the compressor output is obtained by apply-ing Equation 27:

$$ex_7 = \Delta\psi_{compressor} \cdot \dot{m}_9 \qquad (27)$$

Donde:

ex_7 : exergy in point 7 (kW)

Irreversibility is calculated with Equation 28:

$$I_7 = \frac{(h_7 - h_9) \cdot \dot{m}_7}{\eta_{compressor}} - ex_7 \qquad (28)$$

The efficiency of the second law of thermodynamics in the compressor is calculated with Equation 29:

$$\eta_{IIcompressor} = \frac{\Delta\psi_{compressor}}{\frac{h_7 - h_9}{\eta_{compressor}}} \qquad (29)$$

Control volume of the CC

In the CC, point 7 is compressed air, point 8 is natural gas and point 6 are exhaust gases (see Figure 2).

In the same way as in the compressor, the entropy difference between the input and output of the CC, the exergy change, the exergy in point 6 and the efficiency of the second law of thermodynamics are calculated in the CC. The calculations are done with equations:

$$(s_6 - s_7) = (s_6^0 - s_7^0) - Rln\left(\frac{P_6}{P_7}\right) \qquad (30)$$

$$\Delta\psi_{cam.comb.} = (h_6 - h_7) - T_0(s_6 - s_7) \qquad (31)$$

$$\Delta ex = \Delta\psi_{cam.comb.}\dot{m}_9 \qquad (32)$$

$$ex_6 = \Delta ex + ex_7 \qquad (33)$$

$$\eta_{IIcam-comb.} = \frac{ex_6}{ex_7 + ex_8} \qquad (34)$$

Turbine control volume

In the turbine, point 6 is the inlet of the exhaust gases to the turbine and point 5 is the outlet (see Figure 2).

In the same way as in the compressor and the CC, the following equations are applied to the gas turbine.

$$(s_6 - s_5) = (s_6^0 - s_5^0) - Rln\left(\frac{P_6}{P_5}\right) \qquad (35)$$

$$\Delta\psi_{turbina} = (h_6 - h_5) - T_0(s_6 - s_5) \qquad (36)$$

$$\Delta ex = \Delta \psi_{turbina} \cdot \dot{m}_9 \tag{37}$$

$$ex_5 = ex_6 - \Delta ex \tag{38}$$

$$\eta_{IIturbina} = \frac{W_{total}}{\Delta_{ex}} \tag{39}$$

Control volume in the CR

In the CR, point 5 is the entry of exhaust gases and point 4 is the outlet of exhaust gases to the environment. On the other side of the CR, point 3 is water and point 1 is superheated steam (see Figure 2).

The exergy of the exhaust gases is calculated with Equation 40:

$$ex_4 = \left[c_p(T_4 - T_0) - T_0 \left(c_p ln \frac{T_4}{T_0} - R ln \frac{P_4}{P_0} \right) \right] \dot{m}_4 \tag{40}$$

The entropy at point 4 is determined with Equation 41:

$$s_4 - s_0 = c_p ln \frac{T_4}{T_0} - R ln \frac{P_4}{P_0} \tag{41}$$

The exergy change between points 4 and 5 is calculat-ed with equations:

$$\Delta ex_{4-5} = \lfloor c_p(T_4 - T_5) - T_0(s_4 - s_5) \rfloor \cdot \dot{m}_5 \tag{42}$$

$$s_4 - s_5 = c_p ln \frac{T_4}{T_5} - R ln \frac{P_4}{P_5} \tag{43}$$

The exergy change between points 1 and 3 is calculat-ed with equations:

$$\Delta \psi_{1-3} = (h_1 - h_3) - T_0(s_1 - s_3) \tag{44}$$

$$\Delta ex_{1-3} = \Delta \psi_{1-3} \cdot \dot{m}_1 \tag{45}$$

The efficiency of the second law in the CR is calculat-ed with Equation 46:

$$\eta_{IICR} = \frac{\Delta ex_{1-3}}{-\Delta ex_{4-5}} \tag{46}$$

Pump control volume

In the pump, points 2 and 3 are water. In this case point 3 shows a pressure greater than point 2 (see Figure 2).

For the exergy in point 3 we have Equation 47:

$$ex_3 = \dot{m}_3 \cdot [(h_3 - h_2) - T_0 \cdot (s_3 - s_2)] \tag{47}$$

For the irreversibility in point 3 we have Equation 48:

$$I_3 = ((h_3 - h_2) \cdot \dot{m}_3) - ex_3 \tag{48}$$

To calculate the efficiency of the second law in the pump, we have Equation 49:

$$\eta_{IIbomba} = \frac{ex_3}{P_{bomba}} \tag{49}$$

Exergy system efficiency

The total efficiency of the second law of thermodynamics is calculated with Equation 50:

$$\eta_{IIbomba} = \frac{P_{turbine} + \Delta ex_{1-3} - P_{pump}}{PCI_{natural\ gas} \cdot \dot{m}_8} \tag{50}$$

3.3. Economic analysis

The economic analysis determines the cost of electricity and steam produced by the cogeneration system. For this analysis, we considered the value of the equipment, maintenance value, the plant's operational costs, tax rates, time of return of the investment, and the cost of the natural gas.

3.3.1. Cost of equipment

According to Castro [16] and Silveira [22] the following equations are applicable to calculate the value of the equipment:

Investment in the gas turbine:

$$I_{TG} = \left(\frac{US\$}{kW} \cdot E_{PTG} \right) \tag{51}$$

Where:
$\frac{US\$}{kW} = 234\ \frac{US\$}{kW}$ [19]
E_{PTG} = power produced by the turbine (kW)

Investment in the recovery boiler:

$$I_{CR} = 4745 \cdot \left(\frac{h_1}{log(T_5 - T_1)} \right) + 11820 \cdot \dot{m}_1 + 658 \cdot \dot{m}_5 \tag{52}$$

Cost of electric power and steam

To calculate the cost of electricity and steam produced, equations 53 and 54 are used respectively:

$$C_{elec} = \frac{I_{TG} \cdot f}{H \cdot E_{PTG}} + \frac{C_{comb}\left(E_{comb} - E_c - \frac{P_{er}}{2}\right)}{E_p} \cdots \\ + Cm + Co \tag{53}$$

$$C_v = \frac{I_{CR} \cdot f}{H \cdot Q_p} + \frac{C_{comb}\left(E_{comb} - E_c - \frac{P_{er}}{2}\right)}{E_v} \cdots \\ + Cm_{CR} + Co \tag{54}$$

Donde:

C_{comb} = fuel cost $\frac{US\$}{kWh}$

C_{elec} = electricity cost $\frac{US\$}{kWh}$

Cm = maintenance cost of GT $\frac{US\$}{kWh}$

Cm_{CR} = maintenance cost of CR $\frac{US\$}{kWh}$

C_v = Steam production cost $\frac{US\$}{kWh}$

Co = cost of operation staff $\frac{US\$}{kWh}$

E_{comb} = fuel power (kW)

E_p = electricity produced (kWh) $\frac{US\$}{kWh}$

E_v = steam produced (kWh) $\frac{US\$}{kWh}$

For the annuity factor we have Equation 55 and for the value of capital Equation 56:

$$f = \frac{q^k \times (q-1)}{q^k - 1} \tag{55}$$

$$q = 1 + \frac{r}{100} \tag{56}$$

Where:

k = amortization period (years)

r = tipo de interés anual annual interest rate (%)

4. Results and discussion

4.1. Results of thermodynamic analysis

The results of the thermodynamic analysis are shown in Tables 3 and 4. Table 3 shows the energetic and exergetic efficiencies.

Table 3. Energy and exergy efficiencies

Equipment	Energy Efficiency	Exergy Efficiency
Compressor	-	86%
Combustion chamber	-	76%
Gas turbine	39%	79%
Recovery boiler	-	59%
Pump	-	47%
Total efficiency	67%	56%

From Table 3 we can see how the total efficiency of the system (energy) is almost two times higher than the efficiency of the turbine. This is due to the fact that exhaust gases from the gas turbine are used to generate steam (cogeneration).

The works of Castro [16] and Paula Santos et al. [23] show similar technical studies in CC systems where efficiencies greater than 50% were obtained, which corroborates the results of this work.

On the other hand, Table 4 presents the thermodynamic parameters for each point of the co-generation system.

Table 4. Summary of the energy and exergy analysis

#	m kg/s	P kPa	T °C	h kJ/kg	s kJ/kg·K	ex kW
1	50	6860	530	3484	6,9	67871,5
2	50	245	126,8	532,5	2,27	0
3	50	7860	128,1	543,4	1,6	254,44
4	419	94,3	227,9	503	2,31	25020
5	419	94,3	634,6	941,6	2,92	112071
6	419	1462	1208	1612	2,73	417112
7	408	1462	407,5	692,5	1,75	153508
8	8,1	94,3	25	-	-	393611
9	408	94,3	25	298,6	1,69	0

For a better representation of the results in terms of energy, a Sankey diagram is presented in Figure 6. This diagram represents the energy flows from the system input to the system output, as well as the losses of each component.
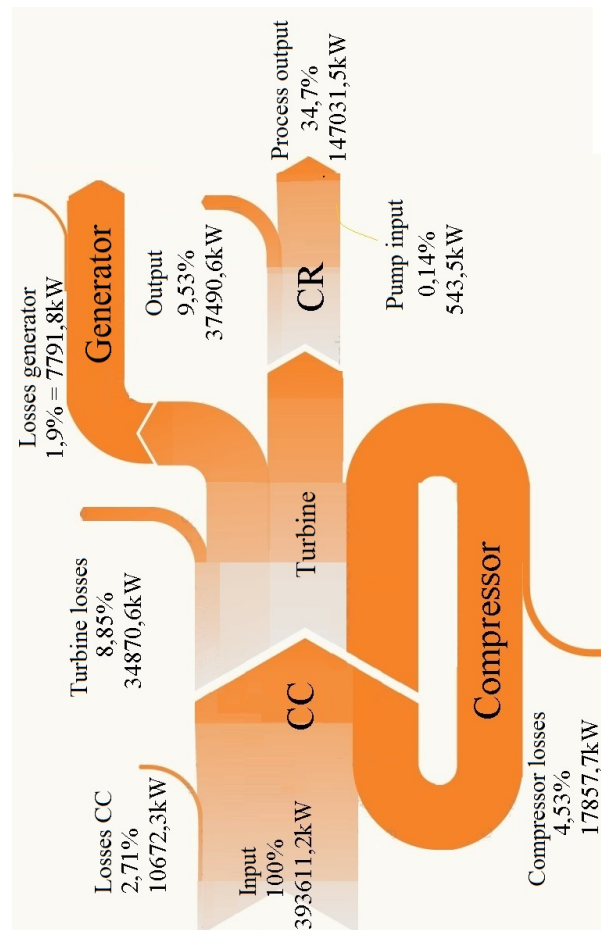
Figure 6. Sankey diagram

In the same way, for the exergy analysis the Grassman diagram is presented in Figure 7.

Llerena / Energetic, exergetic and economic analysis of a cogeneration system: Case for a sugarcane plant of São Paulo

37
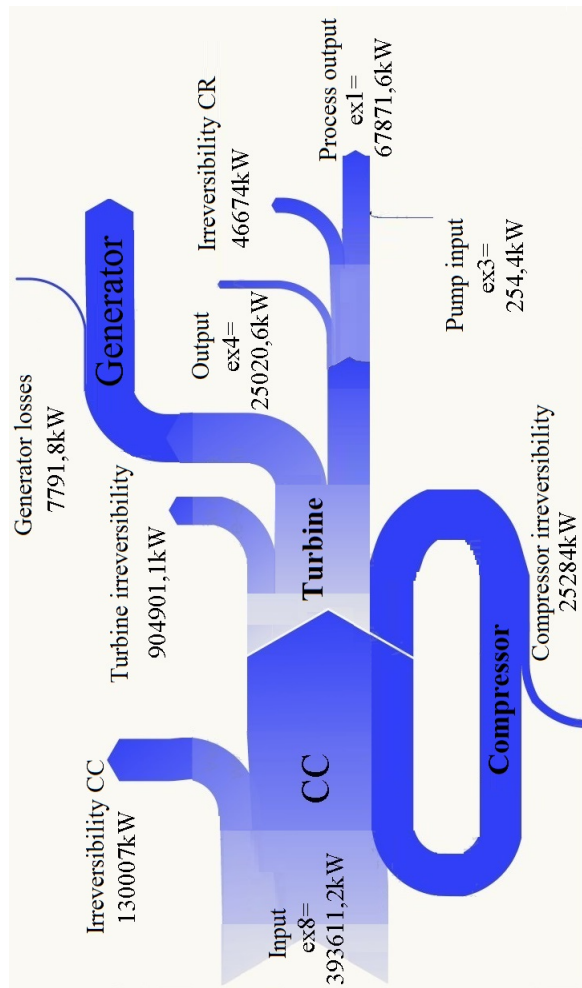
Figure 7. Grassman diagram

Figure 8. Cost of the electric power produced
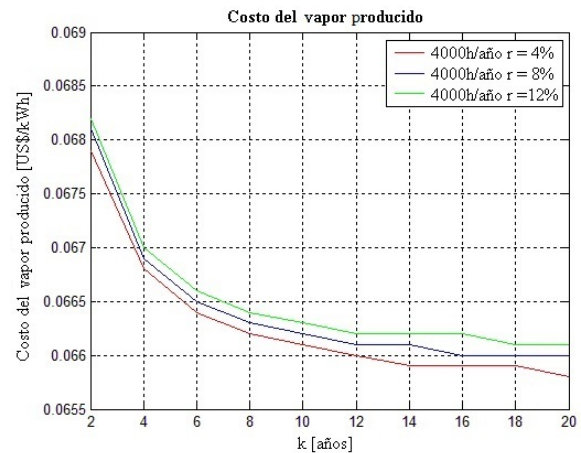
Figure 9. Cost of steam produced

The results of this analysis are the costs of electricity and steam produced by the plant considering a tax rate of 4, 8 and 12% and a repayment period of up to 20 years. It also takes into account that the plant works only 4000 hours, as the intent is to conduct the analy-sis in the most drastic conditions.

On the one hand, Figure 8 presents the cost of the electricity produced.

As can be seen in Figure 8, the highest value (price) of the electricity produced is 0.108 US$/kWh (r = 12%) while the lowest value is 0.103 US$/kWh (r = 4%), which applies when the plant is newly installed.

After 20 years this value is reduced by approximately 30%.

Finally, Figure 9 presents the cost of the steam produced by the process.

In the same way, as observed in Figure 9, the highest price of steam produced is 0.068 2US$/kWh (r = 12%) and the cheapest is 0.0678 US$/kWh (r = 4%) when the plant is newly installed. These values are reduced by approximately 5% after 20 years.

4.2. Discussion of economic analysis

According to the National Electric Energy Agency in Brazil, the sale price of electric energy in 2015 was 191,11 R$/MWh. Considering the exchange rate of dollars to reais in the first quarter of that same year (1 US$ = 2 R$), the price of energy is 0.095 US$/kWh. Thus, the implementation of this system can be considered acceptable since, in addition to producing electricity, steam is being produced. Additionally, this price can be considerably improved if the plant works 7200 h/year and if the bagasse is gasified to produce synthesis gas and replace the use of natural gas. These last two hypotheses are being studied and results will be presented in future publications.

5. Conclusions

In this work, a technical study was carried out based on the first and second law of thermodynamics and the

economic study of a cogeneration system. On the one hand, the energy analysis shows that the plant has an output capacity of 148.045 MW and a thermal capacity of 147.031 MW. In addition, this analysis shows that the total efficiency of the system is approx-imately twice as high (67%) as the efficiency of the turbine. This is due to the fact that the turbid exhaust gases are used to generate steam.

On the other hand, the exergy analysis shows that the capacity of electric energy is the same, while the thermal capacity decreases to 67 MW due to irreversibilities. In this case, the total efficiency of the system is 56%. The economic analysis shows that the prices of electricity and steam produced are 0.105 and 0.068 (US$/kWh) when the plant is initially installed; this cost is reduced by 30% in the case of electric energy and 5% in the case of steam after 20 years.

Finally, the dimensioning section leads to conclude that the flow of exhaust gases of the selected turbine at thermal parity revealed to be sufficient to supply the electrical and thermal needs of the cogeneration sys-tem without the need for additional fuel burning.

Continuing with this study, we intend to carry out the thermodynamic analysis of the gasification process of cane bagasse to produce synthesis gas with the objective of replacing the use of natural gas and reducing the cost of energy production.

References

[1] D. Tomofuji, Y. Morimoto, E. Sugiura, T. Ishii, and A. Akisawa, "The prospects of the expanded diffusion of cogeneration to 2030 - Study on new value in cogeneration," *Applied Thermal Engineering*, vol. 114, Supplement C, pp. 1403–1413, 2017. [Online]. Available: https://doi.org/10.1016/j.applthermaleng.2016.09.071

[2] N. M. Isa, C. W. Tan, and A. Yatim, "A comprehensive review of cogeneration system in a microgrid: A perspective from architecture and operating system," *Renewable and Sustainable Energy Reviews*, vol. 81, Part 2, pp. 2236–2263, 2018. [Online]. Available: https://doi.org/10.1016/j.rser.2017.06.034

[3] R. Carapellucci and A. Milazzo, "Repowering combined cycle power plants by a modified STIG configuration," *Energy Conversion and Management*, vol. 48, no. 5, pp. 15 901–1600, 2007. [Online]. Available: https://doi.org/10.1016/j.enconman.2006.11.024

[4] A. Rovira, C. Sánchez, M. Muñoz, M. Valdés, and M. Durán, "Thermoeconomic optimisation of heat recovery steam generators of combined cycle gas turbine power plants considering off-design operation," *Energy Conversion and Management*, vol. 52, no. 4, pp. 1840–1849, 2011. [Online]. Available: https://doi.org/10.1016/j.enconman.2010.11.016

[5] D. Mahto and S. Pal, "Thermodynamics and thermo-economic analysis of simple combined cycle with inlet fogging," *Applied Thermal Engineering*, vol. 51, no. 1, pp. 413–424, 2013. [Online]. Available: https://doi.org/10.1016/j.applthermaleng.2012.09.003

[6] G. Heyen and B. Kalitventzeff, "A comparison of advanced thermal cycles suitable for upgrading existing power plant," *Applied Thermal Engineering*, vol. 19, no. 3, pp. 227–237, 1999. [Online]. Available: https://doi.org/10.1016/S1359-4311(98)00044-1

[7] J. Silveira and C. Tuna, "Thermoeconomic analysis method for optimization of combined heat and power systems. Part I," *Progress in Energy and Combustion Science*, vol. 29, no. 6, pp. 479–485, 2003. [Online]. Available: https://doi.org/10.1016/S0360-1285(03)00041-8

[8] ——, "Thermoeconomic analysis method for optimization of combined heat and power systems–Part II," *Progress in Energy and Combustion Science*, vol. 30, no. 6, pp. 673–678, 2004. [Online]. Available: https://doi.org/10.1016/j.pecs.2003.06.001

[9] M. A. Kordlar and S. Mahmoudi, "Exergeoconomic analysis and optimization of a novel cogeneration system producing power and refrigeration," *Energy Conversion and Management*, vol. 134, Supplement C, pp. 208–220, 2017. [Online]. Available: https://doi.org/10.1016/j.enconman.2016.12.007

[10] M. Gambini and M. Vellini, "High efficiency cogeneration: Electricity from cogeneration in CHP plants," *Energy Procedia*, vol. 81, Supplement C, pp. 430–439, 2015, 69th Conference of the Italian Thermal Engineering Association, ATI 2014. [Online]. Available: https://doi.org/10.1016/j.egypro.2015.12.117

[11] D. Gvozdenac, B. G. Urošević, C. Menke, D. Urošević, and A. Bangviwat, "High efficiency cogeneration: CHP and non-CHP energy," *Energy*, vol. 135, Supplement C, pp. 269–278, 2017. [Online]. Available: https://doi.org/10.1016/j.energy.2017.06.143

[12] B. B. Kanbur, L. Xiang, S. Dubey, F. H. Choo, and F. Duan, "Thermoeconomic assessment of a micro cogeneration system with

Llerena / Energetic, exergetic and economic analysis of a cogeneration system: Case for a sugarcane plant of São Paulo

39

LNG cold utilization," *Energy*, vol. 129, Supplement C, pp. 171–184, 2017. [Online]. Available: https://doi.org/10.1016/j.energy.2017.04.071

[13] Z.-G. Sun, "Energy efficiency and economic feasibility analysis of cogeneration system driven by gas engine," *Energy and Buildings*, vol. 40, no. 2, pp. 126–130, 2008. [Online]. Available: https://doi.org/10.1016/j.enbuild.2007.01.013

[14] A. Abusoglu and M. Kanoglu, "Exergetic and thermoeconomic analyses of diesel engine powered cogeneration: Part 1 – Formulations," *Applied Thermal Engineering*, vol. 29, no. 2, pp. 234–241, 2009. [Online]. Available: https://doi.org/10.1016/j.applthermaleng.2008.02.025

[15] R. Passolongo, "Avaliação termodinâmica, termoeconômica e econômica da integração de sistemas de gaseificação da biomassa em uma usina sucroalcooleira," Master's thesis, Universidade Estadual Paulista, Faculdade de Engenharia de Ilha Solteira, 2011. [Online]. Available: https://goo.gl/uj3k4s

[16] I. A. de Castro Villela, "Combined fault detection and classification of internal combustion engine using neural network," Ph.D. dissertation, Universidade Estadual Paulista, Facultade de Engenharia de Guaratinguetá, 2007. [Online]. Available: https://goo.gl/w4hmYA

[17] Y. Çengel and M. Boles, *Termodinámica (8a. ed.):.* McGraw Hill, 2015. [Online]. Available: https://goo.gl/YoY7HE

[18] Uniongas. (2017) Chemical composition of natural gas. [Online]. Available: https://goo.gl/1ME1zf

[19] GTW. (2012) Gasturbine world handbook. Pequet. [Online]. Available: https://goo.gl/SNsJv1

[20] D.-C. Sue and C.-C. Chuang, "Engineering design and exergy analyses for combustion gas turbine based power generation system," *Energy*, vol. 29, no. 8, pp. 1183–1205, 2004. [Online]. Available: https://doi.org/10.1016/j.energy.2004.02.027

[21] Unitrove. (2017) Natural gas calorific value calculator. [Online]. Available: https://goo.gl/rU6Uir

[22] J. L. Silveira, "Cogeração disseminada para pequenos usuarios : estudo de casos para o setor terciario," Ph.D. dissertation, Universidade Estadual de Campinas, Facultade de Engenharia Mecânica, 1994. [Online]. Available: https://goo.gl/oBjSeK

[23] C. F. de Paula Santos, R. F. Silva Paulino, C. E. Tuna, and J. L. Silveira, "Thermodynamics analysis and ecological efficiency of a combined cycle power plant," *Engenharia Térmica*, vol. 13, no. 2, pp. 3–8, 2014. [Online]. Available: https://goo.gl/9Ei1Se

ANALYSIS OF ENERGY SAVING MEASURES IN A PRODUCTION COMPANY

ANÁLISIS DE MEDIDAS DE AHORRO DE ENERGÍA EN UNA EMPRESA DE PRODUCCIÓN

Luisa Salazar[1,*], Víctor Guzmán[2], Alexander Bueno[1]

Abstract

This work analyzes possible measures of energy saving in a production company, with the purpose of establishing recommendations that contribute to the efficient use of energy. This research is descriptive-documentary, based on fieldwork, where the different production processes and industrial services were analyzed. Using data supplied from working hours, an estimate of monthly consumption was made to determine the impact of processes on electricity billing. The analysis was restricted to the calculation of consumption index (Ton/kWh), which allows the use of the most efficient equipment to be prioritized over others performing the same functions. The analysis of the consumption characteristic yields optimum consumption points which allow establishing a graph of Energy vs Production called Goal. The result is that by applying all the proposed actions, the monthly consumption would decrease by 138,024.84 kWh, representing an energy saving of around 25% with respect to the current average consumption.

Keywords: Energy Saving, Characterization, Goal, Production

Resumen

Este trabajo analiza las medidas de ahorro de energía posibles en una empresa de producción, con la finalidad de establecer recomendaciones que contribuyan al uso eficiente de la energía. Esta investigación es de tipo descriptivo-documental, sustentada en un trabajo de campo, en donde se analizan los diferentes procesos de producción y servicios industriales. Utilizando datos suministrados de horas de trabajo, se realiza una estimación del consumo mensual para determinar el impacto de los procesos en la facturación de electricidad; el análisis se restringe al cálculo de índices de consumo (t/kWh) con lo que se puede priorizar el uso de los equipos más eficientes sobre otros que realicen las mismas funciones. El análisis de la característica de consumo arroja puntos óptimos de consumo con los cuales se establece un gráfico de energía *vs.* producción llamado meta. Se obtiene como resultado que aplicando todas las acciones propuestas, el consumo mensual disminuiría en 138 024,84 kWh, lo que representa un ahorro de energía del orden del 25 % respecto con el consumo promedio actual.

Palabras clave: ahorro de energía, caracterización, meta, producción.

[1,*]Department of Energy Conversion and Transportation, Universidad Simón Bolívar – Venezuela. Author for Author for correspondence ✉: luisalazar@usb.ve. ⬤ http://orcid.org/0000-0002-0824-8516
[2]Department of Electronics and Circuits, Universidad Simón Bolívar – Venezuela
⬤ http://orcid.org/0000-0002-7029-5727, ⬤ http://orcid.org/0000-0001-9167-522X

1. Introduction

The evolution of man on Earth has been, to a great extent, made possible by the development of technologies that make day-to-day life much easier. Human beings went from using their muscular strength and that of domesticated animals, to the use of diverse energy sources such as wind, water, fire, steam, among others, reaching the current energy scheme, where the burning of fossil fuels plays a preponderant role. It should be noted that this energy source is finite and highly contaminating.

Many electricity generating plants use it as a driving force to supply the electric demand. This implies a high emission of gases into the Earth's atmosphere that affect the ecosystem. In addition to pollution, it must be borne in mind that oil shortages in the future will represent a major global energy problem, which is why decreasing electricity consumption implies savings of this important source of energy.

For humanity, the beginning of the third millennium represents a crossroads of a new energy choice, in face of the depletion of fossil fuels on the one hand, but above all, due to the threat of an ecological catastrophe, where the limits of the planet's capacity to as-similate their impact is exceeded [1].

In general, Venezuelan society has not been characterized by having a culture of energy saving, since in the past the country's great energy wealth has supported an offer well above the national demand in terms of electricity services. However, in recent years, the appearance of long periods of drought has directly affected the main source of electricity generation in the country, which is hydraulic (Figure 1).
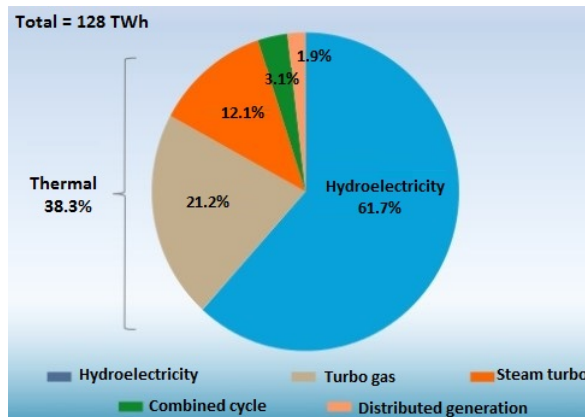
Figure 1. Energy balance in Venezuela by type of plant, estimates for 2015 [2].

In addition, the exponential growth of the population and of the various industrial and commercial sectors brings, therefore, an increase in the demand for electricity (Figure 2). Both factors have taken a turn, not only regarding the energy situation, but also the resulting environmental impact and the reduction of oil reserves.

Nowadays, there is no capacity to generate enough electrical power to supply the entire population if the traditional consumption level is maintained. This is why the need arises to implement awareness plans regarding the efficient use of energy, with the purpose of reducing unnecessary consumption.
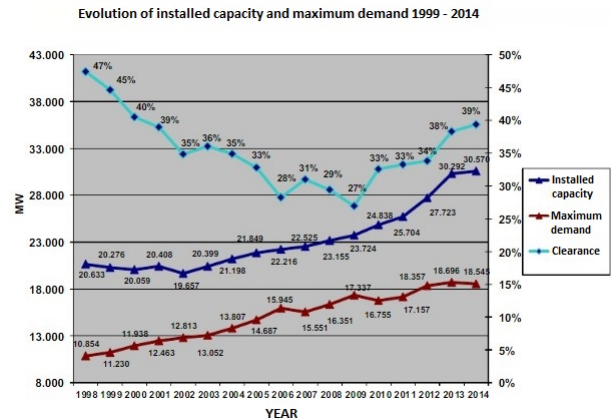
Figure 2. Average power demand of the National Electricity System (Sistema Eléctrico Nacional, SEN) 1999-2014 period [2].

The company that is the subject of this study, Mon-tana Gráfica, a subsidiary of the Corimon Pintura Group, C.A., is dedicated to the manufacture of flexible labels and packaging for various high consumption products such as food, beverages, candies, among others. It is located in Mariara, Carabobo state, Vene-zuela, and has about 30 000 m^2 of construction.

It is powered by a three-phase 13.8 kV line supplied by the national electricity service company Corporación Eléctrica (Corpoelec), which is connected to three internal substations, equipped with a total of seven three-phase transformers with a rated power of 6590 kVA. These reduce the voltage to 460 V, 440 V or 220 V, depending on the unit, according to the one-line diagram shown in Figure 3.

The plant has an average monthly consumption of about 637 000 kWh, and its contracted demand is 1860 kVA. It is classified as a high consumer, as it invoices above 30 000 kWh/month [3]. It is a factory with considerable energy consumption in active systems, such as high consumption lighting and equipment that is relatively inefficient compared to new technologies. The decisions and strategies that man-agement has taken regarding the optimization of consumption have not been as effective as expected. Therefore, this study has been commissioned to achieve a significant effect in terms of efficient use of energy.
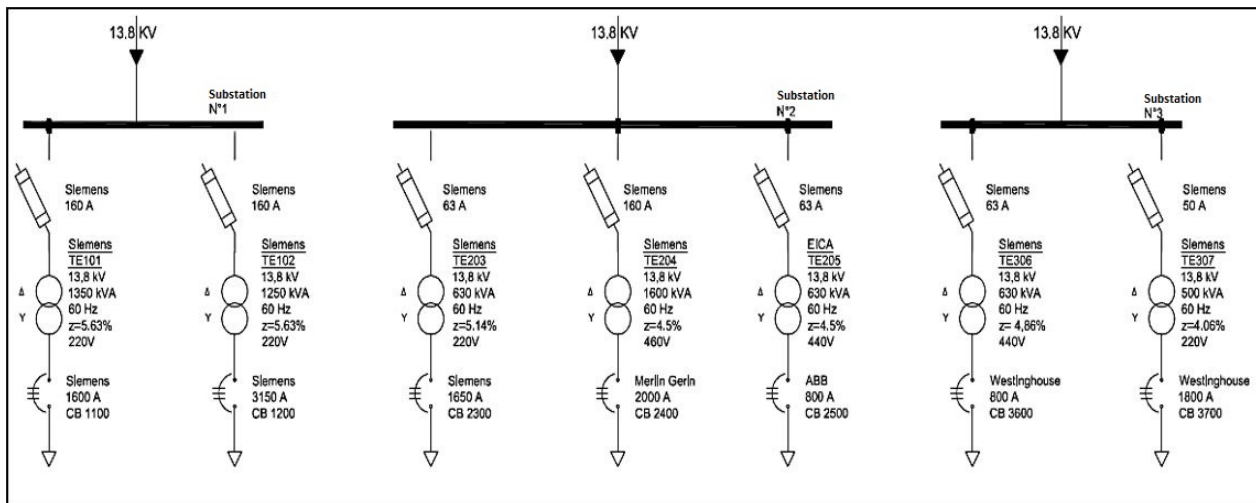
Figure 3. General single line diagram [3].

2. Development and method

The consumption and the availability of energy are preponderant factors in production costs. For this reason, the need to carefully manage energy to increase competitiveness is evident in the manufacturing and services sector [4].

Energy efficiency can be defined as the capacity of a use, equipment, installation or process to perform its function with the lowest possible energy consumption. Likewise, energy savings can be understood as the reduction of primary energy consumption of an a center through the implementation of technical or non-technical measures [4]. The implementation of these concepts in a company's energy management increases its productivity and competitiveness.

This has made it necessary for companies to create their own energy "management models" in order to motivate and encourage the development of a new organizational culture for the efficient use of energy.

By design, this is a documentary, descriptive and field research defined by activities framed in the collection of information that enable the energy characterization of the company Montana Gráfica, a subsidi-ary of the Corimon Pintura Group C.A., through the application of management tools that are part of the procedures presented in the International Standard ISO 50001. This energy review determines the performance of the organization based on data and other information, aimed at identifying opportunities for improvement contemplated in one of the ISO 50001 core requirements, energy planning, which involves a re-view of the company's activities that may affect ener-gy performance [5] for the implementation of an energy management system.

To carry out the energy characterization of the company, the following activities were carried out To

carry out the energy characterization of the company, the following activities were carried out [5]:

1. Define the productive energy diagram: flow chart of the main production processes.

2. Carry out the load census: consumption by ar-eas and representative teams.

3. Calculate the Pareto diagram and stratification: 20% of equipment and areas that consume approximately 80% of electric power.

4. Propose control diagrams: simultaneous variation of energy consumption with production carried out over time, for areas and equipment. These include the elaboration of a control graph, energy production vs. time graph, energy vs. produc-tion graph, goal vs. production graph, and consumption index vs. production graph.

The development of these activities is presented below.

2.1. Productive energy diagram

It is very important to know the areas of the plant and the different processes that take place in it, as well as the equipment and raw materials involved. This provides a clear idea of how the company creates its final product, identifies which processes have the greatest impact on monthly electricity billing, determines percentages of automatization in the plant by analyzing different processes, among other characteristics. Identifying the processes will also allow the work to be broken down, so that it is easier to collect and analyze the results.

2.1.1. Identification of areas

The different processes carried out in the company are:

Cylinder preparations

In this process, images are recorded in several copper cylinders, which will then be inserted in the rotogravure machines for the printing of the image that the client wishes for their product.

Ink preparation

In this process, mixtures of base inks are created to achieve the desired color. Sometimes the inks are mixed with gold or varnish so they adhere more easily to some types of printing materials.

Rotogravure

In this process, the rotogravure machines print the image that the client requires at high speed, on their product and in the material they request.

Laminating

In this process, two layers of different materials adhere according to what the client requires for their product. They can be made with different adhesive materials such as hot wax, adhesives with solvents or without solvents. The materials that normally come together are paper and plastics of different natures.

Metallizing

This process is unique and scarcely done by the company, but, when carried out, it causes a very significant energy consumption, which is why it was preferable to separate it from the laminating process although its objective is basically the same: to join a layer of some kind of metal to a layer of some kind of plastic material.

Cutting and finishing

In this process the printing rolls delivered by the rotogravure process, after passing through the laminating or metallizing area when required, are cut according to the client's requirements (rolls or sheets).

2.1.2. Process flowcharts

Flowcharts of the different processes in the plant were drawn to illustrate the knowledge regarding procedures followed for the elaboration of the company's final product.

Figures 4 to 9 present the respective flow diagrams for each process
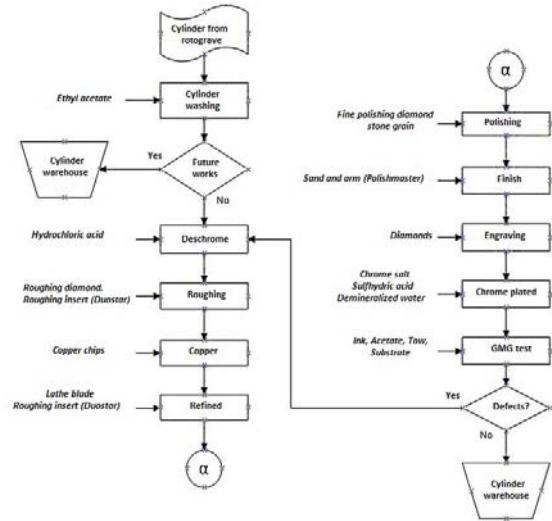
Figure 4. Flowchart for the cylinders area process.
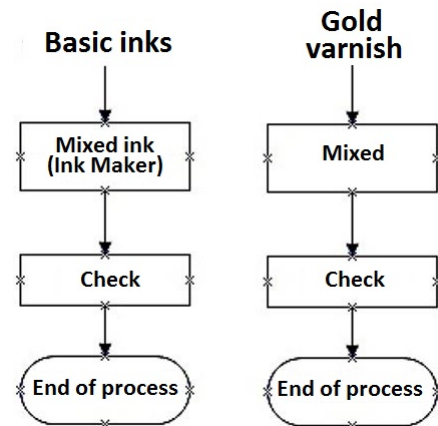
Figure 5. Flowchart for the Ink area process.
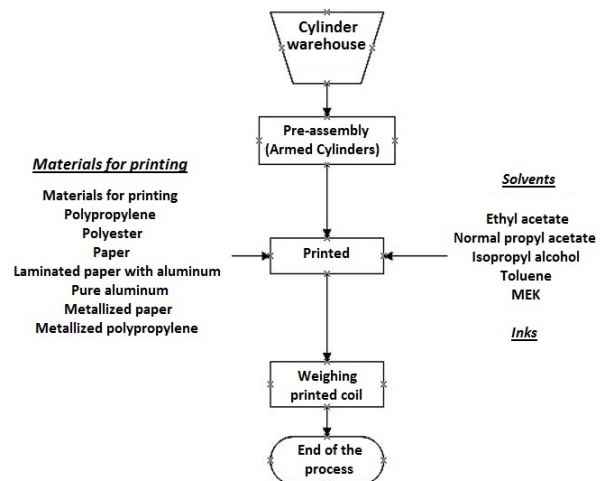
Figure 6. Flowchart for the cylinders area process.
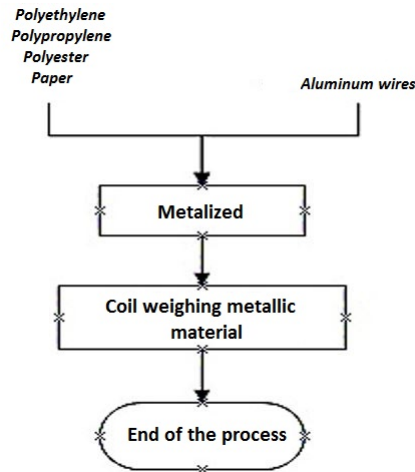
Figure 7. Flowchart for the Metallizing area process.
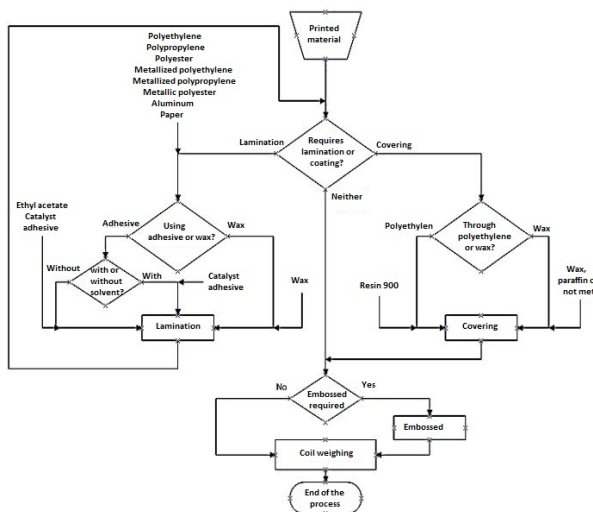
Figure 8. Flowchart for the Laminating process.
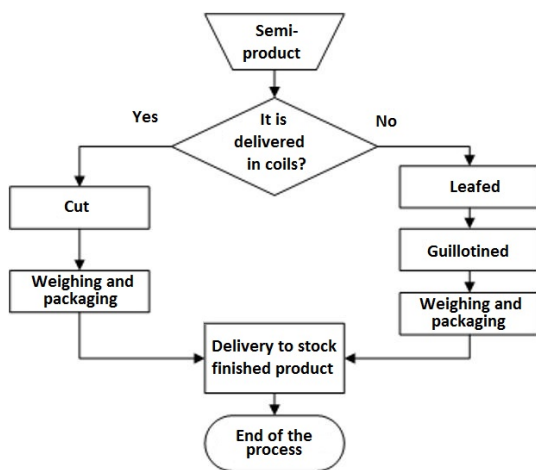
Figure 9. Flowchart of the Cutting and Finishing Process.

2.2. Load census

In the load census, a total of 56 machines composed of motors and various elements were identified; approximately fifty independent engines in the six areas described above, plus office equipment in a total of 45 work areas (offices, workshops, warehouses, etc.), for a total of 5946.35 kVA connected load.

Table 1 presents the independent motors with the highest consumption at the plant.

Table 1. Load estimation of a cooling unit, Chiller 2 – Westing-house – 460 V

Description	P (HP)	Vn (V)	In (A)	kVA
Compressor	20	460	32,5	25,89
Compressor	25	460	40	31,87
Compressor	20	460	32,5	25,89
Compressor	25	460	40	31,87
Fan	2	460	3,3	2,63
Fan	2	460	3,3	2,63
Fan	2	460	3,3	2,63
Approximate power of the machine (kVA)				**123,4**

2.3. Pareto diagram and stratification

Once the load census of the plant has been completed and the load data connected to it is known, the machines, equipment and motors involved are separated for each process carried out in the plant, in order to identify potential savings. Savings potentials were identified using a Pareto diagram.

Figure 10 presents the Pareto diagram of general processes, where the percentage (%) of process load is presented.
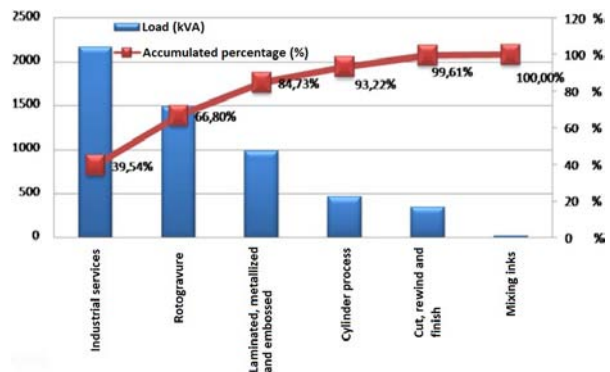
Figure 10. Pareto diagram of general processes.

It is very important to identify the elements that can have a significant impact on the plant's general energy consumption, since these represent possible savings points. Therefore, these devices were measured for real energy consumption.

Low consumption elements have little importance in terms of analysis, since any measurement or recommendation taken will not have a significant impact on the desired energy saving totals.

Figure 10 indicates that there are three processes and one area that represent almost 85% of the plant's total load: metal rolling and winding process, rotogravure and the industrial services area.

– Metallized rolling and winding process:

Dos equipos consumen en conjunto 15 884 kWh al mes, representando un 72 % del consumo mensual estimado de este proceso. Uno de los equipos sobresale por su consumo debido a su operación continua durante el mes y el otro equipo por su elevado consumo puntual.

– Rotogravure:

Three pieces of equipment have an equal production, two of them with the same technology, whose production is superior to the third piece of equipment. The equipments with the same technology consume altogether 105 440 kWh per month, almost 89% of the total monthly energy of this process, and the third piece of equipment consumes only 13 830 kWh.

– Industrial services:

The equipments that consume the most energy monthly are air conditioning equipment and chillers; together they represent 135,000 kWh per month, almost 45% of the monthly consumption in this area.

2.4. Control diagrams

With the data of the last two years of the monthly elec-tricity billing, plus the monthly production data, graphs were made to show the information on the variation of energy consumption based on the plant's production, consumption not associated with production, optimal points of production, establishments of goals, among others.

2.4.1. Control chart

Control charts are linear diagrams that illustrate the behavior of a variable according to certain established limits. They are used as instruments of self-control and are very useful as a complement to the cause and effect diagrams to detect phases of the analyzed process in which the alterations occur.

This graph is used to discard the points located outside the established limits ($\pm 3\sigma$), since these represent abnormal values and, if included in this study, they would give incongruent results. In addition, it allows for the identification of points that come remarkably close to the limits, and find the causes of this deviation. To make this graph, payment records to the electricity service company from the last two years were used. Figure 11 shows the control chart generated for the company. No point of monthly con-sumption exceeds the established limits, so all points are valid for this study.
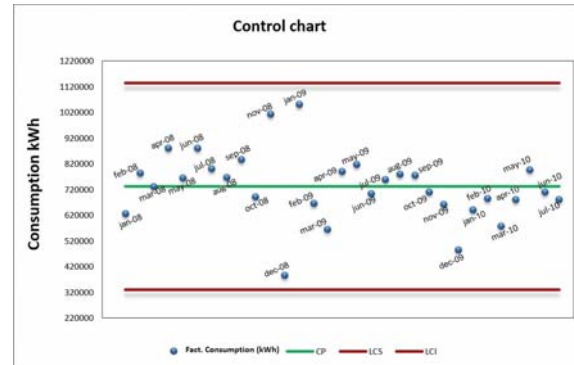
Figure 11. Control chart

2.4.2. Energy production vs. time graph

This graph, presented in Figure 12, simultaneously shows energy consumption and production over time, which illustrates the independent variation of the electrical energy consumed (kWh) and the amount of production (Ton) over time in order to identify any abnormal behavior in a period (month) and the reasons that produce such abnormal behavior [6].
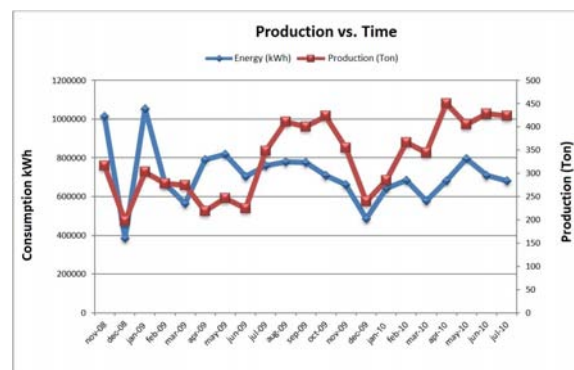
Figure 12. Electric power – Production vs. time graph.

The energy production vs. time graph shows that there is no uniform behavior in the November 2008 to June 2009 period, as well as the existence of a notable change in the relationship between production and electric power billed from July 2009 onwards, due to changes in high consumption equipment, when the production of the company increased significantly.

2.4.3. Energy vs. production graph

The purpose of this graph is to establish the trend that exists between production and energy consumption, and thus quantitatively define the value of energy not associated with production. For industrial and service companies, making a scatter diagram of the energy used in a given time with respect to the production carried out or the services provided during that same period reveals important information about the pro-cess, since when performing the line of characteriza-tion of consumption vs. production, energy consump-tion not associated with production can be established [6].

In the case of the company under study, as shown in Figure 12, two very different energy consumption trends were presented, due to two fundamental reasons: the first is the incorporation of more efficient machines and the second is the regulations published in November of 2009 in the Official Gazette of the Bolivarian Republic of Venezuela Number 39.298 [7], ordering a 20% reduction in electricity consumption, in order not to be subject to penalizations in the form of cuts in the electric supply.

For this reason, individual graphics were made for both trends, one for the period between November 2008 (date from which production data are available) and August 2009, Figure 13, and another for the peri-od from September 2009 to July 2010, Figure 14.
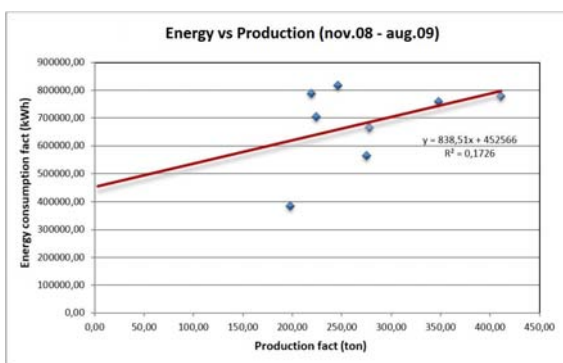
Figure 13. Energy graph vs. production (Nov. 08 - Aug. 09).

Before September 2009, Figure 13, consumption not associated with production was 452 566 kWh. After September 2009, Figure 14, consumption not associated with production was 300 054 kWh (66% of what it was before). This is due to the order to reduce consumption, since the company adopted energy sav-ing measures such as replacing luminaires, switching off lighting circuits, shutting off large pressurizers, acquisition of a more efficient air compressor, among others.

Figure 13 shows a very low point correlation for various reasons that only the company is aware of

(confidential information). There is no proportionality between what is produced and what is consumed. It is also noteworthy that November 2008 and January 2009 were the two months of greatest consumption in the plant and no specific cause for this increase was found, since the production of this period does not justify this fact. It is important to note that these two points further reduce the existing correlation between the plotted data, which indicates the existence of an irregular event in the plant during those months, or an error in the measurement-estimate made by the electric power service company.

Figure 14 shows a correlation of 57% between the graphed data, which indicates their greater reliability, thus the energy consumption study will be made based on this period (September 2009 - July 2010).
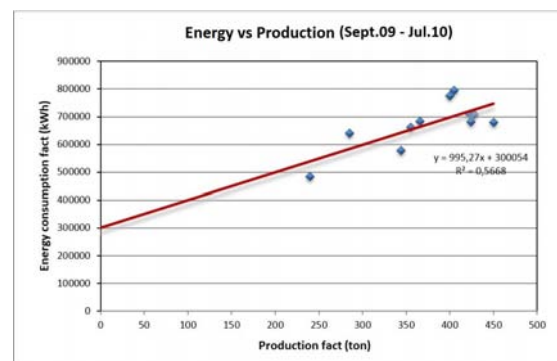
Figure 14. Energy vs. production graph (Sept. 09 - Jul. 10).

2.4.4. Establishment of the goal vs. production graph

Once the energy vs. production graphics are completed, the consumption goals are established.

In order to establish the goals and make them achievable, the months of the plant's best work efficiency were initially selected, that is, those that are below the line drawn in Figure 14. Through these selected points a new consumption trend it is established, which is defined as the goal trend, shown in Figure 15.

In Figure 15 the established goal trend is parallel to the current trend, but vertically displaced downward. This new trend indicates what the consumption of electrical energy for each production value should be so the plant works more efficiently. Consumption not associated with production of the goal trend is 213 871 kWh, while that of the current trend is 300 054 kWh, this implies that if the plant manages to maintain its production within the goal trend, it will achieve 29% energy savings.
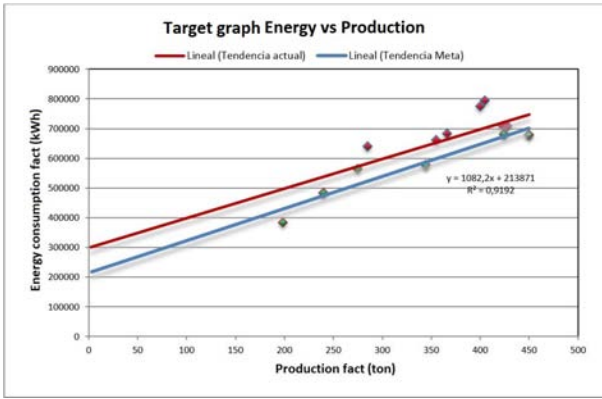
Figure 15. Goal - energy vs. production graph.

It should be noted that the previously established goal was set based on real values that the plant has already reached, so if the plant works to implement new savings systems, the results can be even more efficient.

2.4.5. Consumption index vs. production graph

With the values of the current consumption trend and the goal consumption trend, and dividing these by the production, a graph for the consumption index vs. production is obtained as shown in Figure 16, which indicates the energy needed to produce a ton for a given production value.
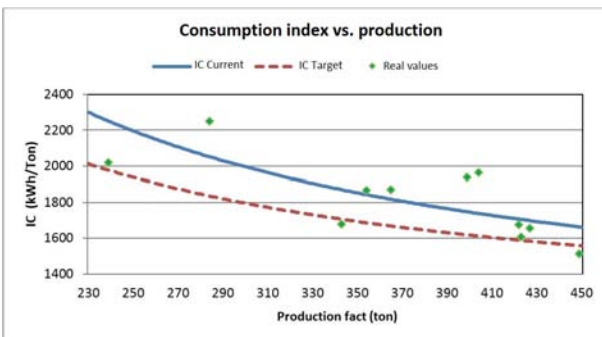
Figure 16. Consumption index vs. production graph.

As can be seen in Figure 16, the greater the production in the plant, the lower the impact of electric power on the cost of a ton of production. Due to this fact, it is important that production in the company is maintained at a high level, in order to reduce the amount of kWh per ton produced. In addition, two theoretical consumption index curves can be observed, one for the current consumption trend and another for the goal consumption trend.

The analysis of the consumption index, summarized in Table 2, indicates that in addition to maintaining high production, it is necessary to meet the established goals to significantly reduce the impact of energy per ton of product.

Table 2. Analysis of the consumption index chart

Tonne	IC current kWh/t	IC goal kWh/t
250	2196,0	1937,0
350	1852,0	1693,0
450	1662,0	1557,0

2.4.6. Measures proposed on the basis of the energy goal vs. production graph

Once the value of electric power (kWh) that can be saved monthly through the application of the proposed measures is quantified, change of luminaires, switching off of luminaires during resting hours, reduction of 20% plant and exterior lighting, change of motors, shutdown of air conditioning and office equipment during resting hours and use of the new compressor 100% of the time; the established goal consumption trend will undergo a modification, since this graph was initially formed by the best values actually achieved by the plant in its operation.

Afterwards, two new goal graphs are established, one considering only the measures that do not require monetary investment in machinery and equipment, and another that includes all energy saving proposals. To lay the foundations of economic analysis, both cases will result in a trend parallel to the previous goal but displaced downwards, that is, with consumption not associated with lower production.

In the establishment of the new goal graphs, factors were applied to the energy saving values for lighting, office equipment and air conditioning in order to give more realism to the results, since in some areas measures such as turning off the lights and computers in resting hours are already applied, and the air conditioning equipment does not work at 100% capacity during its entire work period. These factors are the following:

1) A factor of 0.6 was applied to the value obtained by saving when the luminaires were turned off.

2) A factor of 0.8 was applied to the value obtained through savings when office equipment was turned off.

3) A factor of 0.9 was used at the nominal consumption of air conditioning.

These factors were defined by observing the habits of the company's personnel; Tables 3 and 4 summarize the monthly energy values saved (kWh) as a result of each proposal.

Table 3. Analysis of the consumption index chart

Proposal	Monthly savings kWh
Lighting of luminaires during rest hours	1992,42
20% reduction in floor and exterior lighting	6163,20
Shutdown of A / C during rest hours	4303,28
Shutdown of office equipment during rest hours	155,20
Use of the new compressor 100% of the time	7148,00
TOTAL	**19 762,10**

Table 4. Monthly electricity savings for all the proposed measures

Proposal	Monthly savings kWh
Changing luminaires from 4 × 40 W to 3 × 32 W	2647,04
Lighting of luminaires during rest hours	1765,40
20% reduction of floor and exterior lighting	6163,20
Change of engines (decrease losses)	30 778,73
Shutdown of A / C during rest hours	4303,28
Shutdown of office equipment during rest hours	155,20
Use of the new compressor 100% of the time	7148,00
TOTAL	**52 960,85**

Figures 17 and 18 show the new energy goal vs. production graphs respectively for the measures without investment and for all the proposed measures.
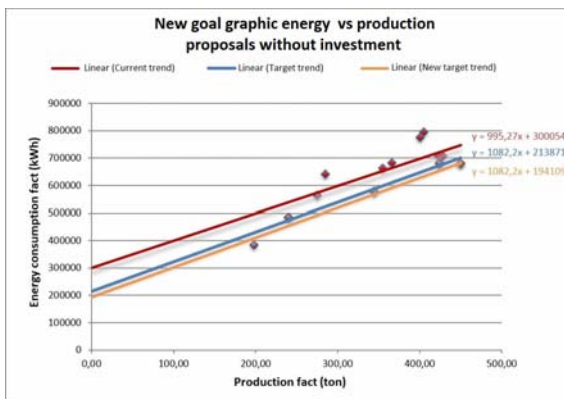
Figure 17. New goal graph – energy vs. production – proposals without investment.
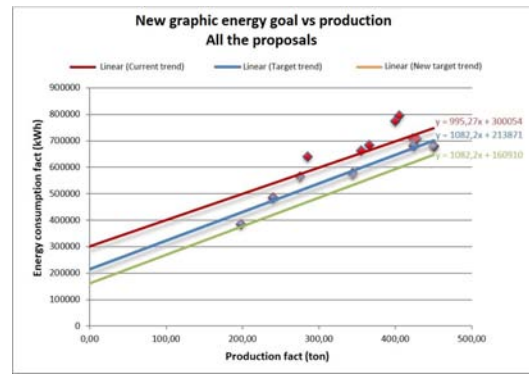
Figure 18. New goal graph – energy vs. production – all proposed measures.

Figures 17 and 18 show the plant's current trend, where consumption not associated to production is 300 054 kWh per month, in red, and the goal trend established for the plant without including changes, whose value is not associated to the production is 213 871 kWh per month, in blue.

Figure 17 shows, in orange, the new goal trend established on the basis of the implementation of savings measures without investment, whose value associated with non-production is 194 109 kWh per month. This represents 35% compared to the current trend and 9% with respect to the established goal trend, Figure 8.

Figure 18 shows, in green, the new goal trend established in accordance with the implementation of all the proposed measures, which yields a consumption value not associated with the production of 160 910,00 kWh per month, representing 46% of current consumption not associated with production, and 25% additional savings compared to the previously established goal.

By way of comparison, Table 5 shows the amount of residences that could be supplied for with the ener-gy savings obtained by implementing the measures proposed for the Montana Gráfica company, subsidiary of the Corimon Pintura Group C.A., taking as average a normal house-hold monthly consumption of 500 kWh per month, the minimum rate for general residential service, typified according to a tariff scheme as Rate 02: General resi-dential service, present in Article 9 point 9.2, published on April 3, 2002 in the Official Gazette of the Bolivar-ian Republic of Venezuela Number 37.415 [8], taking legal rates into consideration. It is possible to supply energy for 40 houses by launching the proposals with-out monetary investment in equipment and machinery, 106 houses if all proposals for energy savings are con-sidered, and, in an ideal case where the company man-ages to operate at optimal points of consumption in accordance with production, besides the implementa-tion of all the actions proposed in this work, it would be possible to supply up to 278 residences with the energy that would no longer be wasted.

Table 5. Number of housing units that could be supplied for with the energy saved

Actions to implement	Energy saved per month (kWh)	N.° of houses
Proposals without investment	19 762,10	40
All the proposals	52 960,85	106
New goal (all proposals)	139 144,00	278

3. Monitoring and control

This section presents an evaluation of the project based on the results obtained due to the implementation of the proposed saving measures, in addition to the company being able to maintain itself in the optimum points of goal consumption established.

The Executive branch introduced a policy for reduction of consumption in 2009 due to the national energy crisis. The management of the Corimon Group, of which the company Montana Gráfica is a subsidiary, has since implemented a series of measures, Figure 19, to reduce energy consumption in the different plants that conform it.

Generators were purchased to supply energy to critical processes during interruptions or rationing.

Situations such as sub-loaded engines, imbalances in the power network, operation at reduced voltage and harmonic content introduced by non-linear loads that impact energy consumption were solved.

A study was carried out on the operation of the most important machines that presented the highest consumption in the processes according to the Pareto diagram.

The energy savings obtained range between 18% and 26% according to the conditions, the policies of the company and the level of commitment reached by the staff.
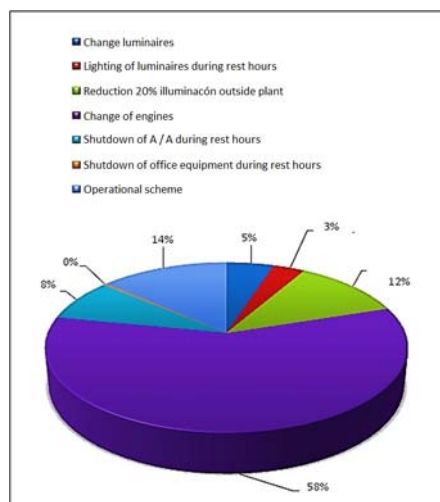
Figure 19. Average percentage of distribution of savings of the proposed measures.

From the constant characterization of the company we can intuit the possibility of improving energy saving goals as new measures are analyzed and implemented.

The economic feasibility of the project was obtained on the assumption that the company operates under optimal conditions in terms of consumption vs. production (goal trend), in addition to the proposed measures without investment over a period of 7 years (short and medium-term measures). The minimum rate of return was considered constant at 17% during the study period.

For the first year (t = 0) only the cost of the project was estimated as monetary flow. For subsequent years, the annual savings obtained through the proposals without investment and operation of the plant under the goal consumption vs. production trend are considered as net flows, but increasing as the measures were implemented. The electric rate is considered constant throughout the study period.

The income exceeds the costs, Table 6, so that economically, in 7 years the benefit is higher than the minimum required according to the analysis of the project (2009-2016).

4. Conclusions

This paper presents a methodology to quantify the energy savings possible in an industry, through a procedure based on control charts that allows for the systematization of the calculation of possible energy savings, which is a way to help solve the current energy problem.

The systematic study of possible savings based on the method allows for the improvement of results obtained previously with non-systematic changes.

The proposals made according to the presented method achieved monthly savings in terms of the electricity generation system of a total of 138,024.84 kWh, on average. Additionally, the company managed to operate at optimal points of consumption according to production. In addition to the implementation of measures, the savings are equivalent to the electric power needed to power up to 278 residences with the energy that is no longer wasted. The generalized application of the proposed methodology would allow for the reduction of the national energy problem in a systematic way, eliminating waste of energy without affecting levels of industrial production.

Table 6. Interpretation of the project's value 2009-2016

Year	Investment to recover at the beginning	Net flow	Minimum performance	Recovered invertment	Invertment to recover
1	98 104,00	12 230,25	16 677,68	-4447,43	102 551,43
2	102 551,43	24 460,50	17 433,74	7026,76	95 524,67
3	95 524,67	36 690,75	16 239,19	20 451,56	75 073,12
4	75 073,12	48 921,24	12 762,43	36 158,81	38 914,31
5	38 914,31	48 921,24	6 615,43	42 305,81	-3 391,5
6	30 582,87	65 228,64	5 199,08	74 797,60	-1 757,98
7	15 852,69	65 228,64	2 694,95	87 513,19	-153,21
8	12 458,67	86 971,94	2 117,96	154 725,23	-79,41

References

[1] Colectivo de autores, *Gestión Energética Empresarial*, Centro de Estudios de Energía y Medio Ambiente, Ed. Universidad de Cien Fuegos, 2001. [Online]. Available: https://goo.gl/UPpCnv

[2] Comisión Eléctrica Nacional Colegio de Ingenieros de Venezuela (CIV). (2017). [Online]. Available: https://goo.gl/WbVNFm

[3] D. Manosalva and A. Abramoff, "Implantación de un sistema integral de la energía en la empresa montana gráfica, filial del grupo corimon c. a." in *Tesis de grado*. Facultad de Ingeniería, Escuela de Ingeniería Eléctrica, Departamento de Potencia, Universidad de Carabobo, Valencia, Estado Carabobo, Venezuela, 2011.

[4] J. Aller, L. Salazar, A. Bueno, and M. P. na., "Metodología para la implantación de un sistema integral de gestión de la energía," in *IX Congreso de Instalaciones Eléctricas: "Hacia la eficiencia en los servicios de electricidad y telecomunicaciones"*, 2010, pp. 1–8. [Online]. Available: https://goo.gl/UPo6pa

[5] *ISO 50001:2011. Energy management systems – Requirements with guidance for use*, International Organization for Standardization Std., 2011. [Online]. Available: https://goo.gl/XLWo5s

[6] A. Borroto and J. Monteagudo, "Gestión energética en el sector productivo y los servicios," in *Universidad de Cienfuegos, Cuba*, 2006, pp. 227–237.

[7] "Gaceta oficial de la República Bolivariana de Venezuela, año CXXX, mes I, Caracas Artículo 1, p. 2." 3 de noviembre de 2009,.

[8] "Gaceta oficial de la República Bolivariana de Venezuela, año CXXIX, mes VI, Caracas Artículo 9," 3 de abril de 2002,.
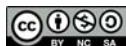
Factors for selecting Petroleum Liquefied Gas conduction pipes in Ecuador

Factores para seleccionar tuberías de conducción de gas licuado de petróleo en el Ecuador

Diego Venegas[1,*], César Ayabaca[2], Santiago Celi[3], Juan Rocha[3], Euro Mena[4]

Abstract

In order to build residential, commercial and industrial installations of Liquefied Petroleum Gas (LPG) in Ecuador, the INEN 2260: 2010 Ecuadorian Technical Regulation establishes the minimum safety guidelines that must be taken into account in this type of installations. To conduct this hydrocarbon, the Standard accepts several materials of pipes, methods of union with accessories, forms of installation, which makes the responsible for the sizing and planning of this type of systems have several options to choose from when directing a determined project. This paper shows some factors that affect the selection of the most suitable pipeline for LPG systems, complying with the mandatory Technical Standard in Ecuador. The mechanical strength, hardness and weight are compared as properties of the accepted materials; the execution times of pipes and fittings and, finally, the costs associated with materials, labor and maintenance that must be given to these systems are compared.

Resumen

Para realizar instalaciones residenciales, comerciales e industriales de gas licuado de petróleo (GLP) en el Ecuador, rige la norma técnica ecuatoriana INEN 2260:2010, la cual establece los lineamientos mínimos de seguridad que se deben tener en cuenta en este tipo de instalaciones. Para conducir este hidrocarburo, la norma acepta varios materiales de tuberías, métodos de unión con accesorios, formas de instalación, lo que hace que el responsable del dimensionamiento y planeación de este tipo de sistemas tenga varias opciones para escoger al momento de encaminar un proyecto determinado. El presente trabajo muestra algunos factores que inciden en la selección de la tubería más adecuada para sistemas de GLP, cumpliendo con la norma técnica obligatoria en el Ecuador. Se compara la resistencia a la tracción, dureza y peso como propiedades de los materiales aceptados; tiempos de ejecución de uniones entre tuberías y accesorios y, finalmente, se comparan los costos asociados a los materiales, mano de obra y mantenimiento que debe darse a estos sistemas.

Keywords: Recommended materials, Technical Standard, pipes, best application, properties.

Palabras clave: materiales recomendados, norma técnica, tuberías, mejor aplicación, propiedades.

[1,*]Faculty of Engineering at Universidad de Concepción, Concepción – Chile.
   Author for correspondence ✉: diegofvenegas@udec.cl. ⓘ http://orcid.org/0000-0002-7376-6272
[2]Departament of Mechanical Engineering, Escuela Politécnica Nacional, Quito – Ecuador.
   ⓘ http://orcid.org/0000-0002-3728-7514
[3]Faculty of Architecture and Engineering, Universidad Internacional SEK, Quito – Ecuador.
   ⓘ http://orcid.org/0000-0002-8302-3413, ⓘ http://orcid.org/0000-0003-0660-7199
[4]Departament of Energy and Mechanics, Universidad de las Fuerzas Armadas, Latacunga – Ecuador.
   ⓘ http://orcid.org/0000-0001-7872-0292

1. Introduction

Liquefied Petroleum Gas (LPG) is a fuel used for residential, commercial and industrial applications [1, 2]. In Ecuador, use of this hydrocarbon is very frequent, and, as such, the National Government has foreseen a subsidized price for the residential sector [3, 4], since it offers several advantages, among which we can mention [5–8]:

El gas licuado de petróleo (GLP) es un combustible utilizado para aplicaciones residenciales, comerciales e industriales [1, 2], y en el Ecuador el consumo de este hidrocarburo es muy frecuente, por lo que para el sector residencial el Gobierno nacional ha previsto un precio subsidiado [3, 4], ya que brinda varias ventajas entre las que se pueden mencionar [5–8]:

- High calorific power compared to other energy sources.
- Clean in terms of emissions of polluting gases.
- It satisfies several energy needs.

As it is a very explosive and flammable fuel [9], much caution is required when planning, sizing and selecting storage systems (containers), transport (pipes), consumer equipment, and protection and safe-ty elements [10].

The risk in a LPG system is always present and can not be eliminated [11], but it can be minimized if the systems that contain it are conceived technically [12, 13], in accordance with the guidelines established in technical standards [14] where the minimum safety requirements are indicated at the time of installation.

In Ecuador, the INEN 2260: 2010 standard is in force: «Fuel gas installations for residential, commercial and industrial use. Requirements» [15], which establishes the minimum mandatory safety parameters in the national territory, and covers all the necessary components in an installation, from storage tanks, pipes, regulation and control systems, prevention sys-tems, maintenance, among others.

In nature, LPG is in a gaseous state, but to facilitate its storage in containers it is converted to a liquid state by increasing its pressure and lowering its temperature [16]. Inside these containers, a phenomenon of natural vaporization of the liquid occurs as a result of heat exchange between it and the environment [17], and it is in this state that it is transported through pipes for consumption.

These pipelines must at minimum comply with the following [18, 19]:

- Manufacturing materials must be compatible with the fuel they are transporting.
- Their dimension must be adequate to drive the flow that is required in the operation of consumer equipment.

- They must withstand pressure tests and the ser-vice pressure to which they will be subjected.
- They must withstand the physical conditions of the environment in which they will be in-stalled.

The types of pipe materials that the technical standard accepts for the installation of LPG systems are shown in Table 1.

Table 1. Load estimation of a cooling unit, Chiller 2 – West-inghouse – 460 V

Pipeline	Manufacturing standard
Carbon steel	ASTM A 53 [20] ISO 65 (serie Heavy) [21]
Stainless steel	ANSI/AGALC1 [22] ASTM A 240 [23]
Copper	ISO 1640 [24] ASTM B88 [25]
Polyethylene	ISO 4437 [26] ASTM D2513 [27]
P-Al-P*	AS-4176 [28] ISO 17484-1 [29]

* P-Al-P Polyethylene aluminum polyethylene.

The table shows that accepted materials can be metal-lic or plastic, and there is a procedure or method of joining pipes with their accessories for each of them. Table 2 shows the most commonly used procedures for joining pipes with their accessories.

Table 2. Methods for joining pipes with accessories [30]

Pipeline	Union procedure
Carbon steel	SMAW o threaded
Stainless steel	Pressing fit
Copper	Oxyacetylenic
Polyethylene	Thermofusion or electrofusion
P-Al-P	Thermofusion or electrofusion

For ease of inspection, maintenance and repair in case of leaks, it is recommended that the pipes that conduct LPG be installed in plain sight. However, users prefer that they are hidden for aesthetic reasons.

The technical standard accepts that pipes for conducting LPG can be hidden if they are installed:

- inside ducts,

- jacketed in a pipe of greater mechanical strength,

- embedded in walls and floors, provided they are covered with an easily removable material,

- buried if they are given adequate protection against physical damage or corrosion.

Table 3. Ways to install pipes [31]

Way to instalation	Stainless	Steel steel	Copper	Polyethylene	P-Al-P
View	Yes	Yes	Yes	No	No
Embedeed	Yes	Yes	Yes	No	Yes
In pipeline	Yes	Yes	Yes	No	Yes
Buried	Yes	Yes	Yes	Yes	Yes
Recessed*	No	No	No	No	No

*Recessed: That pipe that is fused in the building becomes a structural part of it.

Table 3 shows the accepted forms of pipe installation according to the materials used.

With these options of pipe materials, joining procedures with accessories and ways to install them, there are several additional factors that can affect the proper selection for an LPG installation in Ecuador. This paper presents several of these influencing factors to obtain a selection that is more in line with the characteristics of each user, and the particular conditions that surround them.

2. Materials and methods

2.1. Properties of the material

The following physical and mechanical properties of the materials indicated in Table 1 were compared: tensile strength, hardness and weight per meter of pipe.

– To measure the mechanical strength, a Tinius Ol-sen universal testing machine model Super L-20, series 80700-1 was used. The criteria for the measurement is based on ASTM E-8M [32].
– The Rockwell durometer used to measure the hardness is a Mitutoyo, Durotwin model, BG000062 series, diamond penetrator for ADC scales, 1/16" steel ball penetrator for FBG scales, with analog reading. To validate the hardness measurement procedure, the ASTM E18 03 Standard method for Rockwell hardness by in-dentation [33] and ASTM D785 Standard test method for Rockwell hardness of plastics and electrical insulating materials [34] were used.
– To measure the weight of pipes, the Shimadzu Unibloc balance was used. Cap 220 g.

2.2. Installation times

Each of the procedures described in Table 2 has its particularities, its form of execution, its complexity and therefore, its installation time.

Joints were made for 1" pipe and under the procedures established in Table 2, all of them by qualified personnel with vast experience in the assembly of LPG systems.

– The first procedure consisted of making a joint and measuring the time between the start and the end, from the time the tool is operated until the joint is finished.

– For the second procedure, the necessary connections were made to obtain a pipe section of 60 m, with a joint at each end that could then be joined to another accessory. The total time required was recorded.

In both procedures, a Steren chronometer model CLK-150 was used. It should be noted that the external conditions (ambient temperature, atmospheric pressure) for the two procedures were similar.

2.3. Cost ratio

A fundamental aspect that a user of this type of system takes into account is the installation cost, which depends directly on:

– Prices of materials (Table 1) and compatible ac-cessories, plus consumables, according to the joining procedures (Table 2). These prices have been requested from 3 local suppliers and the lowest value quote has been chosen.

– Qualified workforce carries out the assemblies and installations (in welding procedures, the personnel must be qualified by a certifying body). These costs have been obtained with the help of installation companies with several years of experience in LPG systems.

– Preventive maintenance of an installation must be carried out every 5 years [35]. These maintenance values have been estimated in installations of similar size for each of the materials (Table 1) and installed forms of pipe (Table 3).

The cost relationship expresses a value taken as a unit, and from this value and according to the expressed criterion, it is compared as many times as con-tains the unit for the following values.

3. Results and discussion

3.1. Properties of the material

Each material displays certain characteristics, physical and chemical properties, which make them more ad-vantageous than others for a given application.

a) Tensile strength

With this value it is possible to determine what load each one of them can bear before exceeding their elastic limit and deforming without losing their initial properties. Figure 1 shows the tensile strength of the various materials suitable for transporting LPG.
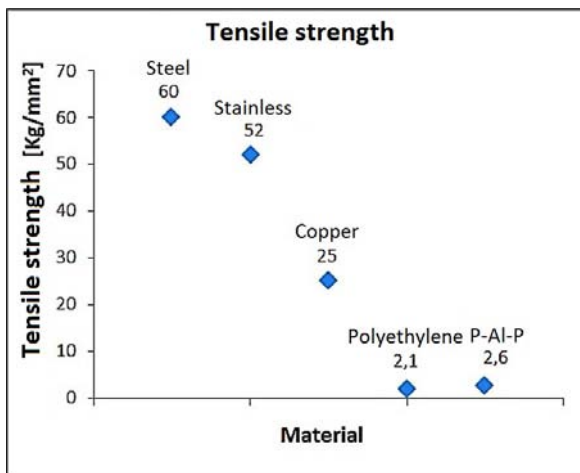
Figure 1. Comparison of tensile strength

The material with the highest tensile strength is steel with 60 kg/mm², followed by stainless steel with 52 kg/mm², then copper with 25 kg/mm², P-Al-P with 2.6 kg/mm² and, finally, polyethylene with 2.1 kg/mm².

b) Hardness

Hardness is the property of resistance of the materials to scratches and perforations, and as a pipe for conduction of LPG is exposed to scratches and blows by external agents, this property is shown in Table 4.

With the results of a) and b), steel pipe is the most recommended to be installed in areas of high shock risk. Due to its low resistance and its degradation when exposed to sunlight, it is recommended that polyeth-ylene pipe is buried when installed.

Table 4. Hardness of materials

Pipeline	Hardness	Scale
Carbon steel	99	Rockwell B
Stainless steel	92	Rockwell B
Copper	37	Rockwell B
Polyethylene	68	Rockwell C
P-Al-P	11*	Rockwell B

* Aluminum hardness

c) Weight

The weight per length unit of pipe for a diameter of 1" determines which type will perform better when ele-vated installations are required, or for long trips that are manageable for crews of installers.

Regarding weight, the polyethylene pipe is lightest (0.146 kg/m), which makes it very versatile when installed in long stretches (Figure 2), and as it comes in rolls, installation is very simple. A similar thing occurs with P-Al-P pipe, with a weight of 0.293 kg/m. It is very versatile for long sections, and this pipe can be embedded in walls and floors, through ducts and jacketing.

Figure 2. Polyethylene pipe ready to be installed.

Next is the stainless-steel pipe with 0.675 kg/m, then the copper pipe with 0.997 kg/m and, finally, the steel pipe, whose weight is 2.478 kg/m, which means that for long stretches it is necessary to install intermediate joining accessories such as flanges or universals. This also makes it difficult to handle in large diameters to perform work in the workshop, which means that the joints for these pipes can only be worked on in situ.

Figure 3 shows the comparison of values of the weights per meter of pipes for LPG conduction.

Table 5 shows the connection times of pipes with fittings, taken for the procedures described in 2.2 (a single connection of pipe with accessory and union of 60 lineal m continuous pipes).

Table 5. Average times to make joints or links in LPG pipes

Time	Steel	Stainless Steel	Copper	Polyethylene	P-Al-P
Connection time for a joint	18 min	15 s	1 min	1 min	1 min
Coonection time for 60m of pipe	4,5 h	3 min	30 min	2,5 min	2,5 min
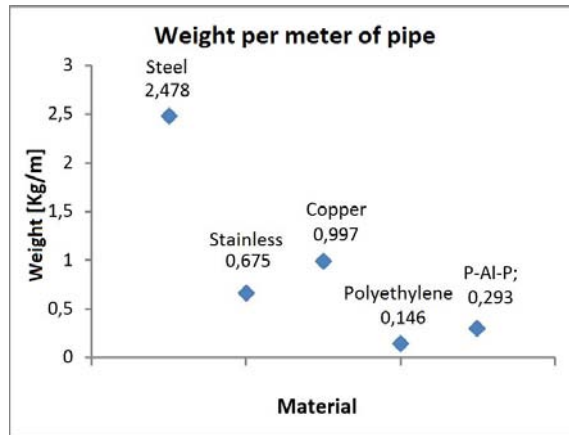
Figure 3. Comparison of pipe weights for conducting LPG

The first measured procedure corresponds to a single joint for a 1" pipe with one joint. The quickest joint to make is the pressing fit. Its value of 15s corre-sponds to the switching on of the tool, closing of the tongs, and subsequent pass—not pass check with the gauges. It is a very fast and clean process. The follow-ing methods have the same joint time of 1 min: poly-ethylene, P-Al-P and copper. The method includes heating the plate for thermofusion, the pipe reaching the required temperature, and joining it with the acces-sory. For copper, the connection time of the pipe with the acces-sory by oxyacetylene is taken into account, using a 5% silver alloy rod which is then melted, and the liquid formed is poured between the pipe and the fitting to achieve fusion. The longest method is the SMAW for steel pipe (18 min.). The time required for 4 steps is taken into account, from the root, to the final finish, including the cleaning of slag.

For the second procedure, the times taken are those necessary to join 60 meters of pipe. The fastest meth-ods are polyethylene and P-Al-P (2.5 min), since only two joints are needed because these pipes are continu-ous and come in rolls. It is followed by the joining method for stainless steel with pressing fit (3 min), then the capillarity method for copper tubing with 30 min and, finally, the SMAW method for steel pipe with 4.5 h.

3.2. Cost ratio

Figure 4 shows the costs associated with the pipes. The measures involved are materials, maintenance and labor. This analysis considers relative costs, taking as a unit lower costs (in materials and labor). Meanwhile, regarding maintenance, 1 is taken as the lowest cost for visible pipe, considering that plastic pipes (poly-ethylene and P-Al-P) can only be installed hidden and requires almost no maintenance.
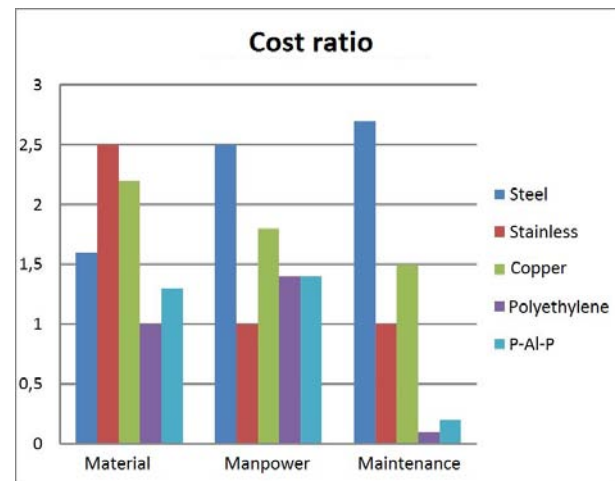
Figure 4. Ratio of pipe costs for LPG services.

The results of the costs presented in Figure 4 can be interpreted as follows:

a) Material

Polyethylene pipe has a value of 1; the P-Al-P pipe is 1.3 times more expensive; steel is 1.6 times more ex-pensive; copper is 2,2; and stainless steel is 2.5 times more expensive.

b) Workforce

The smallest item corresponds to the union of stainless steel pipes by means of pressing fit, since this joining method «only» involves operating a device for closing clamps, the installer does not require more skill or training, therefore, its cost is the lowest of all.

It is followed by polyethylene pipes and P-Al-P with 1.4 since the hot melt, although it is not a very complicated procedure to execute, needs greater skill on the part of the installer than in the case of stainless steel. Copper pipes follow with a value of 1.8. This method requires more skill on the part of the installer, who must be qualified and certified according to the technical standard [15].

Finally, the highest labor cost (2.5) corresponds to the steel pipe that requires the electric arc method (SMAW) for joining, whose installer is a person with great skill, experience, qualified and certified.

c) Maintenance

The unit value (for pipes that can be installed in plain sight) corresponds to the stainless-steel pipe, its maintenance is minimal, since it does not corrode and is aesthetically pleasing to the eye. With 1.5 follows the copper pipe, which requires greater care and protection for sections at plain sight.

Finally, the carbon steel pipe stands at 2.7, since its maintenance requires future repainting of sections that have been installed in highly corrosive atmospheres, or even total repainting.

When buried, polyethylene pipe has the lowest value (0.1), since it does not require maintenance; a value of 0.2 is assigned to P-Al-P pipe considering minimum cleaning maintenance in sections installed in ducts.

3.3. Other selection factors

The fact that a certain material has better mechanical properties (resistance) over another can become an indirect selection factor in LPG pipes, for example:

– Due to their greater mechanical resistance, metal pipes (steel, stainless steel and copper) are better resistant to rodent bites than plastic pipes, and this is of the utmost importance, especially in in-stallations located in open areas or ducts, where the presence of these animals is highly probable [31].

– When a pipe is installed in plain sight, it must be marked according to the respective regulations and painted with the respective color [36], yellow ocher for LPG conduction in vapor phase and white for LPG conduction in liquid phase (Figure 5), in order to alert someone out-side the installation of the danger associated with the fuel.

– Similarly, it is important to protect and signal hidden pipes, as well as the elements that are lo-cated as protections. In this way, and in the case of work in the surrounding area, the protections will be found before the pipes.

– From an aesthetic point of view, stainless steel pipes have a better rating than those made of carbon steel.

– The bacterial growth resistance of stainless steel pipes is superior to the rest [31], which makes them ideal in installations where neatness and asepsis are required.

– There are external factors that affect the selection of a given material in a facility, such as availability of all materials and accessories by the suppliers when required, availability of qualified personnel to carry out the installations, among others.

– Additionally, an indirect cost of installation is that of the equipment and tools necessary to make the pipe joints with accessories. This cost, however, has not been taken into account for this analysis, since the allocation of this value to a given project will depend on the projection that the installation company has for work to be done in a certain period of time. In addition, each project has a different execution times, which makes the depreciation of both machin-ery and tools difficult to determine.

Figure 5. Signaling of LPG pipes (yellow LPG vapor, white LPG liquid).

4. Conclusions

Each project has a different reality because of its location, pipe placement, availability of materials in the market, availability of the right personnel to carry out the work. This makes the selection of the appropriate pipeline specific to each project.

It cannot be said that a material is perfect for an in-stallation, since there are many factors that make its selection feasible. However, and depending on the

particular conditions of each installation, there is one that will have several advantages over others.

It is important to indicate that the user that requires an installation of LPG, and when dealing with a fuel where safety criteria must be taken into account, the personnel that must carry out said installation must be qualified and certified by the competent authority.

The installer of an LPG pipe system is the one who must guarantee technical consistency by using materials, joining procedures, and correct ways to install pipes according to the conditions of each project, and it is the one who must evaluate the best alternatives according to the case.

Joining the criteria of mechanical strength and hardness will allow us to better evaluate applications of pipes near areas of vehicular flow, transport of goods, which at a certain time can directly affect and cause damage to said pipes. All the comparisons made correspond to the instal-lation of pipes and fittings by qualified personnel and under the minimum criteria established in the technical standard.

A LPG pipe must be leak-proof and leak tight, so performing the bonding procedure correctly will re-duce the risks associated with transporting the fuel through the pipes.

It is recommended that polyethylene pipes are always «buried» when installed, they can never be left in plain sight.

5. Recommendations

It is essential to perform a vacuum seal test on the pipe at a pressure greater than normal working pressure prior to determining the supply of fuel in a new instal-lation, the material used, the joint method used and the type of installation.

P-Al-P pipes can be installed in ducts, embedded or buried, that is, hidden. They can in no way be installed in plain sight as they are affected by solar rays (crys-tallization) which makes them fragile, leading to breakage and leaks.

If a metallic pipe is buried, an effective mechanism to protect it must be provided against the corrosion to which it may be exposed.

Regardless of the pipe material, if it is hidden when installed, it must be protected by some mechanism whose mechanical resistance is superior to that of said pipeline, with the aim that if any person involuntarily performs some activity in the vicinity, they find this mechanism first and avoid damage to the pipe.

If a user who needs this type of installation has several commercial proposals, he should seek quali-fied external advice to help them choose the best op-tion.

References

[1] K. J. Morganti, T. M. Foong, M. J. Brear, G. da Silva, Y. Yang, and F. L. Dryer, "The research and motor octane numbers of liquefied petroleum gas (LPG)," *Fuel*, vol. 108, Supplement C, pp. 797–811, 2013. [Online]. Available: https://doi.org/10.1016/j.fuel.2013.01.072

[2] P. Boggavarapu, B. Ray, and R. Ravikrishna, "Thermal efficiency of lpg and png-fired burners: Experimental and numerical studies," *Fuel*, vol. 116, Supplement C, pp. 709–715, 2014. [Online]. Available: https://doi.org/10.1016/j.fuel.2013.08.054

[3] K. Troncoso and A. S. da Silva, "Lpg fuel subsidies in latin america and the use of solid fuels to cook," *Energy Policy*, vol. 107, Supplement C, pp. 188–196, 2017. [Online]. Available: https://doi.org/10.1016/j.enpol.2017.04.046

[4] B. Creamer and R. Becerra., "Cuantificación de los subsidios de derivados del petróleo a los hidrocarburos en el Ecuador," in *Petróleo al día. Boletín Estadístico del Sector de Hidrocarburos*, vol. 2, pp. 9–26, 2016. [Online]. Available: https://goo.gl/3oPCQi

[5] L. Raslavičius, A. Keršys, S. Mockus, N. Keršenė, and M. Starevičius, "Liquefied petroleum gas (lpg) as a medium-term option in the transition to sustainable fuels and transport," *Renewable and Sustainable Energy Reviews*, vol. 32, Supplement C, pp. 513–525, 2014. [Online]. Available: https://doi.org/10.1016/j.rser.2014.01.052

[6] H. Rijpkema, H. Roebers, and M. Mekes, "Tuberiías de plástico para gas en edificios y las consecuencias de los incendios," in *Conferencia Internacional de Tuberias de Plastico*, 2012. [Online]. Available: https://goo.gl/cHEBh2

[7] R. K. Andadari, P. Mulder, and P. Rietveld, "Energy poverty reduction by fuel switching. impact evaluation of the lpg conversion program in indonesia," *Energy Policy*, vol. 66, Supplement C, pp. 436–449, 2014. [Online]. Available: https://doi.org/10.1016/j.enpol.2013.11.021

[8] F. Chica, F. Espinoza, and N. Rivera., "Gas licuado de petróleo como combustible alternativo para motores diésel con la finalidad de reducir la contaminación del aire," *INGENIUS, Revista de Ciencia y Tecnología*, no. 4, pp. 73–81, 2010. [Online]. Available: http://dx.doi.org/10.17163/ings.n4.2010.08

[9] M. Johnsen and G. Nardini, "Manual de seguridad: Aspectos técnicos de la inflamabilidad de los

gases hidrocarburos," Programa de las Naciones Unidas para el Medio Ambiente, 2005. [Online]. Available: https://goo.gl/VpkGxa

[10] D. Venegas, "Seguridad en la instalación de sistemas de gases industriales (glp)," in *II Congreso Internacional de Energía, XXIV Asamblea COPIMERA*. Santo Domingo, República Dominicana, 2016. [Online]. Available: https://goo.gl/EZVwHj

[11] J. Moncada., "Riesgo o peligro," *NFPA Journal Latinoamericano*, 2015. [Online]. Available: https://goo.gl/yypQMZ

[12] D. Venegas and O. Farias., "La bleve, un motivo para la seguridad en las instalaciones de GLP," in *13er Congreso Iberoamericano de Ingeniería Mecánica*. Lisboa, Portugal, 2017. [Online]. Available: https://goo.gl/32aSg3

[13] D. Venegas, M. Arrocha, S. Celi, J. Rocha, C. Ayabaca, and E. Mena., "Manejo inseguro del gas licuado de petróleo en Panamá," *I+D Tecnológico*, vol. 13, no. 2, pp. 22–30, 2017. [Online]. Available: https://goo.gl/TU8uB3

[14] NFPA. (2014) NFPA 58 código del gas licuado de petróleo edición 2014. [Online]. Available: https://goo.gl/yS9rpu

[15] INEN, *NTE INEN 2260:2010 Instalaciones de gases combustibles para uso residencial, comercial e industrial. Requisitos, 2da Rev*, Servicio Ecuatoriano de Normalización Std., 2010. [Online]. Available: https://goo.gl/LHmvsu

[16] M. Leporini, A. Terenzi, B. Marchetti, G. Giacchetta, F. Polonara, F. Corvaro, and R. C. Grifoni, "Modelling the pressurization induced by solar radiation on above ground installations of lpg pipeline systems," *Journal of Physics: Conference Series*, vol. 923, no. 1, pp. 1–9, 2017. [Online]. Available: https://goo.gl/4ghqFL

[17] D. Venegas and C. Ayabaca, *Instalaciones de gas licuado de petróleo*. Editorial Académica Española, 2017. [Online]. Available: https://goo.gl/N4NE1f

[18] Rego, "Catálogo L-102SV, equipo de GLP y amoniaco anhidro," Tech. Rep., 2011. [Online]. Available: https://goo.gl/o5LiuF

[19] J. Fuentes and J. Celis, "Instalaciones de gas natural," 2004. [Online]. Available: https://goo.gl/J3HVij

[20] ASTM, *ASTM A53/A53M - 12, Especificación normalizada para tubos de acero negro e inmersos en caliente, galvanizados, soldados y sin costura*, ASTM International, West Conshohocken, PA Std., 2012. [Online]. Available: https://goo.gl/czayAt

[21] ISO, *ISO 65:1981: Carbon steel tubes suitable for screwing in accordance with ISO 7-1*, International Organization for Standardization Std., 1981. [Online]. Available: https://goo.gl/DBGVBf

[22] ANSI/CSA, *ANSI LC 1-2016/CSA 6.26-2016, Sistemas interiores de tuberías de gas combustible que utilizan tuberías de acero inoxidable corrugado*, CSA Group, Std., 2016. [Online]. Available: https://goo.gl/zkZias

[23] ASTM, *ASTM A240 / A240M-17, Standard Specification for Chromium and Chromium-Nickel Stainless Steel Plate, Sheet, and Strip for Pressure Vessels and for General Applications*, ASTM International, West Conshohocken, PA Std., 2017. [Online]. Available: https://goo.gl/JH3WuY

[24] ISO, *ISO 1640:1974: Wrought copper alloys – Forgings – Mechanical properties*, International Organization for Standardization Std., 1974. [Online]. Available: https://goo.gl/Jde7eN

[25] ASTM, *ASTM B88-16, Standard Specification for Seamless Copper Water Tube, ASTM International, West Conshohocken*, ASTM International, West Conshohocken, PA Std., 2016. [Online]. Available: https://goo.gl/AVRQR3

[26] ISO, *ISO 4437:2007: Buried polyethylene (PE) pipes for the supply of gaseous fuels – Metric series – Specifications*, International Organization for Standardization Std., 2007. [Online]. Available: https://goo.gl/PAuTNi

[27] ASTM, *Mathematical modelling of solute segregation in solidifying materials*, ASTM International, West Conshohocken, PA Std., 2016. [Online]. Available: https://goo.gl/xmMkni

[28] AS, *Polyethylene/aluminium and cross-linked polyethylene/aluminium macro-composite pipe systems for pressure applications.*, Australian Standard Std., 1994. [Online]. Available: https://goo.gl/jj3chW

[29] ISO, *ISO 17484-1:2006: Plastics piping systems- Multilayer pipe systems for indoor gas installations with a maximum operating pressure up to and including 500 kPa (5bar).Part. 1: Specifications for systems.*, International Organization for Standardization Std., 2006. [Online]. Available: https://goo.gl/AZpzoh

[30] D. Venegas, J. Yanez, S. Celi, C. Ayabaca, L. Tipanluisa, D. Bastidas, and M. Arrocha, "Materiales recomendados por las normas internacionales para utilizar en una instalación de GLP," in *XI Congreso Nacional de Ingeniería Mecánica*, Elche – España, 2016. [Online]. Available: https://goo.gl/bLb54Y

[31] D. Venegas, M. Melendrez, and M. Arrocha, "Materiales para instalaciones de gas licuado de petróleo según National Fire Protection Association (NFPA)," in *Congreso Internacional de Metalurgia y Materiales 16 SAM CONAMET*, 2016. [Online]. Available: https://goo.gl/E4DnGs

[32] ASTM, *ASTM E8M-00b, Standard Test Methods for Tension Testing of Metallic Materials [Metric]*, ASTM International, West Conshohocken, PA Std., 2001. [Online]. Available: https://goo.gl/rH1ADB

[33] ——, *ASTM E18 - 03: Standard Test Methods for Rockwell Hardness and Rockwell Superficial Hardness of Metallic Materials.*, ASTM International, West Conshohocken, PA Std., 2003. [Online]. Available: https://goo.gl/Me5Yjm

[34] ——, *ASTM D785 - 08: Standard Test Method for Rockwell Hardness of Plastics and Electrical Insulating Materials.*, ASTM International, West Conshohocken, PA Std., 2015. [Online]. Available: https://goo.gl/fQYos4

[35] D. Venegas, J. YÁnez, S. Celi, C. Ayabaca, L. Tipanluisa, D. Bastidas, and M. Arrocha, "Mantenimiento necesario en instalaciones de GLP," in XXI Congreso Nacional de Ingeniería Mec ánica, Elche–España, 2016. [Online]. Available: https://goo.gl/KfujuH

[36] INEN, *NTE INEN-ISO 9095 Tubos de acero – Marcado de caracteres continuos y código de colores para la identificación de materiales.*, Servicio Ecuatoriano de Normalización Std, 2014. [Online]. Available: https://goo.gl/ixg1rn

Incentive pertaining to energy the generation distributed in Ecuador

Incentivo a la generación distribuida en el Ecuador

Jorge Patricio Muñoz-Vizhñay[1,*], Marco Vinicio Rojas-Moncayo[1],

Carlos Raúl Barreto-Calle[1]

Abstract

Reducing solar infrastructure costs is one of the main reasons for its global growth. In Ecuador adjustments to the legal framework have to be made to encourage the installation of small photovoltaic solar structures for electricity customers connected to low voltage distribution networks for their personal consumption, and any surplus energy be injected into the grid. Three business models pertaining to the distributed microgeneration of PV have been considered, for which we consider two applicable measurement systems: the first one is called "net metering" where the net value of the energy (the difference between the one injected into the network and the one consumed) is determined, and the second known as "Feed-in Tariff" - FIT where the energy injected into the grid is set at a special incentive price. The cost of energy produced by a photovoltaic system in Ecuador is USD/kWh 0.1342 with a discount rate 7%, CF (capacity factor) at 15%, while a discount rate 10%, CF at 20% the cost reduces to USD / kWh 0.1229. These values however, do not take into account the bank of batteries or the land, these values are increasingly more competitive in relation to non-conventional renewable sources.

Keywords: solar, photovoltaic, measurement, microgeneration, net, harmonic.

Resumen

La reducción de los costos de la infraestructura solar es una de las principales razones de su crecimiento mundial. En Ecuador se requiere realizar reajustes al marco jurídico que incentive la instalación de pequeños emprendimientos solares fotovoltaicos (de clientes del servicio eléctrico) conectados a las redes de distribución de baja tensión para consumo propio, y los excedentes sean inyectados a la red. Se plantean tres modelos de negocios para la microgeneración distribuida fotovoltaica, mismos que consideran dos sistemas de medición aplicables: el primero denominado *netmetering* donde se determina el valor neto de la energía (diferencia entre la inyectada a la red y la consumida), y el segundo conocido como «*Feed-in Tariff*» – FIT donde se determina la energía inyectada a la red a un precio especial como incentivo. El costo de la energía producida por un sistema fotovoltaico en el Ecuador es de USD/kWh 0,1342 con la tasa de descuento del 7 %, el CF (factor de capacidad) = 15 %, mientras que con la tasa de descuento del 10 %, CF = 20 % el costo de la energía alcanza a USD/kWh 0,1229, valores que no contemplan el banco de baterías ni de los terrenos, estos valores son cada vez más competitivos en relación con las fuentes renovables no convencionales.

Palabras clave: solar, fotovoltaico, medición, microgeneración, red, armónico.

[1,*]Faculty of Energy, Industries and Non-Renewable Natural Resources, Universidad Nacional de Loja, Ecuador. Author for correspondence ✉: jorgemunozv@yahoo.com ⓘ http://orcid.org/0000-0003-1293-5017, ⓘ http://orcid.org/0000-0002-1338-0095. ⓘ http://orcid.org/0000-0002-4886-2887.

1. Introduction

The intensive use of energy sources of fossil origin has caused significant environmental impacts in global terms, especially through the emission of CO_2, one of the main gases responsible for global warming of the planet or the socalled «greenhouse effect», which is a cause for climate change. Studies have determined that out of a total of 1 trillion tons of CO_2 released on the planet since the beginning of industrialization, 80% corresponds to emissions of the last 50 years [1]. For this reason, more and more non-conventional renewable energies are taking precedence around the world, with the development of new forms and applications, such as distributed or embedded generation in electrical distribution systems. Generally, distributed generation is defined as the generation of electricity by relatively small plants (less than 10 MW) in relation to the centralized plants, with sufficient capacity to allow their interconnection at any point of the electrical system considering the following aspects: end and location; nominal power and voltage level; and, characteristics of the energy delivery zone.

It is estimated that the installation of distributed generation leads to benefits by reducing costs in transmission and distribution losses in the order of 5 to 10% of all generated kWh, and there are also costs avoided in the expansion or repowering of transmission and distribution systems, cost reduction for infrastructure maintenance, increased reliability for consumers close to distributed generation, and faster attention to the growth of demand due to shorter implementation times in relation to centralized generation. Among the main disadvantages of distributed generation is the lack of coordination of protection equipment, the desensitization of protections, difficulties in reconnection, voltage variations, overvoltages, overvoltage resonance, harmonics [2].

2. Analysis of photovoltaic solar energy worldwide

2.1. Production of photovoltaic solar energy

The world energy supply went from 6,642 million tons of oil equivalent (TOE) in 1980, to 10,939 million TOE in 2005; to 12,170 million TOE in 2010; and, to 13,105 million TOE in 2015; with an average annual growth rate of 1.8%, in the last decade (2005-2015) [3]. In this period of 35 years, the global energy matrix did not present significant structural modifications in terms of the use of primary sources of energy. Thus, it is essential to consider new sources of less polluting primary energies, such as natural gas and renewable energies. In this field, photovoltaic solar energy has shown the greatest growth among renewable energies in recent years.

The installed global capacity of electricity in photovoltaic solar panels experienced exponential growth, reaching around 227 GWe by the end of 2015, producing about 1% of total electricity or 0.5% of total primary energy in the world [3–15]. This type of energy has been installed mainly in regions with fewer solar resources (Europe and China), while high resource regions (Africa and the Middle East) are still not exploited. During the last decade, Germany has been the leader of photovoltaic capacity installation, followed by China, Japan, Italy and the United States. The solar energy projections made for 2050 considers a high level of penetration with which participation may be between 18 and 31% of total generation [4–17].

Cost reduction of the solar infrastructure is one of the main reasons for global growth. The global costs of photovoltaic panels fell by 50% in the United States between 2006 and 2011, with an even more accentuated fall of 60% between 2011 and 2015 [5].

2.2. Distributed generation in low voltage mesh networks

The dynamic behavior of distributed generation is different from that of conventional machines (generators) because the time constants of the elements that compose them are small. Currently, the potential of distributed generation to contribute reactive power during and after a failure, thus improving short-term voltage stability, is emphasized. However, the greatest concern lies in the disconnection resulting from disturbances. Consequently, it is likely that in the case of disconnections, regulations impose an injection of reactive power in order to ensure the system's safety.

Consolidated Edison of New York Inc., a major American distribution company that serves densely populated metropolitan areas, points out the difficulty of sending power to the low voltage meshed grid with distributed generation points, and suggests using adequate protection systems to eliminate possible disconnections. Furthermore, it recommends dimensioning the generation in relation to the demand (keeping the distributed generation always lower than the minimum demand). The protection systems to be used can be minimum load relays or reverse power relays, or the use of dynamically controlled inverters that modulate the generation according to the load [7].

The difficulty of sending power to the network is due to the difficulty of coordinating distributed generation protection systems with those of the network.

2.3. Distributed generation business models (international case)

For companies in the electricity sector, the results cannot be only economic, they must also be measured in

terms of improving the quality of the service and of environmental benefits.

In the international arena, and specifically in the North American solar market, three business models are applied. Currently, with the modernization of the sector and the in-troduction of environmental goals for the generation of en-ergy, hybrid forms of these models have emerged.

Model 1. The electricity distributing companies own the photovoltaic solar generation assets and perform the installation, opera-tion and maintenance of the infrastructure in the company's own premises or those of residential or commercial custom-ers who receive payment for the use of roof space. The energy injected into the network belongs to the electricity companies.

Model 2. The electric distribution companies finance solar photovol-taic generation systems for customers and other stakehold-ers, taking into account the high initial investment costs for the acquisition of panels and other complementary equip-ment. Under this model, the excess generated energy is in-jected into the grid and customers can enjoy the economic compensation of energy (net of energy).

Model 3. The electric distribution companies hire solar photovoltaic energy generated by third parties through a PPA (power purchase agreement), avoiding any relationship with the microgenerators (consumers with generation). In this model, distribution compa-nies carry out traditional energy contract-ing activities for resale to consumers. The contracts are es-tablished with few generators avoiding relationships with micro generators or roof owners.

To facilitate the use of the energy resources of distribut-ed generation, it is essential that the agents of the wholesale and retail market have transparent and non-discriminatory access to electricity networks and measurement infor-mation. This can be consid-ered as something normal; how-ever, concerns grow when the local distribution company is also a market participant [8].

2.4. Intelligent networks for the control of distrib-uted generation

The fundamental key of a smart grid is the integra-tion of all the elements that are part of the electrical network. The concept refers to the incorporation of technologies to take a census, monitor, analyze the information of its elements and transmit it in real time for the best performance of the electrical net-works, controlling the power flows among which the distributed generation is located, detecting faults to produce automatic reconnection without affect-ing per-formance. This allows the areas of coordina-tion of protections, control, instrumentation, meas-urement, quality and energy management, etc., to be linked in a single management system with the primary ob-

jective of achieving an efficient and ration-al use of energy [9]. The implementation of smart grid systems in Ecuador is aligned with the execu-tion of distributed microgeneration projects.

2.5. Technical aspects for interconnection with the electrical network

Figures 1 and 2 presents forms of connection be-tween a home with photovoltaic generation and the electrical network, corresponding to model 2 de-scribed above. Figure 3 corresponds to model 3.
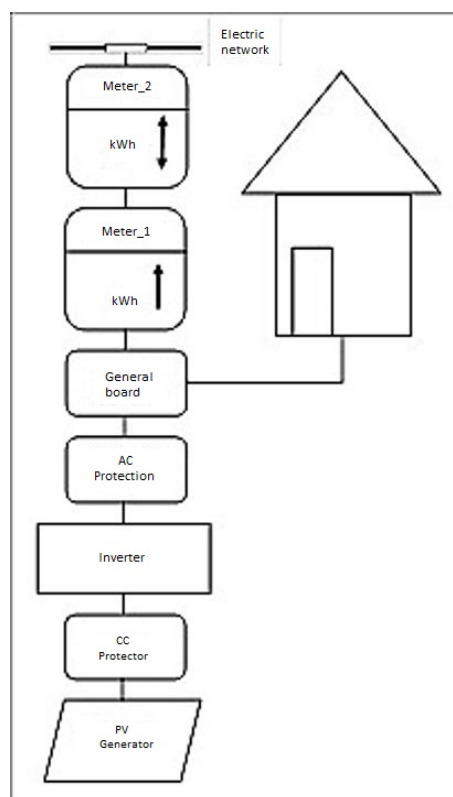
Figure 1. Recommended connection point when there is no incentive for photovoltaic distributed generation [9].

In Figure 1, photovoltaic energy is delivered to the load and the surplus is injected into the electricity net-work (distribution system). Meter 1 records the energy injected into the network. The advantage is that meter 2 rotates in one direction when energy is consumed by the client and in the opposite direction when it is injected into the network (the meter de-termines the net value of energy), this measurement system is known as netmetering [9].

In radial distribution systems with distributed gen-eration, the power flow can be in the substation—load direction, as well as in the load—substation direction. Therefore, the voltage drop can also occur in both directions. In this last case, situations could arise in which the upper voltage limits are exceeded in some

nodes depending on the amount of photovoltaic generation.

In the case of having some kind of remuneration to the surplus of photovoltaic energy, the connection indicated in Figure 2 can be started, prior to the regulation of the price of this surplus energy (meter 1 will record the surplus of injected energy to the network and meter 2 the energy consumed by the client, with the possibility of implementing a single smart meter). This system of surplus energy is known as «Feed-in Tariff» - FIT [9].
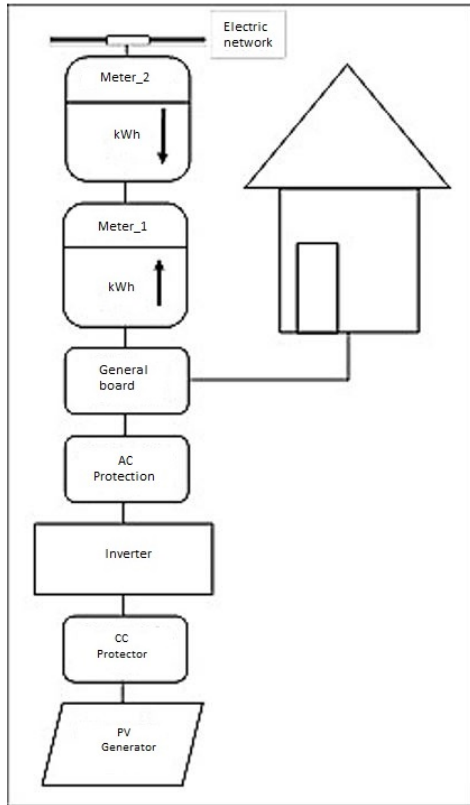
Figure 2. Recommended connection point when the surplus of the distributed photovoltaic generation has an incentive [9].

In Figure 3, corresponding to model 3, the customer is billed according to energy consumption (meter 2) at the applicable tariff, and the photovoltaic generation is sold to the electricity distribution company at a price regulated for that purpose (meter 1 will record the en-ergy injected into the network).

It is concluded that model 3 is the most feasible to install in Ecuador at the present time, because the pric-es of energy sold by distribution companies to final consumers is affected by a direct subsidy from the State, which would prevent a netting of the ex-cesses of photovoltaic generation in suitable economic condi-tions that guarantee investment recovery.

Therefore, it is convenient that the customer is in-voiced independently for the energy consumed by

the network, and that photovoltaic energy produced is billed independently at the appropriate price covering the costs of photovoltaic production established ac-cording to the methodology indicated in section 3.4.
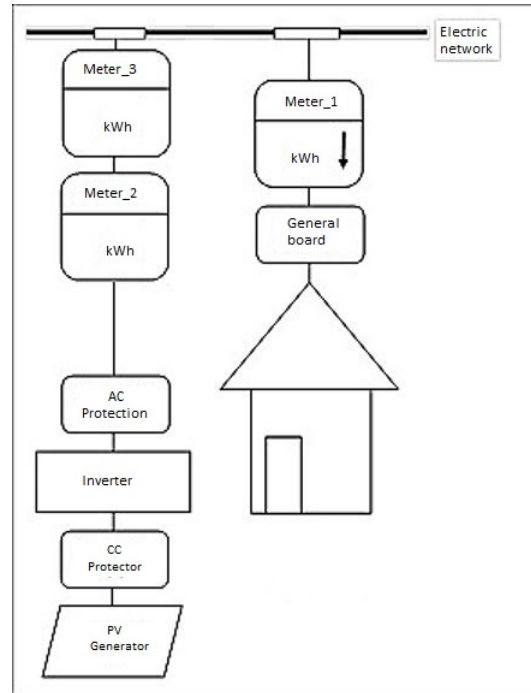
Figure 3. Recommended connection point when are incentives to distributed photovoltaic generation are in place [9].

2.6. Incentives for solar photovoltaic generation (international experiences)

Some countries are adopting financial incentive mechanisms for photovoltaic solar energy through the application of tariff systems such as the so-called feed-in tariff, which is the payment made by electricity distributing companies for energy generated and injected into the distribution networks by customers of the electric service [11].

Since 2006, the federal government of the United States provides a federal tax discount of 30% of the cost of acquiring solar photovoltaic systems for residential and com-mercial customers. In addition to the federal incentive, some states offer discounts on other taxes [11]. For example, Florida proposed an energy premium price over 20 years with a gradual reduction of the annual rate of 5%; Washington offered an incentive to this type of energy for residential and commercial con-sumers as well as public institutions. This incentive consisted of a fixed value (not linked to the kWh pro-duced) for a period of 5 years [16]. However, the net metering system is also one of the regulatory incen-tives used for photovoltaic solar energy in the United States. The model implements the concept that active energy produced with mini or distributed

microgenera-tion compensates the consumption of active energy demanded from the electricity grid by the customer. That is, the consumer pays the electricity distribution company the net value that results between the differ-ence of the energy consumed and the energy generated [12].

The per capita increase in electricity in the metropolitan areas of large cities contrasts the growing difficulty of building transmission and distribution lines and networks in these areas, which in some cases must be buried. For this reason, distributed generation will have a preponderant role in future regulation of the energetic matrix of those areas.

In the case of Brazil, by issuing a decree in 2004, for the first time the figure of distributed generator is created, delineating the market to be served. This mar-ket was basically constituted by the electricity distribu-tion companies, which could acquire up to 10% of their demand from distributed generators [8]. In this way, an important market niche opens up for photo-voltaic distributed generation, especially when commercial and industrial maximum generation coincides with the customers' peak demands.

After the Fukushima nuclear disaster in Japan, and the disabling of nuclear reactors, this country established incentive policies for distributed generation with non-conventional renewable energies, especially solar photovoltaic, for which, starting in 2012, the Feed-in Tariff (FIT) model became effective. The regulation contemplates prices for energy between 39.6 to 47.5 cUSD/kWh depending on generation capacity [9–16].

Germany is another country that has applied distributed generation by applying the Feed-in Tariff (FIT) model for capacities of less than 30 kW, with the dis-tribution companies under obligation to grant access and payment of the energy injected into the grid with prices of 24 cUSD/kWh, in addition to a set of state subsidies for the installation [9–16].

In England, as in Japan and Germany, the prices of distributed generation energy through the Feed-in Tariff (FIT) model are greater than the energy demanded to encourage households to install photovoltaic panels in their houses. Energy prices include values between 19.8 and 24.3 cUSD/kWh for capacity ranges up to 50 kW [9–16].

In Spain, the Feed-in Tariff (FIT) system was implemented, granting a prize price calculated on the base of the market rate, financing lines, providing spe-cial investment conditions and fiscal incentives [16].

The application of preferential prices for distribut-ed generation in these countries has been adequate, considerably increasing generation through non-conventional renewable sources, especially solar photovoltaic energy.

In Ecuador, the Organic Law of Public Electric Power Service does not contemplate the exemption of tariffs, taxes and other charges that affect the importa-tion of materials and equipment not produced in the country, for the installation of systems destined to the use of non-conventional renewable energies such as solar energy.

3. Analysis of photovoltaic generation in Ecuador

3.1. Solar potential in Ecuador

Through the former National Electricity Council - CONELEC, Ecuador developed a solar Atlas for electric generation purposes. The data presented in Figure 4presents the global solar energy averaged from total daily sunlight values (direct and diffuse), expressed in $Wh/m^2/day$. In this Figure we can see the areas with the highest sunlight in the country and, therefore, with the greatest potential for photovoltaic generation, as is the case of the provinces of Loja, Imbabura and Carchi [6].

The approximate average value of global solar radiation in Ecuador is $4,575 Wh/m^2/day$.

The estimated solar potential for power generation purposes in the country is 312 GW equivalent to 456 TWh per year or 283 MBEP (million barrels of oil equivalent) per year. This value is approximately fifteen (15) times the technical and economically usable hydroelectric potential of the country.

In spite of Ecuador having a high energy potential, the development of photovoltaic solar energy is still incipient, particularly in distributed microgeneration; for September 2017, ARCONEL reports that effective capacity for this type of energy was 25.6 MW, which represented 0.34% of the country's total capacity, having produced 35.3 GWh/year equivalent to 0.15% of total production of energy. In addition, in Ecuador there is no information regarding photovoltaic panels that can be categorized as distributed microgeneration. The aforementioned statistical information refers to photovoltaic power plants with a capacity between 0.37 MW and 1 MW, with the vast majority of plants close to the latter val-ue.

3.2. Photovoltaic generation residential load

The analysis of the typical residential load curve in Ecuador, per unit (pu) named P in relation to the pho-tovoltaic generation in pu, named PV, as well as the result of the difference of P — PV (see Figure 5), leads to the conclusion that there will be energy flow in the direction from the electricity network to the res-idence between 16.30 to 9.00, and the flow will be reversed (from PV generation to the electricity grid) from 9.00 to 16.30, relieving the distribution system. This schedule could be shifted in time according to the load curve P. At the time (period) of maximum residential load demand (P) (between 19.00 and 20.00), the
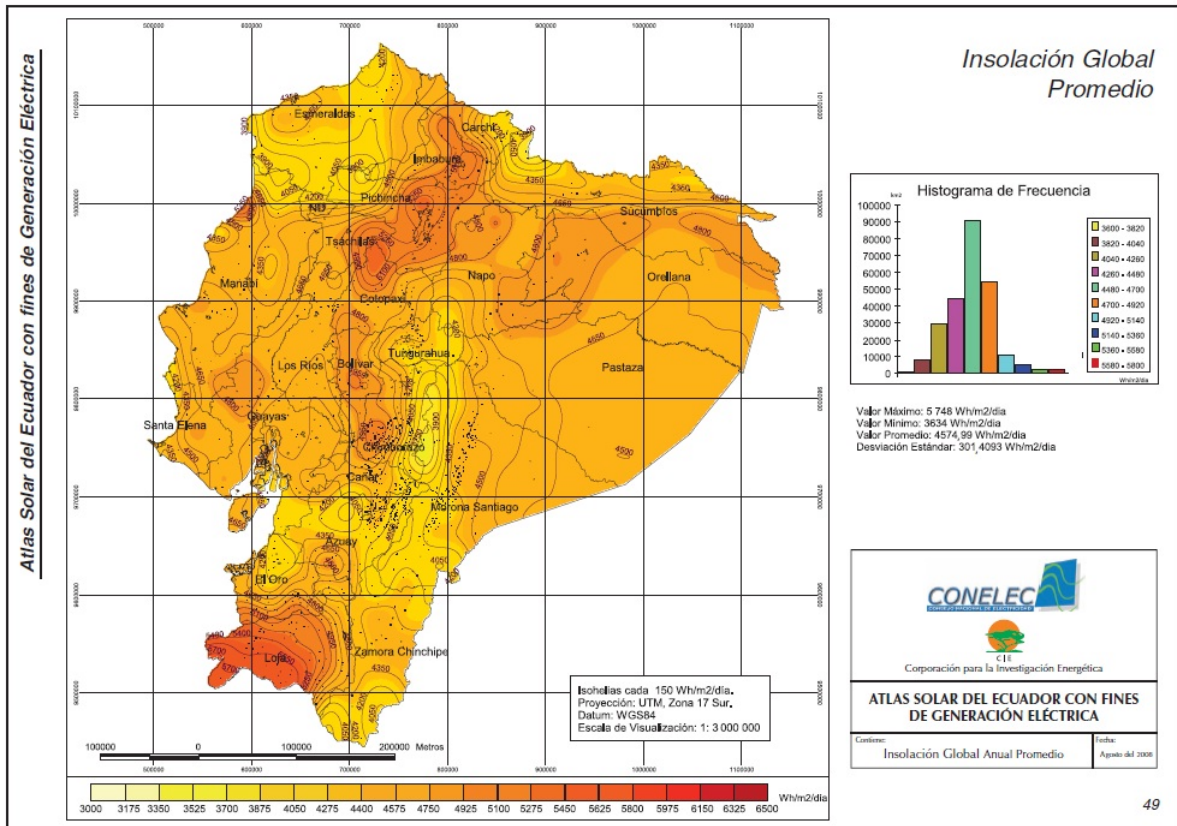
Figure 4. Solar map of Ecuador for power generation purposes [6].

PV photovoltaic generation does not re-duce the flow of energy absorbed by the residence to the electricity network due to the absence of a battery bank.
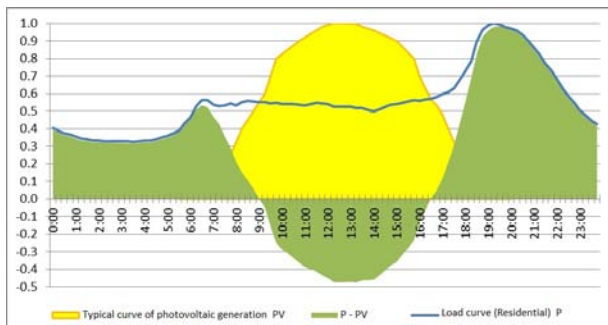
Figure 5. Residential load curve resulting from the use of pho-tovoltaic generation [10].

The power factor of the electric network in the inter-connection node (electricity-customer network) is gradually decreasing as photovoltaic generation in-creases, because active power is decreasing while reac-tive power will be supplied by the network (variation of the power triangle). The IEC 61727 standard states that the power factor must be greater than 0.9 induc-tive when the load of the inverter is greater than 50%.

The harmonic voltage distortions introduced in the network by photovoltaic generation are a consequence of the voltage drop coming from the harmonic currents produced by the inverter that cross the impedances of the network. Total harmonics should be analyzed based on the number of individual photovoltaic panels connected to the network. According to IEC 61727, the total distortion of current harmonics must be less than 5% at the inverter output.

One of the specific requirements of IEC 61727 re-lated to voltage levels, indicates that it should be in the range between 85% and 110% of the nominal voltage of the electrical network. Likewise, the frequency must vary a maximum ± 1 Hz from the nominal fre-quency of the network.

The insertion of photovoltaic panels in the electri-cal networks in low tension leads, as a consequence, to an increased lifespan of distribution transformers (MT/BT) for load relief, in addition to allowing the entrance of new consumers without modifying their capacity [10].

3.3. Ecuadorian regulatory framework

In Ecuador, the Organic Law of Public Electric Power Service does not clearly specify the aspects necessary so that small photovoltaic ventures (natural persons), connected to the distribution networks (low voltage) can produce energy for their own consumption and sur-

pluses for marketing through the electricity net-work. In this area, there is a need for the law to con-template regulations, rules, etc., for the implementation of distributed generation with non-conventional re-newable technologies, especially solar photovoltaics for the residential or domestic sector, due to the high energy potential determined by the levels of sunshine, by granting different types of incentives. Electric dis-tribution companies based on these new regulations should facilitate the participation of distributed genera-tion and carry out ex ante technical validation activi-ties, to ensure that there are no restrictions in the elec-tricity grid and its ex post verification [7].

Taking Japan and Germany, which established higher tariffs for the energy injected into the network in relation to the invoicing price for the customer's consumption, as points of reference with the purpose of establishing incentives for a real possibility of savings in electric payments on a medium and long term, this FIT incentive system presents lower risk to the investor and produces—over the years—a reduction of the incentive (reward) according to the decrease of investment costs of energy technology, differentiating the size of the plant and the geographical location in a way that allows a homogeneous technology distribution. In addition, this regulatory FIT instrument has been widely imple-mented in Spain and Denmark [13–16].

Until recently, Ecuador applied a policy of preferential prices for non-conventional renewable sources (wind, biomass and biogas, geothermal and hydroelectric) in the production of electricity that could be said to correspond to a Feed-in Tariff system, this incentive was established through the Codified Regulation N.° CONELEC 001/13, which was repealed in June 2016 [14]. This regulation did not contemplate any price for photovoltaic solar energy, revealing a strong deficien-cy in the incorporation of this type of renewable energy.
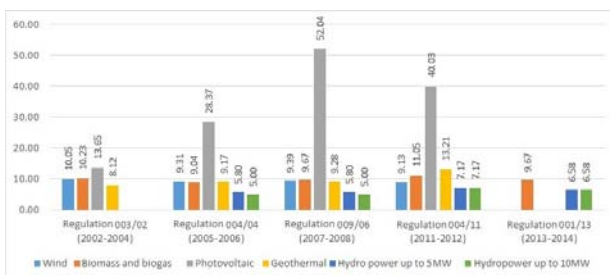
Figure 6. Renewable energy prices in Ecuador.

Figure 6 shows the evolution of prices approved by the former CONELEC in just over a decade, where the highest price for photovoltaic solar energy occurs in 2007 and 2008 (gray bars).

3.4. Costs for implementation of photovoltaic genera-tion in Ecuador

The cost of photovoltaic generation depends on the investment costs of the equipment, the costs of operation and maintenance, the energy delivered by the panels and the capacity factor.

As an example, a contracting process of 75 kWp has been taken through the public procurement platform. The average import cost of the modules reached USD/Wp 1.11 and the investors USD/Wp 0.32. This amount must also include national components of labor, support materials for the modules, wiring, and the necessary protective equipment for the installation, which in sum reaches USD/Wp 0.27 (this does not consider the cost of the land nor batteries). Thus, the total investment cost for photovoltaic generation is USD/Wp 1.69. The cost of energy can be calculated by applying the following expression [8–11]:

$$ C = \left\{ \left[\frac{r \times (1+r)^N}{(1+r)^N - 1} \right] + OM \right\} \frac{I_{nv}}{8.76 \times C_F} \qquad (1) $$

Considering, the discount rate r = 7% as an opportunity cost; The useful life of the system N = 20 years; the annual operation and maintenance costs OM = 1% of the total cost of the investment; the total initial investment Inv = 1690 USD/kWp; and, the capacity factor CF = 15%; in this way, the cost of the energy produced by the photovoltaic system is cUSD/kWh 13.42. Applying the same expression with capacity factor CF = 20% for another place in Ecuador with high levels of sunshine, the cost of energy reaches cUSD/kWh 10.74. These values are increasingly com-petitive in relation to the production of hydroelectric energy and other non-conventional renewable ener-gies. Depending on the geographical location in which the photovoltaic solar panels are installed, the cost of producing the energy could vary between the values recorded. It is estimated that by the year 2020, it will be possible for the cost of solar photovoltaic energy to be reduced to such an extent that it will become a competitive energy source in comparison with conven-tional technologies. Concomitantly, policies should adapt to avoid negative externalities compared to other types of unconventional renewable energies [16].

3.5. Need to create a regulatory framework in Ecuador for the development of photovoltaic generation

It is advisable to adapt the legal framework of the Ec-uadorian electric sector, which would encourage the installation of distributed mini and microgeneration with the use of non-conventional renewable energies, especially solar photovoltaics, considering the ade-quate levels of sunshine existing in Ecuador, allowing for investment in the private sector for this type of

initiatives, and creating the right incentives for such investment to be possible. For this purpose, the first step is to establish a power quota that can be developed in photovoltaic generation for each distribution company and each type of customer, and which does not affect the operation of the distribution system. Additionally, it must be ensured that prices paid for said production, while they incorporate an incentive to the investment, do not cause an economic imbalance to the distribu-tors.

In the reforms to the legal framework, the application of a FIT is recommended, for which prices of the energy injected into the distribution network should be established, which could be in the order of 20.0 cUSD/kWh and capacity ranges of up to 4 kW for residential customers, for a period of 20 years. The range of capacity for commercial and industrial customers should be determined based on studies that demonstrate its feasibility. Distribution companies will carry out traditional energy contracting activities for resale to consumers, which could be referred to as the application of the modified model 3 indicated in section 2.3. In this way, customers who are part of the program would have economic benefits of the 2:1 order in terms of the rela-tionship between the price of the energy injected into the grid versus the billing price of the energy purchased from the distributor.

4. Conclusions and recommendations

The generation of distributed electric power through photovoltaic solar systems is an excellent alternative for the management of supply expansion, especially for models in which distributed generation is considered.

In Ecuador there is no legal framework that encourages the participation of distributed mini and microgeneration with non-conventional renewable energies, especially in the case of photovoltaic solar energy.

A reformation of the Ecuadorian legal framework is adviced, so it includes incentives for the installation of distributed generation by residential, commercial and industrial customers through renewable energy systems, especially photovoltaics. Among the incentives, the elimination of tariffs in the importation of equipment, preferential prices in the sale of energy to the electricity distributing companies, and ease of in-terconnection to the distribution networks should be considered.

The application of the Feed-in Tariff (FIT) model is recommended, for which prices of the energy injected into the distribution network should be established, which could be in the order of 20.0 cUSD/kWh, capacity ranges of up to 4 kW for residential customers, for a period of 20 years. The range of capacity for commercial and industrial customers should be determined based on studies that demonstrate its feasibility.

The Ministry of Electricity and Renewable Energy is leading the implementation process in electricity companies of a series of automation systems (SCADA, intelligent measurement, DMSOMS, etc.), which in the future will facilitate the installation of distributed mi-crogeneration.

Acknowledgements

References

[1] J. A. Aguilera, "Fuentes de energía y protocolo de Kioto en la evolución del sistema eléctrico español," Ph.D. dissertation, Universidad de Oviedo, 2012. [Online]. Available: https://goo.gl/s8A6g3

[2] T. K. V. Hernández, "Uma proposta de integração da geração distribuida, por meio das usinas virtuais, ao sistema elétrico do estado de São Paulo," Master's thesis, Universidade de São Paulo, 2016. [Online]. Available: https://goo.gl/NXABQY

[3] IEA. (2017) Key world energy statistics. International Energy Agency. [Online]. Available: https://goo.gl/SHD6vM

[4] BP. (2017) Statistical review of world energy. [Online]. Available: https://goo.gl/PNqktm

[5] IRENA. (2017) Estadísticas de capacidad renovable 2017. International Renewable Energy Agency. [Online]. Available: https://goo.gl/Lp2F5b

[6] OLADE. (2008) Atlas solar del Ecuador con fines de generación eléctrica. Organización Latinoamericana de Energía. [Online]. Available: https://goo.gl/xyQQTt

[7] G. Barreto, "Metodología de aplicação de geração distribuída fotovoltaica em baixa tensão nos reticulados subterraneos das distribuidoras de energia elétrica," Ph.D. dissertation, Universidade de São Paulo, 2014. [Online]. Available: https://goo.gl/W93aLG

[8] R. Benedito, "Caracterização da geração distribuída de eletricidade por meio de sistemas fotovoltaicos conectados á rede, no brasil, sob os aspectos técnico, econômico e regulatorio," Master's thesis, Universidade de São Paulo, 2009. [Online]. Available: https://goo.gl/q47eJV

[9] IRENA. (2017) Boosting global pv markets: The role of quality infrastructure. [Online]. Available: https://goo.gl/YyaRRa

[10] A. F. Pinto, "Avaliação dos impactos de sistemas fotovoltaicos conectados á rede de distribuição de baixa tensão," Ph.D. dissertation, Universidade de São Paulo, 2016. [Online]. Available: https://goo.gl/Qof7Xs

[11] M. P. Almeida, "Qualificação de sistemas fotovoltaicos conectados á rede," Master's thesis, Universidade de São Paulo, 2012. [Online]. Available: https://goo.gl/MQZ6Pw

[12] IRENA. (2017) Renewable energy benefits leveraging local capacity for solar pv. [Online]. Available: https://goo.gl/UhY1Yn

[13] ——. (2017) Adapting market design to high shares of variable renewable energy. [Online]. Available: https://goo.gl/iMmWei

[14] ARCONEL. (2017) Normativa y regulaciones. [Online]. Available: https://goo.gl/RFuerV

[15] World Energy Council. (2010) World energy. issues monitor 2017. [Online]. Available: https://goo.gl/B1eZvT

[16] S. M. K. Barbosa, "A competitividade das fontes energéticas em uma abordagemde learning curves: Uma proposição de regulação que incentive as tecnologias renováveis," Ph.D. dissertation, Universidade de São Paulo, 2016. [Online]. Available: https://goo.gl/u6i8AN

[17] World Energy Council. (2010) World energy perspectives. renewables integration 2016. [Online]. Available: https://goo.gl/xENr7B

ON THE BEHAVIOUR OF SPHERICAL INCLUSIONS IN A CYLINDER UNDER TENSION LOADS

ESTUDIO DEL COMPORTAMIENTO DE INCLUSIONES ESFÉRICAS EN UN CILINDRO BAJO TRACCIÓN

Sebastián Montero[1], Roger Bustamante[1,*], Alejandro Ortiz-Bernardin[1]

Abstract

In the present paper the behaviour of a hyperelastic body is studied, considering the presence of one, two and more spherical inclusions, under the effect of an external tension load. The inclusions are modelled as nonlinear elastic bodies that undergo small strains. For the material constitutive relation, a relatively new type of model is used, wherein the strains (linearized strain) are assumed to be nonlinear functions of the stresses. In particular, a function is used that keeps the strains small, independently of the magnitude of the external loads. In order to simplify the problem, the hyperelastic medium and the inclusions are modelled as axial-symmetric bodies. The finite element method is used to obtain results for these boundary value problems. The objective of using these new models for elastic bodies in the case of the inclusions is to study the behaviour of such bodies in the case of concentration of stresses, which happens near the interface with the surrounding matrix. From the results presented in this paper, it is possible to observe that despite the relatively large magnitude for the stresses, the strains for the inclusions remain small, which would be closer to the actual behaviour of real inclusions made of brittle materials, which cannot show large strains.

Resumen

En el presente artículo se estudia el comportamiento de un sólido hiperelástico con una, dos y más inclusiones esféricas, bajo el efecto de una carga externa de tracción. Las inclusiones se modelan como sólidos elásticos con comportamiento no-lineal y que presentan pequeñas deformaciones, usando un nuevo modelo propuesto recientemente en la literatura, en donde las deformaciones (caso infinitesimal) se expresan como funciones no-lineales de las tensiones. En particular, se consideran expresiones para dichas funciones que aseguran que las deformaciones están limitadas en cuanto a su magnitud independientemente de la magnitud de las cargas externas. Como una forma de simplificar el problema, el medio hiperelástico y las inclusiones se modelan como sólidos axil-simétricos. El método de elementos finitos es usado para obtener resultados para estos problemas de valor de frontera. El objetivo del uso de los nuevos modelos para cuerpos elásticos para el caso de las inclusiones, es estudiar el comportamiento de dichos cuerpos en el caso de concentración de tensiones, lo cual ocurre cerca de la zona de interface con la matriz. De los resultados mostrados en este trabajo, es posible apreciar que a pesar de los valores relativamente altos para las tensiones, las deformaciones se mantienen pequeñas, lo cual sería mucho más cercano al comportamiento esperado en la realidad, cuando se trabaja con inclusiones hechas de un material frágil, el cual no puede mostrar grandes deformaciones.

Keywords: Nonlinear elasticity, Strain limiting behaviour, Finite element method, Constitutive equations, Elastic bodies, Isotropic bodies

Palabras clave: elasticidad no-lineal, límite para las deformaciones, método de elementos finitos, ecuaciones constitutivas, cuerpos elásticos, cuerpos isotrópicos.

[1,*]Department of Mechanical Engineering, University of Chile – Chile. Author for correspondence ✉:
rogbusta@ing.uchile.cl. ⬦ https://orcid.org/0000-0002-2402-6139, ⬦ https://orcid.org/0000-0002-1072-1042
⬦ https://orcid.org/0000-0001-9221-2470

1. Introduction

In Refs. [1–3] Rajagopal and co-workers have proposed some new types of constitutive relations, which cannot be classified as either Green or Cauchy elastic equations. If $\mathbf{T}$ and $\mathbf{B}$ are used to denote the Cauchy stress tensor and the left Cauchy Green tensor, respectively, one of such relations is $\boldsymbol{f}(\mathbf{T}, \mathbf{B}) = \mathbf{0}$, and two special cases that can be obtained from the above implicit relation are the classical nonlinear constitutive equation for a Cauchy elastic body [4] $\mathbf{T} = \boldsymbol{g}(\mathbf{B})$, and the subclass $\mathbf{B} = \boldsymbol{h}(\mathbf{T})$ (see, for example, Ref. [5]).

As a particular case, we assume that the gradient of the displacement field is small. From the above equation $\mathbf{B} = \boldsymbol{h}(\mathbf{T})$, we obtain $\boldsymbol{\varepsilon} = \boldsymbol{g}(\mathbf{T})$, where $\boldsymbol{\varepsilon}$ is the linearized strain tensor. This last constitutive equation is very important on its own, since it could be used to model the behaviour of some materials that can show a nonlinear behaviour, but where the strains are small, such as rock [6, 7], concrete [8] and some metal alloys [9]. Another important use of $\boldsymbol{\varepsilon} = \boldsymbol{g}(\mathbf{T})$ is in the fracture mechanics analysis of brittle bodies [10], where for some particular expressions for $\boldsymbol{g}(\mathbf{T})$, it can be proved that for a crack in a brittle body, the magnitude of the strains are limited and do not go to infinite near the tip of a crack, contrary to what happens when the classical linearized elastic theory is used (see, for example, Ref. [11]). It is very important to study the behaviour of elastic bodies considering $\boldsymbol{\varepsilon} = \boldsymbol{g}(\mathbf{T})$ for as many different boundary value problems as possible, in order to understand the capabilities and drawbacks of these new constitutive models, and that is the main objective of the present communication.

We are interested in studying the behaviour of a hyper-elastic (Green solid) cylindrical sample that can contain 1, 2 and 5 spherical inclusions, which are located in a row in the central axis of the cylinder, and which are equally separated from each other. The inclusions are assumed to behave as nonlinear elastic solids, using the new constitutive equation $\boldsymbol{\varepsilon} = \boldsymbol{g}(\mathbf{T})$ mentioned above[1]. For simplicity the composite sample is modeled as an axial-symmetric body and a tension load is applied on the upper part of the cylinder. The finite element method is used to obtain results for the boundary value problem. We are particularly interested in studying the behaviour of the stresses and strains near the interface of the inclusions and the surrounding hyper-elastic body. It is assumed that the spherical inclusions are perfectly attached to the hyper-elastic matrix. The hypothesis of our work is that the new classes of constitutive equations $\boldsymbol{\varepsilon} = \boldsymbol{g}(\mathbf{T})$ can be useful for the modelling of brittle bodies, in particular in the case we have large stresses, but where the strains must remain small. For a cylindrical sample with inclusions, such concentration of stresses appear near the interface of the matrix and the inclusion, and as it is shown in the present work, considering a particular expression for $\boldsymbol{g}(\mathbf{T})$, that we indeed obtain small strains for the spherical inclusions. For the modelling of such composite materials is very important to obtain results as precise as possible of the stresses near the interface, as the most common failure, which such composites show, corresponds to the debonding of the particles with the surrounding matrix.

This work is structured into the following sections. In Section 2 we present the basic equations for the models, in particular, the constitutive equations used for the spherical inclusions. In Section 3 we give details about the models to be analyzed. In Section 4, some numerical results for the different cases analyzed are presented. We end in Section 5 with some concluding remarks about the numerical results presented in this paper.

2. Basic equations

2.1. Kinematics and equation of motion

Let X denotes a point of a body $\mathcal{B}$, the reference and current configurations are denoted as $\mathcal{B}_r$ and $\mathcal{B}_t$, respectively, and the position of point X in such configurations is denoted as $\mathbf{X}$ and $\mathbf{x}$, respectively. It is assumed that there is a one-to-one mapping $\boldsymbol{\chi}$ such that $\mathbf{x} = \boldsymbol{\chi}(\mathbf{X}, t)$, where t is time. The deformation gradient $\mathbf{F}$, the left and the right Cauchy-Green tensors $\mathbf{B}$, $\mathbf{C}$, respectively, the Green Saint-Venant strain tensor $\mathbf{E}$, the displacement field $\mathbf{u}$ and the linearized strain tensor $\boldsymbol{\varepsilon}$ are defined as:

$$\mathbf{F} = \frac{\partial \boldsymbol{\chi}}{\partial \mathbf{X}}, \quad \mathbf{B} = \mathbf{F}\mathbf{F}^{\mathrm{T}}, \quad \mathbf{C} = \mathbf{F}^{\mathrm{T}}\mathbf{F}, \quad (1)$$

$$\mathbf{E} = \frac{1}{2}(\mathbf{C} - \mathbf{I}), \quad \mathbf{u} = \mathbf{x} - \mathbf{X}, \quad (2)$$

$$\boldsymbol{\varepsilon} = \frac{1}{2}(\nabla\mathbf{u} + \nabla\mathbf{u}^{\mathrm{T}}). \quad (3)$$

Where ∇ is the gradient operator with respect to the reference configuration. We assume $0 < J < \infty$, where $J = \det \mathbf{F}$.

The equation of motion is

$$\rho\ddot{\mathbf{x}} = \operatorname{div}\mathbf{T} + \rho\mathbf{b}, \quad (4)$$

where ρ is the density of the body in the current configuration, $\mathbf{T}$ is the Cauchy stress tensor, $\mathbf{b}$ represents the body forces in the current configuration, $(\ddot{})$ is the second derivative in time, and div is the divergence operator defined in the current configuration.

---

[1] See Ref. [12] for a recent work on the modelling of composites considering an extension of such new constitutive equations $\boldsymbol{\varepsilon} = \boldsymbol{g}(\mathbf{T})$ for viscoelastic deformations.

In our work we consider quasi-static deformations, therefore the left side of (4) is zero. More details about the above relations can be found, for example, in Ref. [13].

2.2. Constitutive equations

We consider a body composed of two materials, a matrix which is assumed to be hyper-elastic, filled with spherical inclusions which are assumed to behave as nonlinear elastic bodies undergoing small strains. For the hyper-elastic matrix cylinder, we assume there exists a function $W = W(\mathbf{F})$, called the energy function, such that (see, for example, Ref. [4])

$$\mathbf{T} = J^{-1}\mathbf{F}\frac{\partial W}{\partial \mathbf{F}}, \tag{5}$$

where we use the convention $\left(\frac{\partial W}{\partial \mathbf{F}}\right)_{\alpha i} = \frac{\partial W}{\partial F_{i\alpha}}$. In this work, we use the neo-Hookean compressible model

$$W = \frac{\mu}{2}(\bar{I}_1 - 3) + \frac{\kappa}{2}(J - 1)^2, \tag{6}$$

where $\bar{I}_1 = J^{-1/3}I_1$, $I_1 = \text{tr}(\mathbf{C})$, where tr is the trace of a second order tensor, and μ, κ are material constants.

For the inclusions, we assume that they are elastic bodies that develop nonlinear behaviour when strains are small. As indicated in the introduction section, recently some new types of constitutive relations for elastic bodies have been proposed in the literature [1–3], one of such relations is of the form

$$\boldsymbol{f}(\mathbf{T}, \mathbf{B}) = \mathbf{0}, \tag{7}$$

where the Cauchy elastic body $\mathbf{T} = \boldsymbol{g}(\mathbf{B})$ is a special subclass of the above relation, plus the new constitutive equation

$$\mathbf{B} = \boldsymbol{h}(\mathbf{T}). \tag{8}$$

Assuming that $|\nabla\mathbf{u}| \sim O(\delta)|$ where $\delta \ll 1$, then $\mathbf{B} \approx 2\boldsymbol{\varepsilon} + \mathbf{I}$ (we also have $\mathbf{E} \approx \boldsymbol{\varepsilon}$), and from (8) we obtain (see, for example, Refs. [14,15])

$$\boldsymbol{\varepsilon} = \boldsymbol{g}(\mathbf{T}), \tag{9}$$

where in general $\boldsymbol{g}(\mathbf{T})$ is a nonlinear function of the stress tensor. We consider a special case of (9), where we assume there exists a scalar function $\Pi = \Pi(\mathbf{T})$ such that (see Ref. [16])

$$\boldsymbol{\varepsilon} = \boldsymbol{g}(\mathbf{T}) = \frac{\partial \Pi}{\partial \mathbf{T}}. \tag{10}$$

If Π is assumed to be an isotropic function, we have that $\Pi(\mathbf{T}) = \Pi(J_1, J_2, J_3)$, where J_i, $i = 1, 2, 3$ are the following set of invariants of the stress tensor

$$J_1 = \text{tr}\mathbf{T}, \quad J_2 = \frac{1}{2}\text{tr}(\mathbf{T}^2), \quad J_3 = \frac{1}{3}\text{tr}(\mathbf{T}^3). \tag{11}$$

And from (10), we obtain the representation

$$\boldsymbol{\varepsilon} = \Pi_1\mathbf{I} + \Pi_2\mathbf{T} + \Pi_3\mathbf{T}^2, \tag{12}$$

where $\Pi_i = \frac{\partial \Pi}{\partial J_i}$, $i = 1, 2, 3$.

The following particular expression for Π is considered:

$$\Pi(J_1, J_2) = -\frac{\alpha}{\beta}\ln[\cosh(\beta J_1)] + \frac{\gamma}{\iota}\sqrt{1 + 2\iota J_2}, \tag{13}$$

where α, β, γ and ι are constants.

Eq. (13) has been used in Ref. [17] to study problems, where independently of the magnitude of the stresses, the strains remains small. It is necessary to point out that this form for Π and the numerical values of the constant that are shown in Chart 1, have not been obtained from experimental data. In Figures 1, 2 presented in Ref. [17], some plots for the behaviour of a cylinder under tension are shown, where it is possible to observe that the strains remain always small independently of the magnitude of the stresses. As indicated in the introduction section, such particular expressions could be important for fracture analysis of brittle bodies.

Finally, in Chart 1 the numerical values of the constants used in (6) and (13) are presented.

Chart 1. Values for the constants used in (6) and (13).

α	β	γ	ι	μ	κ
	1/Pa	1/Pa	1/Pa^2	Pa	Pa
0.01	9.277×10^{-8}	4.020×10^{-9}	10^{-14}	80.194×10^6	150×10^6

2.3. Boundary value problems

For the hyper-elastic cylinder, the boundary value problem is the classical formulation in nonlinear elasticity, where the function $\boldsymbol{\chi}(\mathbf{X})$ is found by solving the equilibrium equation in the reference configuration (see, for example, Ref. [4])[2]:

$$\text{Div}\mathbf{S} = \mathbf{0}, \tag{14}$$

where $\mathbf{S} = J^{-1}\mathbf{F}\mathbf{T}$ is the nominal stress tensor. From (5), $\mathbf{S} = \frac{\partial W}{\partial \mathbf{F}}$, and Div is the divergence operator with respect to the reference configuration. Eq. (14) must be solved using the boundary conditions

$$\mathbf{S}^{\text{T}}\mathbf{N} = \hat{\mathbf{s}} \quad \mathbf{X} \in \partial\mathcal{B}_r^s, \quad \boldsymbol{\chi} = \hat{\mathbf{x}} \quad \mathbf{X} \in \partial\mathcal{B}_r^x, \tag{15}$$

where $\partial\mathcal{B}_r$ is the boundary of the hyper-elastic body in the reference configuration, $\partial\mathcal{B}_r^s \cup \partial\mathcal{B}_r^x = \partial\mathcal{B}_r$, $\partial\mathcal{B}_r^s \cap \partial\mathcal{B}_r^x = \varnothing$, $\mathbf{N}$ is the outward normal vector to the surface of the body in the reference configuration, $\hat{\mathbf{s}}$ is the external traction (described in the reference

---

[2]In this paper we do not consider the effect of body forces.

configuration), and $\hat{\mathbf{x}}$ is a known deformation field on some part of the surface of the hyper-elastic body.

For the inclusions we consider small strains and displacements. And following what has been presented in Refs. [16, 17], for the boundary value problem corresponds to find $\mathbf{T}$ and $\mathbf{u}$ by solving (see (3), (4) and (10))

$$\text{div}\mathbf{T} = \mathbf{0}, \quad \frac{1}{2}(\nabla\mathbf{u} + \nabla\mathbf{u}^{\mathrm{T}}) = \frac{\partial\Pi}{\partial\mathbf{T}} \qquad (16)$$

simultaneously. In the above system we have 9 equations for a fully 3D problem, and 9 unknowns that correspond to the components of the stress tensor and the displacement field. Regarding the boundary conditions we have in general

$$\mathbf{Tn} = \hat{\mathbf{t}} \quad \mathbf{x} \in \partial\mathcal{B}_t^t, \quad \mathbf{u} = \hat{\mathbf{u}} \quad \mathbf{x} \in \partial\mathcal{B}_t^u, \qquad (17)$$

where $\partial\mathcal{B}_t$ is the surface of the inclusion and $\mathbf{x} \in \partial\mathcal{B}_t^t \cup \partial\mathcal{B}_t^u = \partial\mathcal{B}_t$, $\partial\mathcal{B}_t^t \cap \partial\mathcal{B}_t^u = \varnothing$, $\mathbf{n}$ is the normal vector to the surface of the inclusion, $\hat{\mathbf{t}}$ is the external load and $\hat{\mathbf{u}}$ is a known displacement field on a part of the surface of the inclusion. Since for the inclusion we assumed that $|\nabla\mathbf{u}| \sim O(\delta)|$ where $\delta \ll 1$, then there is no need for distinguishing between the reference and the current configuration for that body.

3. Axial-symmetric models

For simplicity, the hyper-elastic matrix is considered to be a cylinder of radius R and length L (see, for example, Figure 1).

For a cylinder with one inclusion, it is assumed that the inclusion is located in the center of the cylinder, and that the radius of that spherical body is r_i (see Figure 1). It is assumed that there is axial symmetry, therefore, we study a plane problem using the coordinates r and z (radial and axial axis, respectively).
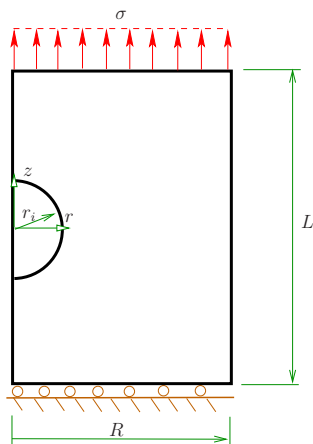
Figure 1. Hyper-elastic cylinder with one inclusion.

The center of the sphere is located at $z = L/2$. On the surface $z = L$ we apply a uniform axial load σ. On

the surface $z = 0$ we assume that the cylinder cannot move in the axial direction, but it is free to expand in the radial direction, i.e., $u_z(r, 0) = 0$. On the surface $r = R$ we assume that the cylinder is free. Finally, the spherical inclusion is assumed to be perfectly bonded to the the surrounding hyper-elastic cylinder, i.e., the displacement field is continuous across the surface of the inclusion.

In Figure 2, an hyper-elastic cylinder with two inclusions is depicted.
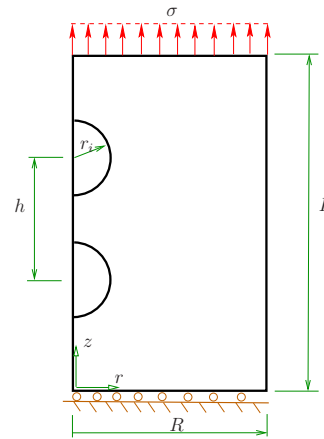
Figure 2. Hyper-elastic cylinder with two inclusions.

These two inclusions are of the same radius, are separated by a distance h between centers (the central point between them is located in the middle of the cylinder in the axial line defining it.) The two inclusions are assumed to behave as nonlinear elastic bodies using (10). The rest of the boundary conditions for the problem are the same as the problem presented in Figure 1.

In Figure 3, the case of an hyper-elastic cylinder with five inclusions in a row is presented.
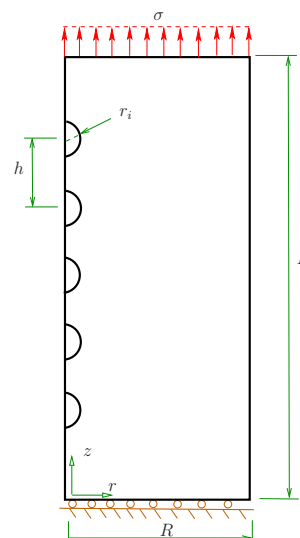
Figure 3. Hyper-elastic cylinder with five inclusions.

The inclusions are separated to each other by the same distance h. As in the previous case, they are modelled using (10), and the center point for all the inclusions is located in the center of the cylinder.

For the different models mentioned previously, it was assumed that $r_i = 1$ mm. Regarding R, L and h, different cases were considered as indicated in Tables 2-4.

Chart 2. Cases studied for the cylinder with one inclusion.

R	$2\,r_i$	$3\,r_i$	$4\,r_i$	$5\,r_i$
L	$6\,r_i$	$8\,r_i$	$10\,r_i$	

For the case of a cylinder with two inclusions, we assume $R = 5\,r_i$ and $L = 10\,r_i$ (the parameter h is presented in Chart 3.)

Chart 3. Cases studied for the cylinder with two inclusions.

h	$2.1\,r_i$	$2.2\,r_i$	$2.3\,r_i$	$2.4\,r_i$	$2.5\,r_i$	$3\,r_i$	$4\,r_i$	$5\,r_i$

Finally, for the case of a cylinder with five inclusions, we assume $R = 5\,r_i$ and $L = 4(h + r_i)$, and for h we have the cases presented in Chart 4.

Chart 4. Cases studied for the cylinder with five inclusions.

h	$2.1\,r_i$	$2.2\,r_i$	$2.3\,r_i$	$2.4\,r_i$	$2.5\,r_i$	$3\,r_i$	$4\,r_i$	$5\,r_i$	$6\,r_i$	$7\,r_i$

The boundary value problems were solved using the finite element method with an in-house finite element code (details of the method in which the code is based can be found, for example, in Ref. [16].)

4. Numerical results

4.1. Results for one inclusion

In this section we show some results for a cylinder with one spherical inclusion located on its center (see Figure 1), for the cases indicated in Chart 2.

In Figure 4, results are presented for the axial and radial components of the normalized stress and the components of the strain, for different values for R, for the case $L = 10 r_i$.
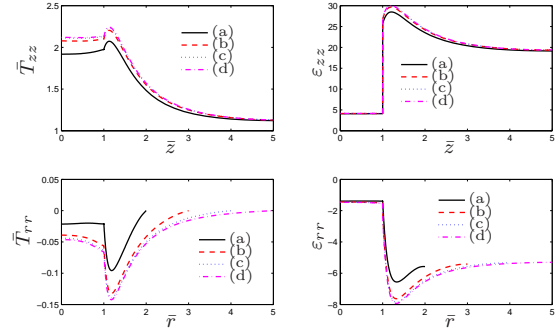
Figure 4. Results for the normalized components of the stress $\bar{T}_{zz}$ and strain ε_{zz}, for the line $r = 0$, $0 \leq \bar{z} \leq \bar{L}/2$, and the component $\bar{T}_{rr}$ of the stress and ε_{rr} of the strain, for the line $z = 0$, $0 \leq \bar{r} \leq \bar{R}$. This is for the case $L = 10\,r_i$, where: (a) $R = 2\,r_i$ (b) $R = 3\,r_i$ (c) $R = 4\,r_i$ (d) $R = 5\,r_i$.

The normalized components of the stress that appear in Figure 4 are defined as

$$\bar{T}_{zz} = \frac{T_{zz}}{\sigma}, \quad \bar{T}_{rr} = \frac{T_{rr}}{\sigma}, \qquad (18)$$

where σ is the uniform load applied on the upper surface of the cylinder (see Figure 1). The strains are in %.

The results for the axial components of the normalized stress and strain $\bar{T}_{zz}$ and ε_{zz} presented in Figure 4, respectively, are shown for the line $r = 0$, $0 \leq \bar{z} \leq \bar{L}/2$, where

$$\bar{z} = \frac{z}{r_i}, \quad \bar{L} = \frac{L}{r_i}. \qquad (19)$$

The results for the radial components of the normalized stress and strain $\bar{T}_{rr}$ and ε_{rr} presented in Figure 4, respectively, are shown for the line $z = 0$, $0 \leq \bar{r} \leq \bar{R}$, where

$$\bar{r} = \frac{r}{r_i}, \quad \bar{R} = \frac{R}{r_i}. \qquad (20)$$

In Figure 5 we show similar results as in Figure 4, for $R = 5\,r_i$ and different cases for L.
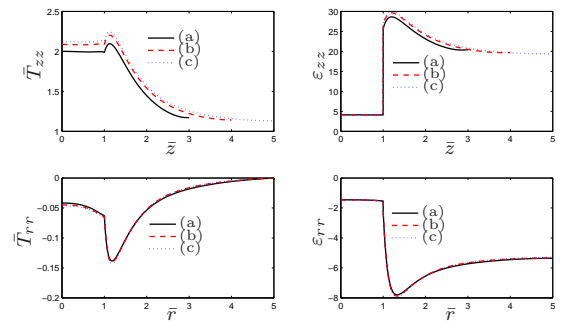
Figure 5. Results for the normalized components of the stress $\bar{T}_{zz}$ and strain ε_{zz}, for the line $r = 0$, $0 \leq \bar{z} \leq \bar{L}$, and the component $\bar{T}_{rr}$ of the stress and ε_{rr} of the strain, for the line $z = 0$, $0 \leq \bar{r} \leq \bar{R}$. This is for the case $R = 5\,r_i$, where (a) $L = 6\,r_i$ (b) $L = 8\,r_i$ (c) $L = 10\,r_i$.

The results for $\bar{T}_{zz}$ and ε_{zz} are shown for the line $r = 0$, $0 \leq \bar{z} \leq \bar{L}$, while for $\bar{T}_{rr}$ and ε_{rr}, the results are shown for the line $z = 0$, $0 \leq \bar{r} \leq \bar{R}$.

In both Figures 4 and 5 the inclusion is located in the region $\bar{r} \leq 1$, $\bar{z} \leq 1$, and due to the symmetry of the problem, only the upper half part of the inclusion and the cylinder is considered (see Figure 1).

In Figures 6-9 we show results for the radial and axial components of the strain and the stress, for the case $R = 5r_i$, $L = 10r_i$. The stresses are presented in Pa.
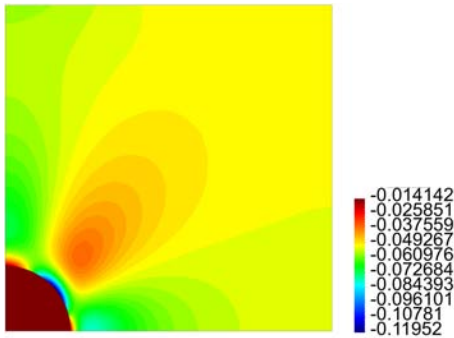
Figure 6. Contour plot for ε_{rr} for the problem of one inclusion.
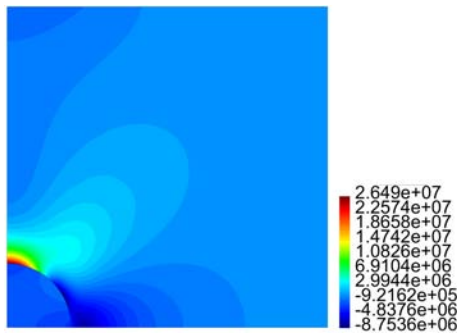
Figure 7. Contour plot for T_{rr} in Pa for the problem of one inclusion.
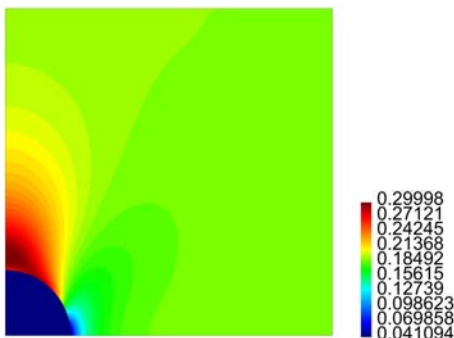
Figure 8. Contour plot for ε_{zz} for the problem of one inclusion.
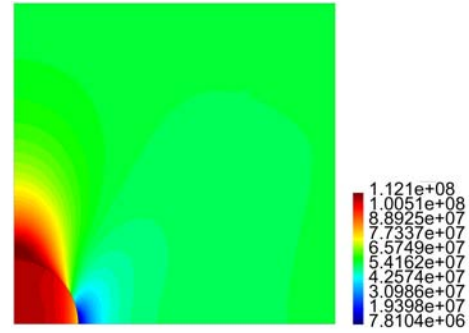
Figure 9. Contour plot for T_{zz} in Pa for the problem of one inclusion.

4.2. Results for two inclusions

Figure 10 depicts results for the axial and radial components of the stress (normalized stresses, see (18)) and the strain, for the line $r = 0$, $0 \leq \bar{z} \leq \bar{L}$, for different values for h as presented in Chart 3 for a hyperelastic cylinder with two inclusions (see Figure 2).
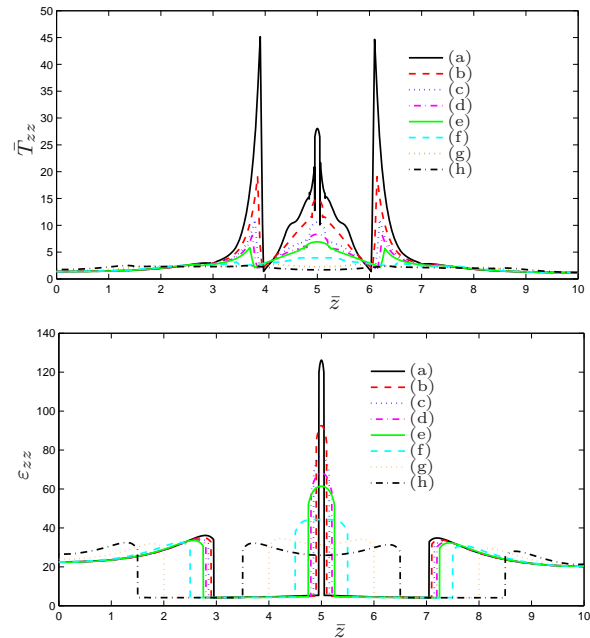
Figure 10. Results for the normalized components of the stress $\bar{T}_{zz}$ and strain ε_{zz}, for the line $r = 0$, $0 \leq \bar{z} \leq \bar{L}$, where (a) $h = 2.1\,r_i$ (b) $h = 2.2\,r_i$ (c) $h = 2.3\,r_i$ (d) $h = 2.4\,r_i$ (e) $h = 2.5\,r_i$ (f) $h = 3\,r_i$ (g) $h = 4\,r_i$ (h) $h = 5\,r_i$.

In Figures 11-14 we present results for the radial and axial components of the strain and the stress, for the case $h = 2.5\,r_i$ (the stresses are in Pa.)
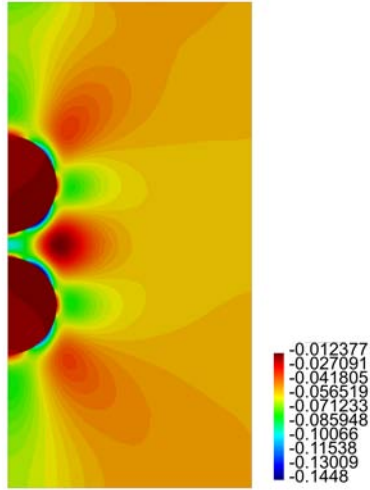
Figure 11. Contour plot for ε_{rr} for the problem of two inclusions.

Figure 12. Contour plot for T_{rr} in Pa for the problem of two inclusions.
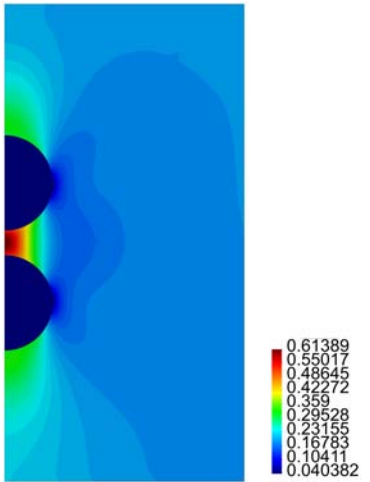
Figure 13. Contour plot for ε_{zz} for the problem of two inclusions.

Figure 14. Contour plot for T_{zz} in Pa for the problem of two inclusions.

4.3. Results for five inclusions

Figure 15 presents results for the axial and radial components of the stress (normalized stresses, see (18)) and the strain, for the line $r = 0$, $0 \leq \bar{z} \leq \bar{L}$ for a hyperelastic cylinder with five inclusions (see Figure 3).
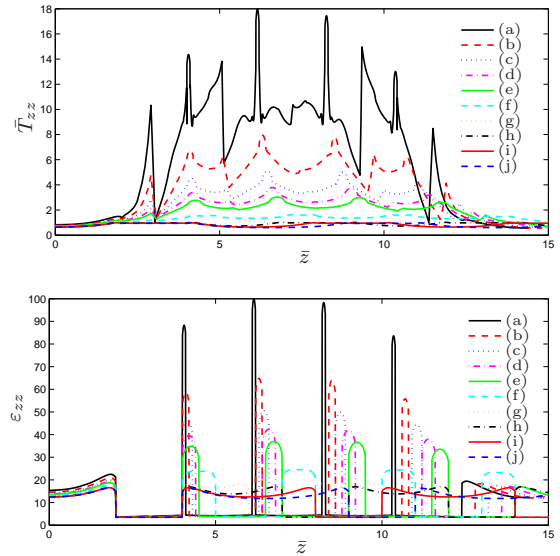
Figure 15. Results for the normalized components of the stress $\bar{T}_{zz}$ and strain ε_{zz}, for the line $r = 0$, $0 \leq \bar{z} \leq \bar{L}$, where (a) $h = 2.1\,r_i$ (b) $h = 2.2\,r_i$ (c) $h = 2.3\,r_i$ (d) $h = 2.4\,r_i$ (e) $h = 2.5\,r_i$ (f) $h = 3\,r_i$ (g) $h = 4\,r_i$ (h) $h = 5\,r_i$ (i) $h = 6\,r_i$ (j) $h = 7\,r_i$.

In Figures 16-19 we present results for the radial and axial components of the strain and the stress, for the case $h = 2.5\,r_i$ (the stresses are in Pa.)
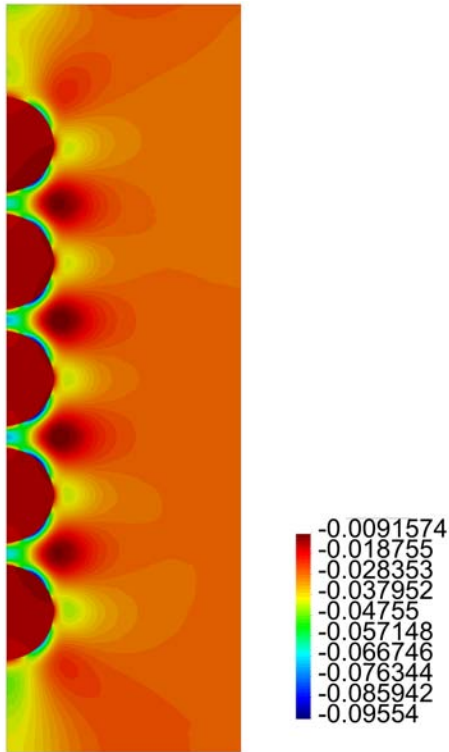
Figure 16. Contour plot for ε_{rr} for the problem of five inclusions.
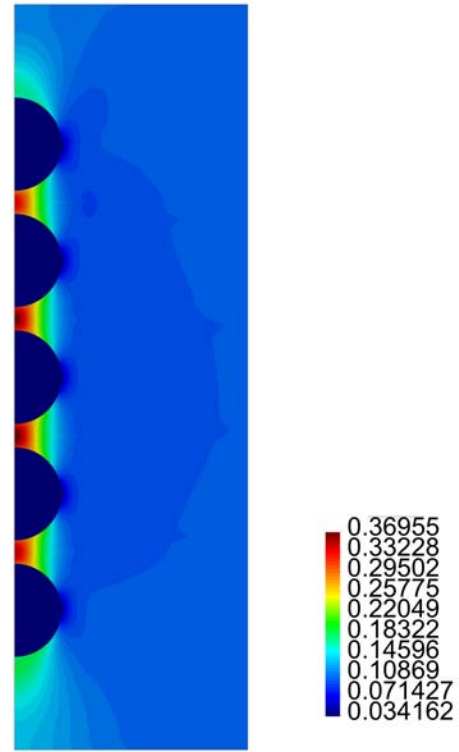
Figure 18. Contour plot for ε_{zz} for the problem of five inclusions.
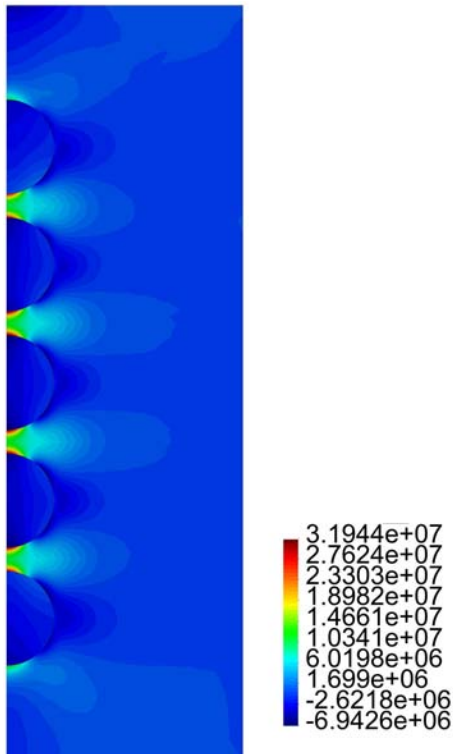
Figure 17. Contour plot for T_{rr} in Pa for the problem of five inclusions.
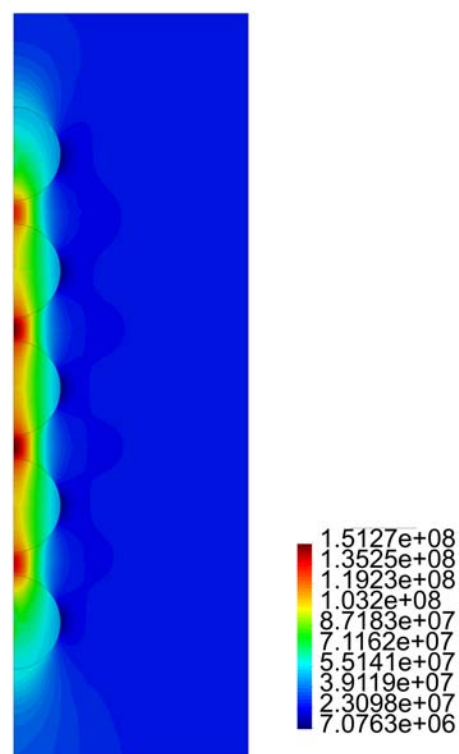
Figure 19. Contour plot for T_{zz} in Pa for the problem of five inclusions.

4.4. Discussion of the results

For the matrix with one particle, from Figure 4 cases (c) and (d), it is observed there is no meaningful difference between the behaviour of the stress and the strain, i.e., as expected for R large enough, the results tend to be invariant of the size of the cylinder. For the results presented in Figure 5, as in the previous case, for L large enough, there is no much difference in the behaviour of the body. From Figures 4 and 5, we observe that the component of the stress are continuous across the surface of the inclusion, but the components of the strain are not. In both cases, it is recognized the presence of large stresses in the matrix material near the interface with the inclusion, and for T_{zz} such stresses are positive, which could eventually lead to debonding of the composite. In fact, in Figure 7 we recognize that there is a zone on the upper part of the spherical inclusion (in the matrix), where the radial stress T_{rr} is positive, and that effect is much stronger in the same zone for T_{zz} (see Figure 9).

For the cylinder with two spherical inclusions, from Figure 10 we observe that there is a considerable difference in the behaviour of the composite if h is varied. Compare for instance the results presented in cases (a), (b) and (d) of that figure, where $h = 2.1\,r_i$, $h = 2.2\,r_i$ and $h = 2.3\,r_i$, respectively. The difference in behaviour between T_{zz} and ε_{zz} is large (in particular for the case (a) for T_{zz}.) In the plot for ε_{zz}, we observe the jump in the value for that component of the strain across the interface between the inclusion and the surrounding matrix. In Figures 12, 14 we notice the large values for T_{rr} and T_{zz} in the matrix, for the zone connecting the two inclusions.

Finally, for the cylinder with five inclusions, as in the previous case, from Figure 15 we notice large values for ε_{zz} for the matrix material between the inclusions. Also large values and rapid variations for T_{zz} in the same zone are observed, especially for the cases (a), (b) and (c). From Figures 16-19 we observe the same large values for the components of the stress and the strain in the zone near the inclusions.

5. Concluding remarks

In the present communication, we have studied the behaviour of a composite consisting of a hyper-elastic matrix with one, two and five spherical inclusions that are modelled using some relatively new classes of constitutive equations, in which, as a particular case such inclusions undergo small strains independently of the magnitude of the stresses. In several of the previous works discussed in the introduction section (see, for example, Refs. [10,17] and the reference mentioned therein), the main idea of studying constitutive equations of the type (10), (13), was to analyse the behaviour of the solutions for problems exhibiting concentration of stresses, where from the physical point of view, it is expected that the strain remain small. This is the case of brittle bodies with cracks (see the discussion in Ref. [14]). In the present work, this has been also the purpose. Herein, problems exhibiting concentration of stresses near the boundary of inclusions were studied. From the results presented in Section 4, it is observed that indeed there exists concentration of stresses, but strains remain small inside the inclusions. The results presented in this paper should be considered as the outcome of a new way to study the problem of modelling the behaviour of composite materials, where there is a soft matrix filled with a relatively stiff and brittle inclusions.

References

[1] K. R. Rajagopal, "On implicit constitutive theories," *Applications of Mathematics*, vol. 48, no. 4, pp. 279–319, 2003. [Online]. Available: https://doi.org/10.1023/A:1026062615145

[2] ——, "The elasticity of elasticity," *Zeitschrift für angewandte Mathematik und Physik*, vol. 58, no. 2, pp. 309–317, 2007. [Online]. Available: https://doi.org/10.1007/s00033-006-6084-5

[3] K. Rajagopal and A. Srinivasa, "On the response of non-dissipative solids," *Proceedings of the Royal Society of London A: Mathematical, Physical and En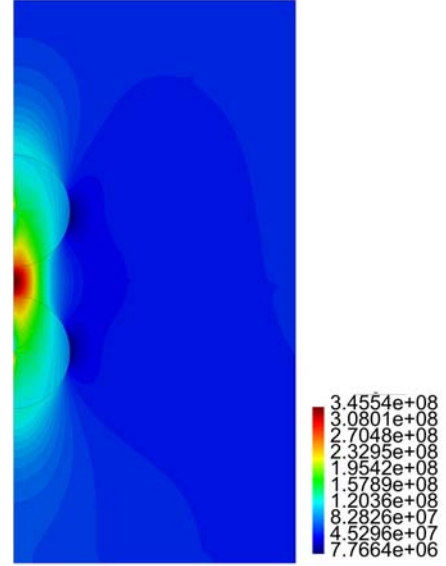gineering Sciences*, vol. 463, no. 2078, pp. 357–367, 2007. [Online]. Available: https://dx.doi.org/10.1098/rspa.2006.1760

[4] C. Truesdell and W. Noll, *The non-linear field theories of mechanics*, 3rd ed., S. Antman, Ed. Springer Berlin Heidelberg, 2004. [Online]. Available: https://goo.gl/t8UfwX

[5] K. R. Rajagopal and U. Saravanan, "Extension, inflation and circumferential shearing of an annular cylinder for a class of compressible elastic bodies," *Mathematics and Mechanics of Solids*, vol. 17, no. 5, pp. 473–499, 2012. [Online]. Available: https://doi.org/10.1177/1081286511423125

[6] R. Bustamante and K. R. Rajagopal, "A nonlinear model for describing the mechanical behaviour of rock," *Acta Mechanica*, pp. 1–22, 2017. [Online]. Available: https://doi.org/10.1007/s00707-017-1968-3

[7] P. A. Johnson and P. N. J. Rasolofosaon, "Manifestation of nonlinear elasticity in rock: Convincing evidence over large frequency and strain intervals from laboratory studies," *Nonlinear Processes in Geophysics*, vol. 3, no. 2, pp. 77–88, 1996. [Online]. Available: https://goo.gl/bnyjUK

[8] Z. Grasley, R. El-Helou, M. D'Ambrosia, D. Mokarem, C. Moen, and K. Rajagopal, "Model of infinitesimal nonlinear elastic response of concrete subjected to uniaxial compression," *Journal of Engineering Mechanics*, vol. 141, no. 7, p. 04015008, 2015. [Online]. Available: https://dx.doi.org/10.1061/(ASCE)EM.1943-7889.0000938

[9] V. Kulvait, J. Málek, and K. R. Rajagopal, "Modeling gum metal and other newly developed titanium alloys within a new class of constitutive relations for elastic bodies," *Archives of Mechanics*, vol. 69, no. 3, pp. 223–241, 2017. [Online]. Available: https://goo.gl/qLkpQP

[10] ——, "Anti-plane stress state of a plate with a v-notch for a new class of elastic solids," *International Journal of Fracture*, vol. 179, no. 1–2, pp. 59–73, 2013. [Online]. Available: https://doi.org/10.1007/s10704-012-9772-5

[11] M. L. Williams, "On the stress distribution at the base of a stationary crack," *Journal of Applied Mechanics*, vol. 24, no. 1, pp. 109–114, 1956. [Online]. Available: https://goo.gl/q9uZUn

[12] H. Zhu, A. Muliana, and K. Rajagopal, "On the nonlinear viscoelastic deformations of composites with prestressed inclusions," *Composite Structures*, vol. 149, Supplement C, pp. 279–291, 2016. [Online]. Available: https://doi.org/10.1016/j.compstruct.2016.03.008

[13] C. Truesdell and R. Toupin, *The classical field theories*. Springer, Berlin, Heidelberg: Principles of Classical Mechanics and Field Theory / Prinzipien der Klassischen Mechanik und Feldtheorie. Encyclopedia of Physics / Handbuch der Physik, 1960, vol. 2/3/1, pp. 226–858. [Online]. Available: https://doi.org/10.1007/978-3-642-45943-6_2

[14] K. R. Rajagopal, "On the nonlinear elastic response of bodies in the small strain range," *Acta Mechanica*, vol. 225, no. 6, pp. 1545–1553, 2014. [Online]. Available: https://doi.org/10.1007/s00707-013-1015-y

[15] R. Bustamante and K. R. Rajagopal, "A note on plane strain and plane stress problems for a new class of elastic bodies," *Mathematics and Mechanics of Solids*, vol. 15, no. 2, pp. 229–238, 2010. [Online]. Available: https://doi.org/10.1177/1081286508098178

[16] A. Ortiz-Bernardin, R. Bustamante, and K. Rajagopal, "A numerical study of elastic bodies that are described by constitutive equations that exhibit limited strains," *International Journal of Solids and Structures*, vol. 51, no. 3, pp. 875–885, 2014. [Online]. Available: https://doi.org/10.1016/j.ijsolstr.2013.11.014

[17] S. Montero, R. Bustamante, and A. Ortiz-Bernardin, "A finite element analysis of some boundary value problems for a new type of constitutive relation for elastic bodies," *Acta Mechanica*, vol. 227, no. 2, pp. 601–615, 2016. [Online]. Available: https://doi.org/10.1007/s00707-015-1480-6

Comparison Between Artificial Neural Network And Multiple Regression For The Prediction of Superficial Roughness In Dry Turning

Comparación entre redes neuronales artificiales y regresión múltiple para la predicción de la rugosidad superficial en el torneado en seco

Yoandrys Morales-Tamayo[1,*], Yusimit Zamora-Hernández[2], Paco Vásquez-Carrera[1],

Mario Porras-Vásconez[1], Joao Bárzaga-Quesada[3], Ringo López-Bustamante[4]

Abstract

The simple regression and artificial neural network methods are techniques used in many industrial aplications. This work developed two models in order to predict the surface roughness in dry turning of AISI 316L stainless steel. In its implementation they were considered various cutting parameters such as cutting speed, feed, and machining time. The models obtained by both methods were compared to develop a full factorial design to increase reliability of the recorded values of roughness. The analysis can be corroborated by the values of coefficients of determination that the proposed models are able to predict for surface roughness. The obtained results show that the neural networks techniques are more accurate than the multiple regression techniques for this study.

Resumen

Los métodos de regresión múltiple y redes neuronales artificiales son técnicas usadas en muchas aplicaciones de la industria. En este trabajo se utilizaron dos métodos de predicción: regresión múltiple y redes neuronales artificiales (perceptrón multicapa) con el objetivo de predecir la rugosidad superficial en el torneado en seco del acero AISI 316l. En su implementación fueron considerados varios parámetros de corte como la velocidad, el avance y el tiempo de mecanizado. Las ecuaciones obtenidas por ambos métodos fueron comparadas desarrollando un diseño factorial completo para aumentar la fiabilidad de los valores registrados de rugosidad superficial. En el análisis se puede comprobar mediante los valores de coeficientes de determinación que los modelos propuestos son capaces de predecir la rugosidad superficial. Los modelos obtenidos demuestran que la técnica de redes neuronales artificiales tiene mejor precisión que la regresión múltiple para este estudio.

Keywords: AISI 316L stainless steel, Analysis of variance and regression, Artificial neural network, Dry high-speed turning, Surface roughness.

Palabras clave: acero inoxidable AISI 316L, análisis de varianza y regresión, redes neuronales artificiales, rugosidad superficial, torneado de alta velocidad.

[1,*]Director of Electromechanics, Universidad Técnica de Cotopaxi, Cotopaxi – Ecuador. Author for correspondence ✉:
    yoandrys.morales@utc.edu.ec, ⬚ http://orcid.org/0000-0001-7456-1490, ⬚ http://orcid.org/0000-0003-4734-8584,
    ⬚ http://orcid.org/0000-0002-4119-4812
[2]Department of Mechanical Engineering, Universidad de Granma, Cuba. ⬚ http://orcid.org/0000-0002-0112-1061
[3]Department of Energy and Mechanical Sciences, Universidad de las Fuerzas Armadas, Cotopaxi – Ecuador.
    ⬚ http://orcid.org/0000-0001-9792-7379
[4]La Maná Extension Office, Universidad Técnica de Cotopaxi, Ecuador. ⬚ http://orcid.org/0000-0002-6519-1587

1. Introduction

Stainless steel is one of the most used metallic materials in the industrial sector, due to its favorable combination of mechanical properties, corrosion resistance and cost. This material has been widely used in the aerospace and military fields, where there is a growing demand and increasing surface quality requirements [1].

The characteristics of the machined surface directly affect fatigue resistance, corrosion resistance and the tribological properties of the machined components. Obtaining a high-quality surface increases the life of the product's fatigue capacity. Consequently, control of the machined surface is essential to ensure a correct cutting process. The most important aspect in manufacturing processes is the measurement and characterization of surface properties. In the turning pro-cess, surface roughness is a parameter that has a great influence on the behavior and functionality of me-chanical components and production costs [2].

Surface roughness is affected by several factors, such as: advance, the properties of the working material, cutting speed, depth, tip radius, the conditions of the machine, cutting fluids, the materials of the cutting tools, and the angles of the cutting tool, among others. Within them, it is easy to adjust cutting parameters in order to achieve the expected performance [3].

Austenitic stainless steels are considered difficult to machine, a characteristic related to their low thermal conductivity, high coefficient of thermal expansion, high ductility and high hardening by deformation. Fin-ishing operations carried out on these steels are com-monly executed with coated carbide inserts. The range of recommended speeds for the turning of these steels are very conservative (200-350 m/min) [4].

The use of low cutting speeds leads to a low efficiency in production and consequently high production costs [5]. As this range is unproductive in terms of current technological conditions, it is necessary to de-termine the behavior of surface roughness during the high-speed machining process (HSM).

Surface roughness generated in the machining processes has been studied since [6] by Sata and in [7] by Dickinson. The effect of the tool advancement, the tip radius and the angle of the edge on the surface roughness generated in the turning was described by Groover and named «ideal roughness», enunciated as the minimum roughness that is generated in a turned piece [8].

Surface roughness is one of the quality parameters most studied by researchers who analyze the machinability of austenitic steels. For example, Korkut et al. conducted a study of surface roughness and flank wear to determine the optimum cutting speed with the use of coated carbide inserts. The highest values of surface roughness during turning were achieved at low speeds

(<180m/min) attributed to the presence of cut-ting edge growth [9]. A similar result was achieved by Ciftci during his experimental study to analyze the influence of cutting speed (between 120 m/min and 210 m/min) on surface roughness and cutting forces [9].

Four years later, Galanis and Manolakos developed an empirical mathematical model to predict surface roughness with the application of a surface response methodology. This investigation was developed during the machining of femoral heads with a tool coated with $(TiN/Al_2O_3/TiC)$ [10].

In 2012, Çaydaş and Ekici implemented an artificial neural network to predict surface roughness. The validation of this model was developed through an experimental study that considered the cutting parameters involved in the dry turning of stainless steel AISI 304 [11].

That same year, Ahilan and others conducted an investigation with the purpose of developing a model based on artificial neural networks to predict cutting conditions on CNC lathes. They used the design of experiments (Taguchi method) to train and validate the proposed neural model [12]. In this case, the maxi-mum cutting speed used was 150 m/min.

Selvaraj and others developed a research to optimize cutting parameters in order to minimize surface roughness, cutting force and tool wear. The experiments are analyzed using the Taguchi method, the turning operation was performed dry and at a maximum cutting speed of 120 m/min [13].

Figure 1 shows a summary of the cutting speeds used in the main studies developed during the turning of austenitic steels. These investigations include not only the study of surface roughness, but also of wear of cutting tools, surface integrity, cutting forces, cut-ting power and chip formation.

The literature reveals (Figure 1) that there are few studies related to the dry turning of austenitic stainless steels at cutting speeds higher than 400 m/min. Only four authors exceeded this cutting speed.

Lin evaluates the wear behavior of the tool (flank wear) [14], Fernández-Abia and collaborators did not carry out dry machining [15], Maranhão and Darvim studied the influence of the friction coefficient of the tool-chip interface [16] and finally, Galanis and Manolakos studied the effect of cutting conditions on surface roughness during the machining of AISI 316L stainless steel femoral heads. The cutting length for this study was 28 mm [17].

The objective of this research is to compare two methods in order to predict surface roughness in AISI 316L stainless steel with speeds of 400 m/min and 450 m/min, one based on multiple regression and another in artificial neural networks of the multilayer percep-tron type.

For this purpose, it was necessary to implement a complete factorial design to investigate the effect of

Morales et al. / Comparison Between Artificial Neural Network And Multiple Regression For The Prediction of Superficial Roughness In Dry Turning

81

cutting conditions (speed, advance, time) on surface roughness. Multiple regression models are validated by basic assumptions.

A multilayer perceptron architecture with a back-propagation algorithm is used to develop the neural network and the criterion for updating the weights is a downward gradient. The effectiveness of both models is determined by comparing the coefficients of determination and the absolute average error.
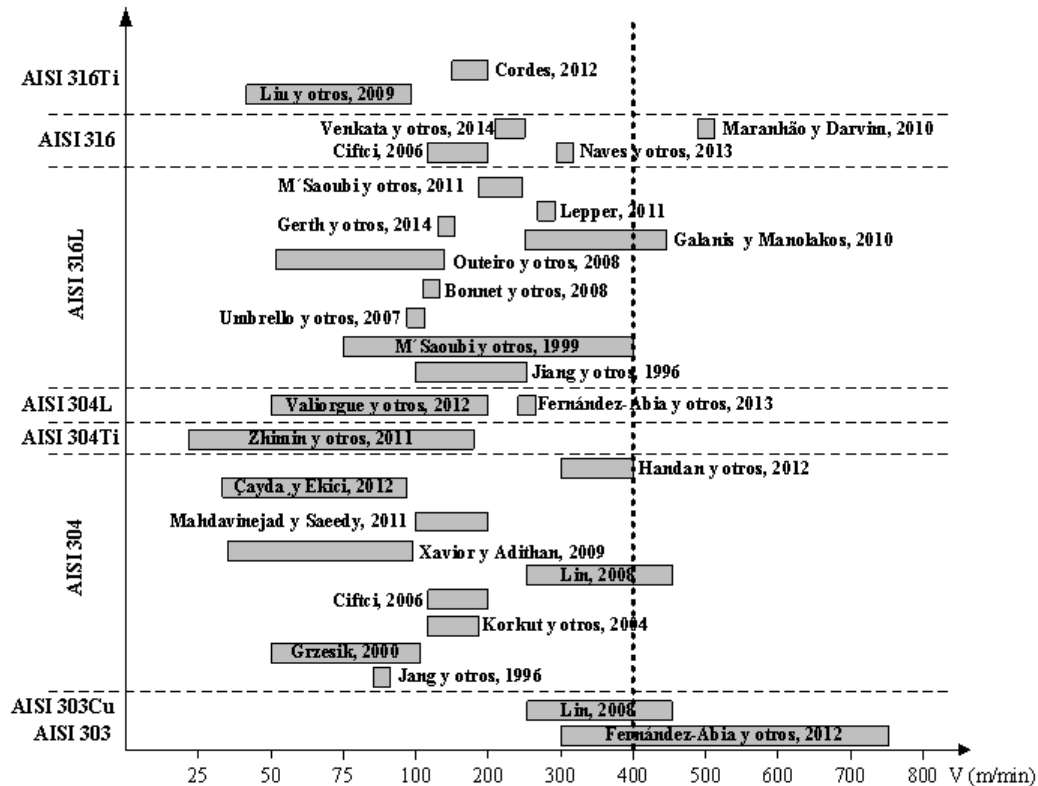
Figure 1. Main investigations in the turning of austenitic stainless steels

2. Materials and methods

2.1. Surface roughness models

In turning, there are many factors that affect surface roughness such as the cutting tool, the work material and the cutting parameters. The factors related to the tools include materials, tip radius, the angle of attack, the geometry of the cutting edge, the vibration of the tool, etc., while the variables related to the material of the piece of work include hardness, physical and me-chanical properties, among others. On the other hand, influential cutting conditions include cutting speed, advance and depth [18].

The appropriate selection of cutting parameters and the geometry of the tool to achieve the required surface quality is complex and difficult [19]. Therefore, it is clear that the selection and obtaining of a model that describes this process is essential for the machining of steels [20].

Surface roughness (Ra) is generally defined based on the ISO 4287 standard as the arithmetic mean of the deviation of the profile of the roughness from the cen-terline throughout the measurement. This definition is given in equation (1).

$$R_a = \frac{1}{L} \int_0^L |y(x)| dx \qquad (1)$$

Where: L is the measurement length; y it is the distance between two points of the profile. The relationship between surface roughness and machining variables can be defined as (equation 2):

$$R_a = C \cdot V^n \cdot f^m \cdot d^p \cdot r^l \cdot \varepsilon \qquad (2)$$

Where, Ra is surface roughness measured in μm; V, f, d, r are cutting speed (m/min), feed (mm/rev), depth (mm), radius of the tool tip (mm), respectively. C, m, n, l are constants and ε is the random error [21]. Equation (1) can be seen as equation (3) to facilitate the representation of constants and parameters. The arithmetic mean roughness (Ra) and the height of the maximum peak (Rt) of the turned surfaces can be de-termined by the following equations (3) and (4):

$$R_a \approx \frac{f^2}{32 \cdot r} \tag{3}$$

$$R_t \approx \frac{f^2}{8 \cdot r} \tag{4}$$

Where r is the tip radius (mm) and f is the cutting advance (mm/rev). Equations (3) and (4) show that surface roughness increases proportionally with the advance and, in addition, the increase in tip radius of the cutting tool reduces surface roughness in the turning.

2.2. Modelación por regresión múltiple

Multiple regression is a statistical technique that allows to determine the correlation that exists between independent variables and two or more dependent variables. Multiple regression can be used to analyze ordinal and categorical data [22]. Generally, a variance analysis (ANOVA) is carried out first to determine the important factors involved and then with the use of regression a quantitative model is obtained that relates the most important factors with the answer [23].

2.3. Prediction strategy using artificial neural networks

Artificial neural networks (ANNs) are widely used in many industry applications. These are very popular in the modeling of systems due to their high efficiency in adaptation and learning through pattern recognition [3].

The network installed in this research is a multilayer perceptronic network which is equivalent to multiple non-linear regression [24]. The multilayer perceptronic network is composed of the association of artificial neurons organized within the network forming levels or layers.

This case presents an input layer in which the patterns are introduced into the network (cutting parameters), a hidden layer with some neurons, and an output layer with the response variable (surface roughness). The structure of the ANN shown in Figure 2 was used to model and predict the dependent variable.

The determination of the optimal number of neurons of the hidden layer was carried out through a trial and error process in which different variants were tested. In any case, the objective was to provide the network with an adequate number of neurons in the hid-den layer to guarantee the ability to learn the characteristics of the possible relationships between the sam-ple's data.
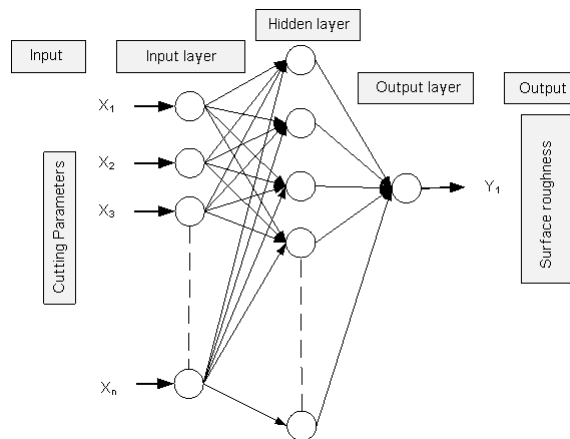
Figure 2. Structure of the multi-layer perceptronic network

2.4. Experimental tests

Experimental turning was executed in dry conditions, with the use of a multifunctional Okuma Multus B200-W type lathe with an engine power of 15 kW and a rotation of the spindle between 50 rpm and 5000 rpm (Figure 3).

Figure 3. CNC multifunctional lathe Okuma model Multus B-200W

AISI 316L stainless steel was the material selected for the test pieces. This steel is used in the manufacture of products resistant to corrosion and to high tem-peratures [25]. The chemical composition is C 0.015%, Si 0.58%, Mn 1.50%, Cr 16.95%, Mo 2.05%, Ni 10.08%, P 0.031%, S 0.029% and N 0.059%.

The specimens of 100 mm in diameter and 200 mm in length were turned with sandvik, GC1115 and GC2015 coated inserts. The coatings of (TiCN-A_2O_3-TiN) with a thickness of 15 μm corresponded to the GC2015 insert and, for the GC1115 insert, the coating was 5 μm thick TiN. After the turning operation, surface roughness (Ra) was measured with a CARL ZEISS rugosimeter model SURFCOM 1500SD2 (Figure 4).

The geometry of the inserts was CCMT 12 04 04-MF with chipbreaker, the Sandvik tool holder code C6-SCLCL-45065-12 and an adapter with code C6-391.01-63 060. The main incidence angle was 7°, the angle of attack was 0° and the radius of the tip of 0.4 mm.

Morales et al. / Comparison Between Artificial Neural Network And Multiple Regression For The Prediction of Superficial Roughness In Dry Turning

83

Figure 4. CARL ZEISS rugosimeter model SURFCOM 1500SD2.

A complete factorial analysis was done to determine the relationship between the independent variables (cutoff parameters) and the dependent variable (surface roughness (Ra)). A total of 64 tests for two replicas were developed with two levels of cutting speeds (v), four levels of time (T), two levels of cutting advances (f) and two levels of tool material. Table 1 shows the variables studied.

Table 1. Factors and levels used in the development of the experiment

Factors	Symbols		Level 1	Level 2	Level 3	Level 4
Advanced (mm/rev)	f		0,08	0,16	-	-
Insert material	Ins		GC1115	GC2015	-	-
Speed (m/min)	v		400	450	-	-
Time (min)	T	400 m/min	2	3	4	5
		450 m/min	0,6	1,2	2	3

3. Results and discussion

Surface roughness is widely used as a parameter to indicate the quality of a product and in most cases, an important technical requirement in mechanical design.

Consequently, achieving the quality of the desired surface is of great importance for the functional behavior of a product [26]. It also has an impact on me-chanical properties, specifically on fatigue resistance and corrosion resistance [19].

Manufacturing industries are in charge of guaranteeing the consumer's increasing demands for superficial quality and availability of less expensive products. Therefore, knowing the effect of these parameters is important to evaluate the effectiveness and productivi-ty of the cutting process [27].

This section compares and discusses the results obtained through multiple regression and artificial neural networks.

3.1. Analysis of multiple regression

The models obtained as a result of the multiple regression analysis with the velocity of 400 m/min are shown in equations (5) and (6) for the GC1115 and GC2015 inserts respectively. The models with the speed of 450 m/min are shown in equations (7) and (8) for the GC1115 and GC2015 inserts respectively.

$$R_a = 0,358933 + 0,0188793 \cdot e^T \cdot f \quad (5)$$

$$R_a = 0,27529 + 0,0109446 \cdot T^2 + 0,69 \cdot f \quad (6)$$

$$R_a = -2,75967 + 2,99435 \cdot e^{(T^3 \cdot f^2)} \quad (7)$$

$$R_a = 0,219579 + 0,0201327 \cdot T^3 + 0,45625 \cdot f \quad (8)$$

The coefficient of determination (R^2) represents the true measure of the correctness of the adjustment in the regression line determined by the model. For these cases the R^2 were at a speed of 400 m/min, 0.92 (GC1115) and 0.80 (GC2015) and for 450 m/min were 0.97 (GC1115) and 0.97 (GC2015).

In all cases, in order to validate the regression results obtained, compliance with the basic regression assumptions was verified, such as: homoscedasticity (White Test), non-autocorrelation of residues (Breusch-Godfrey Test), normality (Jarque-Bera Test) and no mean.

Figures 5 and 6 show the comparisons between the experimentally measured values and the estimated values of surface roughness by the models corresponding to the speeds of 400 m/min and 450 m/min, respectively. In these Figures we can observe a strong relationship between the estimated variables and the response variable.

(a)

(b)
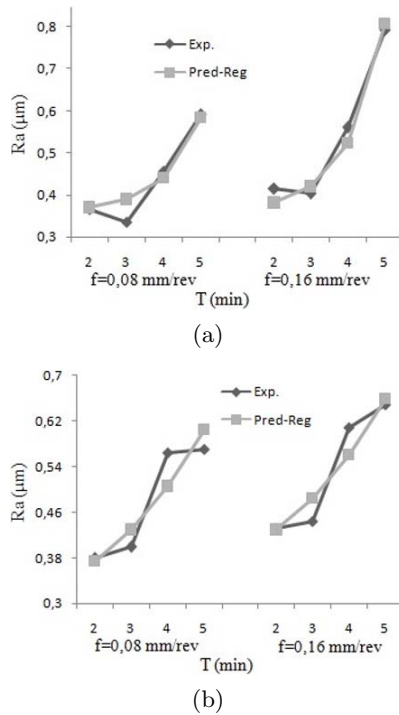
Figure 5. Values measured and estimated by multiple regression for v = 400 m/min, a) GC1115 insert and b) GC2015 insert

(a)

(b)
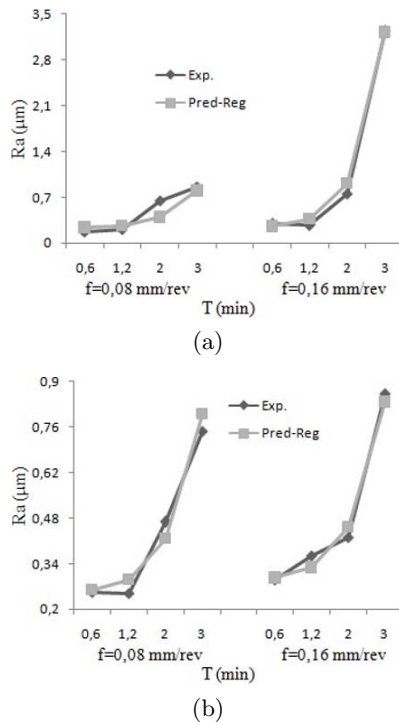
Figure 6. Values measured and estimated by multiple regression for v = 450 m/min, a) GC1115 insert and b) GC2015 insert

3.2. Results of artificial neural networks

The structure of the network applied to model and predict surface roughness in the turning operation corresponds to the multilayer perceptron of the feedforward Backpropagations type. The experimental data were used to construct the model of artificial neural networks.

The training was developed through the Levenberg Marquardt algorithm. The best results were obtained with a 3-5-1 structure, three neurons in the input layer, 5 neurons in the hidden layer and one in the output layer. The neural network software was encoded using Matlab's Neural Networks Toolbox. The parameters of the proposed network structure are shown in Table 2.

The input data were divided by the speeds, therefore, only the machining time, the cutting advance and the type of cutting tool were considered. These data were randomly distributed in the following way: for the training 70% were selected (22 data), 15% (5 data) for the test stage and for the validation the remaining 15% (5 data).

Table 2. Parameters of the artificial neural network implemented in the study.

Number of layers	3
Number of neurons in the layers	Entrada: 3 Oculta: 5 Salida: 1
Activation function	Tansig-purelin
Number of iterations	10000

The results obtained were analyzed by statistical methods, the criteria used were the absolute average error (Emedio, (%)) and the coefficient of determination (R^2).

Equations 9 and 10 are used to calculate these criteria respectively.

$$E_{medio} = \left(\frac{1}{N} \sum_i \left| \frac{t_i - t_0}{t_i} \right| \times 100 \right) \qquad (9)$$

$$R^2 = 1 - \left(\frac{\sum_i (t_i - t_0)^2}{\sum_i (t_0)^2} \right) \qquad (10)$$

Where N, is the number of trials; t_i, experimental values and t_0, estimated values.

Figures 7 and 8 show a comparison between the experimental values and the estimated values of sur-face roughness by the model developed by artificial neural networks.

The results of the neural networks show that the models proposed in this study are suitable for the pre-diction of surface roughness.

The values of the coefficients of determination and of the absolute average errors are within acceptable ranges (Table 3).

Morales et al. / Comparison Between Artificial Neural Network And Multiple Regression For The Prediction of Superficial Roughness In Dry Turning

85

Table 3. Values of coefficients of determination (R^2) and absolute mean errors for each developed neural network.

| Parameter | Neural network | |
	400 m/min	450 m/min
Training	0,98134	0,99836
Test	0,99842	0,99026
General	0,98122	0,9973
$E_{average}$	2,869	6,946

the precision of the values obtained by means of multiple regression and by artificial neural networks. The results are close to those measured experimentally for all models. Therefore, the proposed models can be used to predict surface roughness in the dry turning of AISI 316L steel. However, as can be seen in the same table, the models obtained by artificial neural networks produce better results compared to the models using multiple regression.

(a)

(b)

Figure 7. Values measured and estimated by artificial neural networks for v = 400 m/min, a) GC1115 insert and b) GC2015 insert

(a)

(b)
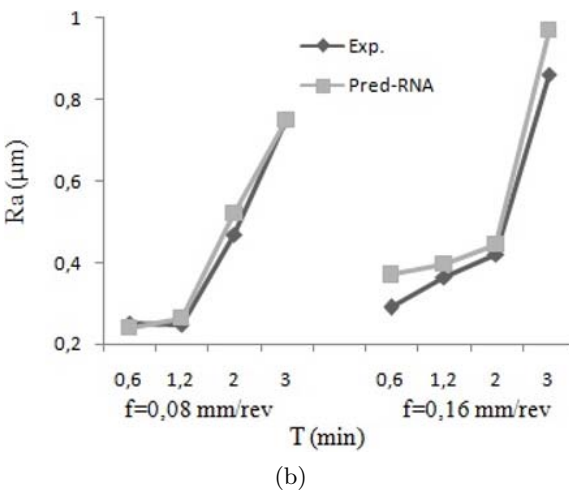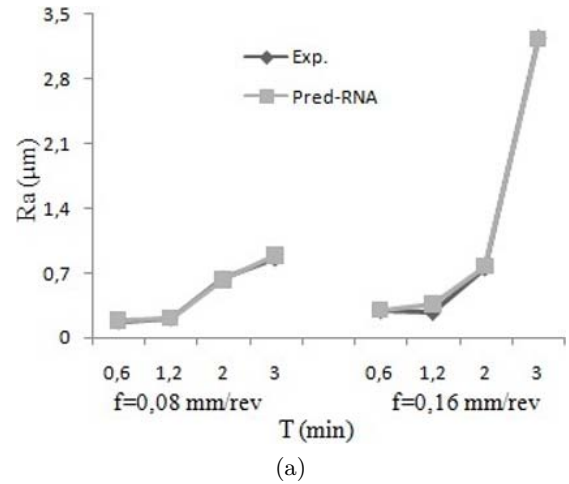
Figure 8. Values measured and estimated by artificial neural networks for v = 450 m/min, a) GC1115 insert and b) GC2015 insert

3.3. General evaluation

A complete factorial experiment design was applied to determine the effects of independent variables (speed, advance, time and cutting tools) of the dry turning process in surface roughness. After each turning test, surface roughness values were recorded for further analysis. In this research, models were developed us-ing artificial neural networks and multiple regression. Table 4 shows a comparison of the results according to

Table 4. Comparison of proposed methods

Method	Equation	$E_{average}$	R2
Multiple Regresión	-1	5,153	0,9
	-2	5,552	0,8
	-3	22,78	1
	-4	8,473	1
Artificial neural network	400 m/min	2,869	1
	450 m/min	6,946	1

4. Conclusions

In this research, a study has been carried out to predict surface roughness in the dry turning of AISI 316L steel. The influence of variables such as speed, ad-vancement and machining time were analyzed through a complete factorial design. The models to predict the surface roughness were developed from the experimental data. According to the results obtained in this work, the following conclusions are presented.

- The developed models were evaluated for their prediction capabilities with the values measured experimentally.

- The proposed models can be used to predict surface roughness in the dry turning of AISI 316L steel.

- The coefficient of minimum determination reached by the models was 80% and the maximum of 99%, indicating the proportion of variability of the data explained by the regression models, in the case of the absolute average error the minimum was of 2,869% and the maximum of 22.78.

- The lowest absolute mean errors were obtained with the models implemented with artificial neural networks.

- In future research, models based on neural networks and multiple regression could be developed to allow a study of the economy of the dry turning process.

Acknowledgments

References

[1] D. Vasumathy, A. Meena, and M. Duraiselvam, "Experimental study on evaluating the effect of micro textured tools in turning aisi 316 austenitic stainless steel," *Procedia Engineering*, vol. 184, no. Supplement C, pp. 50–57, 2017, advances in Material & Processing Technologies Conference. [Online]. Available: https://doi.org/10.1016/j.proeng.2017.04.070

[2] F. Mata-Cabrera, I. Hanafi, A. Khamlichi, A. Jabbouri, and M. Bezzazi., "Predicción de rugosidad en maquinado de compuestos con base de *peek* usando metodologá de superficie de respuesta," *Ingeniería, Investigación y Tecnología*, vol. 14, no. 4, pp. 463–474, 2013. [Online]. Available: https://doi.org/10.1016/S1405-7743(13)72258-3

[3] M. Mia and N. R. Dhar, "Prediction of surface roughness in hard turning under high pressure coolant using artificial neural network," *Measurement*, vol. 92, Supplement C, pp. 464–474, 2016. [Online]. Available: https://doi.org/10.1016/j.measurement.2016.06.048

[4] A. Fernández-Abia, J. Barreiro, L. N. López de Lacalle, and S. Martínez, "Effect of very high cutting speeds on shearing, cutting forces and roughness in dry turning of austenitic stainless steels," *The International Journal of Advanced Manufacturing Technology*, vol. 57, no. 1–4, pp. 61–71, 2011. [Online]. Available: https://doi.org/10.1007/s00170-011-3267-9

[5] J. Zhou, V. Bushlya, and J. Stahl, "An investigation of surface damage in the high speed turning of inconel 718 with use of whisker reinforced ceramic tools," *Journal of Materials Processing Technology*, vol. 212, no. 2, pp. 372–384, 2012. [Online]. Available: https://doi.org/10.1016/j.jmatprotec.2011.09.022

[6] T. Sata, *Surface finish in metal cutting*, 1964, vol. 12, pp. 190–197.

[7] G. R. Dickinson, "Paper 26: Survey of factors affecting surface finish," *Proceedings of the Institution of Mechanical Engineers, Conference Proceedings*, vol. 182, no. 11, pp. 135–147, 1967. [Online]. Available: https://doi.org/10.1243/PIME_CONF_1967_182_311_02

[8] M. P. Groover, *Fundamentos de manufactura moderna: materiales, procesos y sistemas,*. McGraw-Hill Interamericana de España S. L., 2007, no. 4. [Online]. Available: https://goo.gl/aJx7SQ

[9] I. Korkut, M. Kasap, I. Ciftci, and U. Seker, "Determination of optimum cutting parameters during machining of AISI 304 austenitic stainless steel," *Materials & Design*, vol. 25, no. 4, pp. 303–305, 2004. [Online]. Available: https://doi.org/10.1016/j.matdes.2003.10.011

[10] Y. Morales Tamayo, Y. Zamora Hernández, P. Zambrano Robledo, R. Beltrán Reyna, and J. Pino Tarrago, "Investigação da influência dos parâmetros de corte na rugosidade superficial usando regressão múltipla," *Revista Iberoamericana de Ingeniería Mec"anica.*, vol. 20, no. 2, pp. 25–33, 2016. [Online]. Available: https://goo.gl/33SqTx

Morales et al. / Comparison Between Artificial Neural Network And Multiple Regression For The Prediction of Superficial Roughness In Dry Turning

87

[11] U. Çaydaş and S. Ekici, "Support vector machines models for surface roughness prediction in cnc turning of aisi 304 austenitic stainless steel," *Journal of Intelligent Manufacturing*, vol. 23, pp. 639–650, 2012. [Online]. Available: https://doi.org/10.1007/s10845-010-0415-2

[12] C. Ahilan, S. Kumanan, N. Sivakumaran, and J. E. R. Dhas, "Modeling and prediction of machining quality in cnc turning process using intelligent hybrid decision making tools," *Applied Soft Computing*, vol. 13, no. 3, pp. 1543–1551, 2013, hybrid evolutionary systems for manufacturing processes. [Online]. Available: https://doi.org/10.1016/j.asoc.2012.03.071

[13] D. P. Selvaraj, P. Chandramohan, and M. Mohanraj, "Optimization of surface roughness, cutting force and tool wear of nitrogen alloyed duplex stainless steel in a dry turning process using taguchi method," *Measurement*, vol. 49, Supplement C, pp. 205–215, 2014. [Online]. Available: https://doi.org/10.1016/j.measurement.2013.11.037

[14] W. S. Lin, "The study of high speed fine turning of austenitic stainless steel," *Journal of Achievements in Materials and Manufacturing Engineering*, vol. 27, no. 2, pp. 191–194, 2008. [Online]. Available: https://goo.gl/UWA5LL

[15] A. I. Hernández-Abia, J. Barreiro, L. N. López de Lacalle, and S. Martínez Pellitero, "Behavior of austenitic stainless steels at high speed turning using specific force coefficients," *The International Journal of Advanced Manufacturing Technology*, vol. 62, no. 5–8, pp. 505–515, 2012. [Online]. Available: https://doi.org/10.1007/s00170-011-3846-9

[16] C. M. ao and J. P. Davim, "Finite element modelling of machining of aisi 316 steel: Numerical simulation and experimental validation," *Simulation Modelling Practice and Theory*, vol. 18, no. 2, pp. 139–56, 2010. [Online]. Available: https://doi.org/10.1016/j.simpat.2009.10.001

[17] N. I. Galanis and D. E. Manolakos, "Surface roughness prediction in turning of femoral head," *The International Journal of Advanced Manufacturing Technology*, vol. 51, no. 1-4, pp. 79–86, 2010. [Online]. Available: https://doi.org/10.1007/s00170-010-2616-4

[18] K. S. Sangwan, S. Saxena, and G. Kant, "Optimization of machining parameters to minimize surface roughness using integrated ann-ga approach," *Procedia CIRP*, vol. 29, Supplement C, pp. 305–310, 2015, the 22nd CIRP Conference on Life Cycle Engineering. [Online]. Available: https://doi.org/10.1016/j.procir.2015.02.002

[19] E. Kilickap, M. Huseyinoglu, and A. Yardimeden, "Optimization of drilling parameters on surface roughness in drilling of aisi 1045 using response surface methodology and genetic algorithm," *The International Journal of Advanced Manufacturing Technology*, vol. 52, no. 1–4, pp. 79–88, 2011. [Online]. Available: https://doi.org/10.1007/s00170-010-2710-7

[20] R. E. Harber, J. E. Jiménez, A. Jiménez, and J. López-Coronado, "Modelo matemático para la predicción del esfuerzo de corte en el mecanizado a alta velocidad," *Revista de Metalurgia*, vol. 40, no. 4, pp. 247–258, 2004. [Online]. Available: http://dx.doi.org/10.3989/revmetalm.2004.v40.i4.272

[21] I. Asiltürk and M. Çunkaş, "Modeling and prediction of surface roughness in turning operations using artificial neural network and multiple regression method," *Expert Systems with Applications*, vol. 38, no. 5, pp. 5826–5832, 2011. [Online]. Available: https://doi.org/10.1016/j.eswa.2010.11.041

[22] K. V. B. S. Kalyan Kumar and S. K. Choudhury, "Investigation of tool wear and cutting force in cryogenic machining using design of experiments," *Journal of Materials Processing Technology*, vol. 203, no. 1, pp. 95–101, 2008. [Online]. Available: https://doi.org/10.1016/j.jmatprotec.2007.10.036

[23] D. Montgomery, *Design and Analysis of Experiments (fifth edition)*. John Wiley & Sons, Ltd., 2002. [Online]. Available: http://dx.doi.org/10.1002/qre.458

[24] J. Montaño Moreno, "Redes neuronales artificiales aplicadas al análisis de datos," Ph.D. dissertation, Universitat de Les Illes Balears. Islas Baleares, España, 2002. [Online]. Available: https://goo.gl/yVkDrN

[25] V. N. Gaitonde, S. R. Karnik, B. Siddeswarappa, and B. T. Achyuta, "Integrating box-behnken design with genetic algorithm to determine the optimal parametric combination for minimizing burr size in drilling of aisi 316l stainless steel," *The International Journal of Advanced Manufacturing Technology*, vol. 37, no. 3–4, pp. 230–240, 2008. [Online]. Available: https://doi.org/10.1007/s00170-007-0957-4

[26] Z. Zhimin, Z. Yuanliang, L. Xiaoyan, Z. Huiyuan, and S. Baoyuan, "Influences of various cutting parameters on the surface roughness during turnings stainless steel," *Acoustical Physics*, vol. 57, no. 1, pp. 114–120, 2011. [Online]. Available: https://doi.org/10.1134/S1063771011010209

[27] J. Campos Rubio, T. H. Panzera, A. M. Abrao, P. F. Faria, and J. Paulo Davim, "Effects of high speed in the drilling of glass whisker-reinforced polyamide composites (pa66 gf30): statistical analysis of the roughness parameters," *Journal of Composite Materials*, vol. 45, no. 13, pp. 1395–1402, 2011. [Online]. Available: https://doi.org/10.1177/0021998310381540
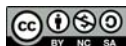
Obtaining of SHW with solar energy in the canton Cuenca and analysis of environmental pollution

Obtención de ACS con energía solar en el cantón Cuenca y análisis de la contaminación ambiental

John Calle Sigüencia[1,*], Óscar Tinoco Gómez[1]

Abstract

This document contains the analysis to determine the feasibility of implementing solar water heaters to obtain Sanitary hot water(SHW) in Ecuador, in the province of Azuay, in the Canton of Cuenca, in order to reduce the environmental pollution caused by the use of fossil fuels. The project considers the implementation of a meteorological network and data collection of global solar radiation in 16 points located in populated areas of the Canton during the years 2014 and 2015. Then, through a field work a diagnosis is made to establish which are the systems which are currently used to obtain SHW, two solar vacuum tube heaters for SHW production are also located and characterized with their corresponding equations. With the measured radiation data, we stablish the model applying the equations and establishing the feasibility of implementation based on the measured solar energy. Finally, a comparison is made to determine what would be the decrease of CO_2 emissions if the implementation would be carried out. The obtained results indicate that in 82% of households it uses SHW and of these 65% use LPG-based systems, which 44% of the energy demand to obtain SHW can be covered with solar energy.Therefore auxiliary systems can be used to guarantee a constant supply and that with the implementation it would be possible to reduce 108537 t CO_2 eq per year.

Keywords: Solar heater, environmental pollution, solar energy, vacuum tubes

Resumen

En este documento se encuentra el análisis para determinar la factibilidad de implementación de calentadores solares para obtener agua caliente sanitaria (ACS) en el Ecuador, en la provincia del Azuay, en el cantón Cuenca, con el fin de disminuir la contaminación ambiental provocada por el uso de combustibles fósiles. El proyecto considera la puesta en marcha de una red meteorológica y toma de datos de radiación solar global en 16 puntos ubicados zonas pobladas del cantón durante los años 2014 y 2015, posteriormente a través de un trabajo de campo se realiza un diagnóstico para establecer cuáles son los actuales sistemas usados para obtener ACS, también se analizan de manera teórica y práctica las eficiencias de dos tipos de calentadores solares de tubos de vacío para producción de ACS; con los datos de radiación medidos se modela aplicando las ecuaciones de transferencia de calor y se establece la factibilidad de implementación en función de la energía solar medida; finalmente, se realiza una comparación para determinar cuál sería la disminución de emanaciones de CO_2 si se ejecutaría esta propuesta. Los resultados obtenidos indican que el 82 % de familias utiliza ACS, de estas el 65 % emplean sistemas a base de GLP y, que el 44 % de la demanda de energía para obtener ACS puede ser cubierta con energía solar necesitando utilizar sistemas auxiliares para garantizar un abastecimiento constante. La implementación de estos sistemas permitiría reducir 108 537 tn CO_2 eq al año.

Palabras clave: calentador solar, contaminación ambiental, energía solar, tubos de vacío

1. Introduction

Since the 70s, concern for the environment has been especially intense, generating a series of actions, conferences and international agreements [1], among whose fundamental points is the decrease in the production of CO_2 and greenhouse gases. Their results have remained as good intentions, but efficient action in favor of this large-scale purpose has not been achieved.

The use of renewable energies has generated an increase in technological development, as they have become increasingly reliable and high performance, which has led to constant increases in their production, marketing and implementation, both for domestic and for industrial use.

By the 70s, solar energy began to be used as one of the main options for the benefit of people. Countries such as the United States, France, Germany, Spain, pay great attention to the use of solar energy for thermal and photovoltaic purposes, and present notable percentages of energy generation. By 2016, 94% of the solar thermal systems installed in the world are used to obtain hot water [2].

Because of its geographical location, Ecuador is a privileged country as far as the solar resource is concerned, since the angle of incidence of solar radiation is almost perpendicular to the surface throughout the year, a situation that does not occur in other parts of the planet where the angle varies according to the seasons of the year. This positional advantage translates into the reception of a greater and constant amount of solar radiation (Figure 1), which varies within the national territory only by local geographic conditions. The aforementioned condition has not been considered to take advantage of systems that favor the reduction of CO_2 emissions with special attention regarding the production of SHW, contemplating a constant flow that maintains the comfort conditions obtained with other sources.
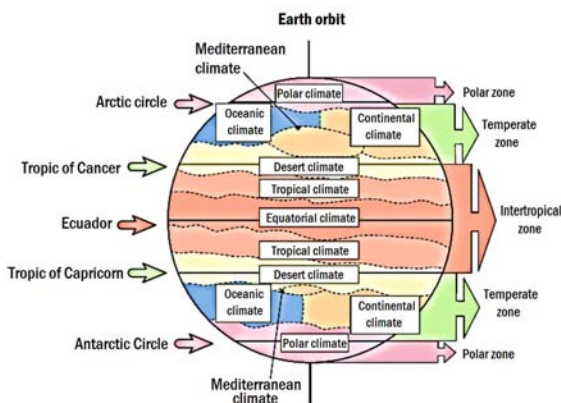
Figura 1. Thermal zones of the Earth [3]

2. Materials and methods

This research is of quasi-experimental nature; since there is no effective control for the selection and development of variables, a set of methodical and technical activities are integrated and carried out to gather the necessary information and data on the subject to be investigated and the problem to be solved [4].

The presented project requires a calculation of the percentage of CO_2 per kg of fuel burned in a defined period without solar thermal systems (control group) and the calculation of the percentage of CO_2 with application of solar thermal systems (experimental group). Four phases have been contemplated for this investigation, as shown in Figure 2.
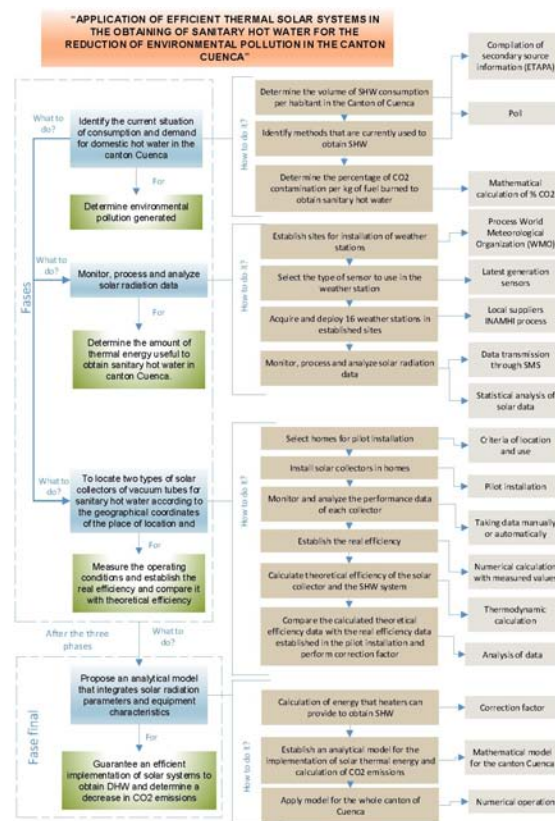
Figura 2. Outline of research design

2.1. Analysis of current SHW consumption and de-mand in the Canton of Cuenca and determination of the percentage of CO_2 emitted into the environment

At this point, water consumption per inhabitant is determined through secondary source data that is, in this case, collected from the Municipal Public Company for Telecommunications, Drinking Water, Sewerage and Environmental Sanitation (Empresa Pública Municipal de Telecomunicaciones, Agua Potable, Alcantarillado y Saneamiento Ambiental, ETAPA) and the analysis is

completed with a survey where the consumption and demand of SHW is identified. In addition, the methods used to produce hot water are identified: gas heaters, electric heaters, solar heaters, others. Finally, a mathematical calculation will determine the percentage of CO_2 contamination per kg of fuel burned to obtain SHW.

For conducting the survey, the projection of the population for the year 2016 is performed using the parabolic method [5], based on the information from the censuses of the years 1990, 2001 and 2010 [6] as shown in Table 1.

Tabla 1. Projected number of inhabitants in the canton of Cuenca for the year 2016

Year	Urban	Rural	Total
1990	194 981 hab.	136 047 hab.	331 028 hab.
2001	277 374 hab.	140 258 hab.	417 632 hab.
2010	331 888 hab.	173 697 hab.	505 585 hab.
2016	**361 781 hab.**	**210 986 hab.**	**572 767 hab.**

The population under study is made up of the number of households in the canton of Cuenca. It is estimated that an average household is composed of 5 members, which results in a total of 114 553 households for the whole canton divided into 72 356 for the urban area and 42 197 in the rural area.

To determine the sample, equation (1) is applied considering reliability level k = 95%, error limit e = 0.06, probability of success p = 0.6 and probability of failure q = 0.4.

$$n = \frac{k^2 \times p \times q \times N}{(e^2 \times (N-1)) + k^2 \times p \times q} \tag{1}$$

The significant sample to be used is 531 households divided into 266 in the urban area and 265 in the rural area. In the latter, a stratification is carried out according to the number of inhabitants of each parish due to the geographical particularities presented by each one; the urban area it is not stratified because the conditions of all the parishes are similar.

A questionnaire is used to obtain instrumental information. Taking into account the variable transit to its dimensions or components, then to the indicators and, finally, to the items or reagents [4], the established analysis is shown in Table **??**.

Tabla 2. Analysis of transit of variables for questionnaire

Analysis on the use of SHW in the Canton of Cuenca			
Variable	**Dimension**	**Indicators**	**Items**
Uso of SHW	Daily cleaning activities	If use or do not use	Use hot water for regular activities such as bathing, washing hands, washing dishes, washing clothes, etc. (Mark with an "X" your answer) YES .... NO........
No use of SHW	Consideration factor	Hierarchy of preference why does not use SHW considering cost, pollution and ease of purchase and installation.	If your answer is NO, write in the box that the numbers from 1 to 4 are blank, considering 1 to the most important and 4 least important. Very expensive............. It contaminates the environment...... Difficult to buy...... Difficult to install..........
Number of inhabitants per household	Accountant	Number of inhabitants per household	Including you, how many people live in your house? .... people
Type of system used to obtain SHW in the home	Identification of the type of system for SHW	Determination of the current system to obtain SHW considering: Gas (LPG); electrical resistance, electric induction, solar heater, solar and gas, solar and electrical resistance, other in regular activities: shower, sink, kitchen sink and laundry	Indicate the type of water heating system you use in your home for the following activities. (Mark with an "X" only in those that use hot water)

Indicate the type of water heating system you use in your home for the following activities. (Mark with an "X" only in those that use hot water)

Activity System	Shower	Handwash	Kitchen sink	Laundry
Gas (LGP)				
Electric resistance				
Electric induction				
Solar heater				
Solar and Gas (LPG)				
Solar - Electric resistance				
Other				

Variable	Dimension	Indicators	Items
Time used for cleaning activities with SHW	Determination of time	Time range for regular activities: shower, sink, kitchen sink and laundry	Considering what is marked in the previous table, determine the total daily time for each activity by adding up the time occupied by each family member. (Mark with an "X" your answer).

Time Activity	30 to 45 min	45 to 60 min	60 to 75 min	More than 75 min
Shower				
Handwash				
Kitchen Sink				
Laundry				

Variable	Dimension	Indicators	Items
Quality of the SHW system used	Attribution of performance	Degree of perception of the quality of the SHW system used	How do you rate the current water heating system that you have? (Mark with an "X" the corresponding answer, the same one that is unique). Very good...... Good...... Regular..... Bad.....
Factors to choose system	Implementation allocation	Degree of perception and ranking of factors to choose a DHW system for housing	What are the factors you considered when choosing your current water heating system? (Write in the box that the numbers from 1 to 4 are blank, considering 1 to the most important and 4 least important). Low cost...... Easy to install...... Does not pollute...... Easy to buy......

For data collection, the questionnaire is applied ac-cording to the analysis made in the previous para-graphs. A group of interviewers visited the homes and re-quested that it be completed.

The amount of energy that is required to cover the demand, considering the average values of SHW consumption in the shower, sink and in the kitchen sink determined in the survey, is obtained from equation (2):

$$D_{ACS} = V_{ACS} \times \rho_a \times C_p \times (T_{uso} - T_{red}) \quad (2)$$

Where:

D_{ACS} = Demand for SHW (J)
V_{ACS} = Volume of SHW consumption (m^3/month)
ρ_a = Water density 1000 kg/m^3
C_p = Specific heat of water (4187 J/(kg·°C))
T_{uso} = Temperature of use (°C)
T_{red} = Network temperature (°C)

To calculate CO_2 emissions generated when obtaining SHW, the energy required to obtain SHW is multiplied by an emission factor of 0.234 kg CO_2 eq/kWh for LPG and 0.385 kg de CO_2 eq/kWh for electricity [7].

2.2. Monitoring, processing and analysis of solar ra-diation data for the canton of Cuenca

For this second phase of the project, work is carried out for the selection and location of meteorological stations in accordance with the recommendations made by the World Meteorological Organization (WMO). Data quality control and corresponding ad-justments are carried out to finally quantify the exist-ing energy in each of the sectors where the meteoro-logical stations are located and which are associated with the urban and rural parishes of the canton of Cuenca.

2.2.1. Location of weather stations in the canton of Cuenca

In 2013, Universidad Politécnica Salesiana, UPS, and the National Institute of Energy Efficiency and Renewable Energies, INER installed a network of 16 me-teorological stations distributed in strategic points of the canton of Cuenca with the purpose of measuring meteorological variables and use the data in projects for the implementation of energy systems based on renewable energies [8].

For the correct geographical definition of the site sites of the stations, work was conducted in six stages as listed below [9].

- Determination of data of possible areas for placement.

- Field visits

- Selection of criteria.

- Spatial analysis

- Assessment and choice of location sites.

- Selection and location of weather stations

2.2.2. Characterization of solar radiation in the canton of Cuenca during the years 2014-2015

For this process, the global radiation information measured by the meteorological station is collected and a quality control of the obtained data is carried out, given that, due to the conditions of the location sites or due to uncontrolled circumstances of the equipment, there may be missing data in certain dates. Then, the corresponding complementation is carried out, the existing radiation is quantified and the energy contribution that the radiation offers in the different zones for each month in 2014 and 2015 is calculated.

The missing information is completed using the Angström – Prescott mathematical model modified by Page, which enables the estimation of the solar re-source in a given area [10]. The procedure consists of making use of several equations correlated to each other, which allow for the calculation of extraterrestrial radiation (He) according to the geographical location of the area of interest, to then use the Page equation and obtain the radiation on a horizontal surface (Ho). The Angström – Page correlation to determine the missing global solar radiation on a horizontal surface is shown in Table 3.

Tabla 3. Angström – Page correlation to determine global solar radiation [10]

Description	Equation
Theoretical hours of solar brightness (h)	$N = \frac{2}{15}cos^{-1}(-tan\ \phi \cdot tan\ \delta)$
Extraterrestrial radiation (J/m^2)	$H_e = \frac{24}{\pi}I_{sc}\left[1 + 0.033cos\frac{360 \times z}{365}\right] \cdot \left[cos\ \rho \cdot cos\ \delta \cdot sin\ h_s + \frac{2\pi h_s}{360}sin\ \phi \cdot sin\ \rho\right]$
Real hours (h)	$HSP_{Ecuador} = 9$
Solar radiation on horizontal surface (Wh/m^2)	$H_0 = H_e\left(a + b\frac{n_{reales}}{N}\right)$

To make the corresponding calculations, the daily supplemented values and the established sun hours are added to find the daily total, and the daily totals of each month are added to obtain the monthly total, fi-nally, the monthly totals are used to obtain the total incident annual energy value.

2.3. Characterization of vacuum tube and heat pipe solar collectors

For the case under study, two types of solar collectors are used, which are installed in two houses in the canton of Cuenca; the first is a vacuum tube heater and the other is a vacuum tube heater with a heat pipe, which are commercially available in Ecuador; For each one, the corresponding theoretical analysis is carried out applying the principles of thermodynamics and heat transfer. With the collectors installed, real effi-ciencies are determined and compared with the theo-retical data calculated, the corresponding correction is established, and the specific mathematical model is obtained for each one.

The useful heat (Qu) that would be equal to the in-cidental heat (Qinc), that is, the one obtained from solar radiation minus heat losses (Qper) that occur in the process of heat transfer, is calculated with equation (3).

$$Q_u = Q_{inc} - Q_{per} \qquad (3)$$

To determine the efficiency η of the solar collectors, equation (4) is used:

$$\eta = \frac{Q_u}{Q_{inc}} \qquad (4)$$

2.3.1. Characterization of a vacuum tube solar heater.

To calculate the incident heat in Watts, we have equation (5)

$$Q_{inc} = I_p \times \alpha_s \times A \qquad (5)$$

Where:

I_p is the average irradiation in the city of Cuenca.
A is the radiation collection area multiplied by the num-ber of tubes.
α_S is the correction factor of the incident radiation that reaches the vacuum tubes and is determined by equation (6):

$$\alpha_s = \frac{\tau\alpha}{1 - (a - \alpha)\rho_d} \qquad (6)$$

Where:
τ is the transmissivity of glass tubes.
α is the absorptivity of the tubes.
ρ_d is the diffuse reflectance of the tubes.

For the calculation of the incidence area (m^2), it must be taken into account that solar radiation, whatever the location of the sun, will only affect half of the vacuum tubes, therefore only half of the periphery will be taken into account as shown in equation (7):

$$A = \frac{d_i \times \pi \times number\ of\ tubes}{2} \qquad (7)$$

The next process is to determine the conduction, con-vection and radiation losses in the entire heater as shown in Figure 3.
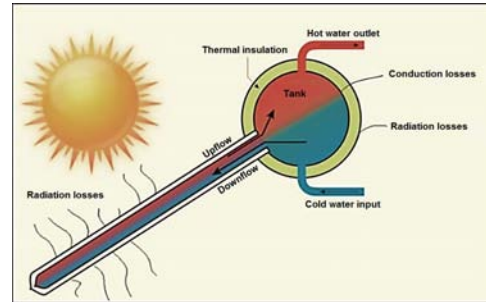
Figura 3. Heat losses in a solar vacuum tube heater [11].

The total of the losses (TQ$_{loss}$) (W) is given by the sum of the losses obtained in the vacuum tubes (Q$_{p-Tubes}$) and the losses of the accumulator tank (Q$_{p-Tank}$). Therefore, the expression for the calculation of the total losses is given by equation (8):

$$Q_{loss} = Q_{p-Tubes} + Q_{p-Tank} \qquad (8)$$

In the case of vacuum tubes, losses are generated only by radiation [12], since this is their advantage over other systems; to calculate the losses in the tubes, we have equation (9):

$$Q_{p-Tubos} = U_{lr} \times A(T_c - T_a) \qquad (9)$$

Where:

U$_{lr}$ is the coefficient of heat loss by radiation of the tubes.
A is the catchment area.
T$_c$ is the temperature of the cover.
T$_a$ is ambient temperature.

The calculation of U$_{lr}$ is carried out using the formula proposed by Duffie & Beckman [13] in which they relate the losses by radiation of the surface from the receiver tube to the cover tube (h$_{r,\ r-c}$) and radiation losses from the cover tube to the environment (h$_{r,\ c-a}$) as shown in equation 10.

$$U_{ir} = \Big[\frac{A_r}{h_w + h_{r,\ c-a} \times A_c} + \frac{1}{h_{r,\ r-c}}\Big]^{-1} \qquad (10)$$

Where:

A_r represents the area of the receiving tube.
A_c is the area of the cover or outer tube.
h$_w$ is the convection coefficient depending on the wind.

For the calculation of the convection coefficient $\left(\frac{w}{m^2 \times °C}\right)$ Equation (11) will be used:

$$h_w = N_u \times \frac{K}{D} \qquad (11)$$

Where:

N_u is the Nusselt number.
K is the coefficient of thermal conductivity.
D is the diameter of the tube.

The heat transfer coefficient between the two concentric tubes, the receiving tube and the cover tube $h_{r,\ r-c}\left(\frac{w}{m^2 \times °C}\right)$ is not attenuated by the vacuum between them, therefore, its value will be calculated by equation (12):

$$h_{r,\ r-c} = \frac{\sigma(T_r^2 + T_c^2) \times (T_r + T_c)}{\frac{1-\varepsilon_1}{\varepsilon_1} + \frac{1}{F_{12}} + \frac{1-\varepsilon_2 \times A_r}{\varepsilon_2 \times A_c}} \qquad (12)$$

Where:

ε_1 is the emissivity of the receiver tube.
ε_2 is the emissivity of the cover tube.
F_{12} is the vision factor.
T_c is the temperature of the cover.
T_r is the temperature of the receiver.

For the calculation of losses in the accumulator tank an analogy is made with thermal resistance networks since the tank is made up of three materials as shown in Figure 4.
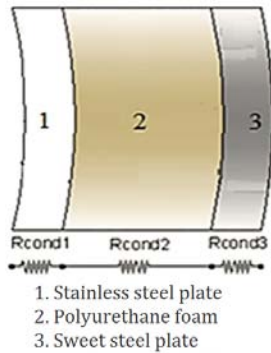
Figura 4. Resistor analogy for the multilayer accumulator tank [11].

Losses are produced in the storage tank by conduction, convection and radiation; ($Q_{p\text{-tanque}}$) and are giv-en by equation (13):

$$Q_{p-Tank} = Q_{p-cond} + Q_{p-conv} + Q_{p-rad} \qquad (13)$$

For the conduction losses in the periphery of the tank, equations (14) and (15) are considered:

$$Q_{p-cond} = \frac{T_i - T_a}{R_{Total}} \qquad (14)$$

$$R_{Total} = R_{cond1} + R_{cond2} + R_{cond3} \qquad (15)$$

Where:

T_i is the temperature inside the tank.
T_a is the temperature of the environment.
R_{Total} is the sum of the thermal resistances by conduction in each of the layers in the accumulator tank.

Equation (16) is applied to the calculation of each of the conduction resistances:

$$R_{cond} = \frac{ln\frac{D}{d}}{2 \times \pi \times L \times K} \qquad (16)$$

Where:

D is the largest diameter of the layer being analyzed.
d is the smallest diameter of the layer.
L is the length of the cylinder.
K is the coefficient of thermal conductivity of the materials.

For the losses in the tank tops, an analogy with thermal resistance networks is used since the tank consists of three materials as shown in Figure 5.
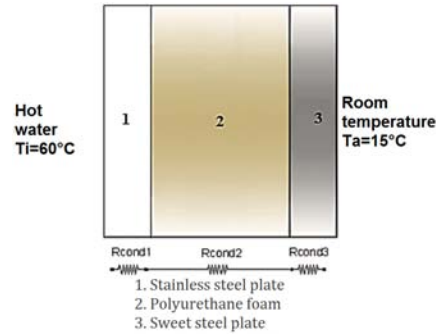
Figura 5. Resistor analogy for the multilayer tank lid [11].

The calculation procedure is the same as explained in the previous paragraphs, but the expression of the re-sistances is modified by equation (17) considering that the surfaces are flat.

$$R = \frac{e}{K \times A} \qquad (17)$$

Where:

e is the thickness of the different layers of insulation.
K is the coefficient of thermal conductivity.
A is the conduction area of the insulation layer.

By summing the total resistance of the cylinder and that of the lids, total resistance is obtained, which implemented in equation (14) allows for the calculation of total losses of conduction in the tank (Q_{p-cond}).

For losses by convection in the tank, equation (18) is used.

$$Q_{p-cond} = hA_t(T_t - T_a) \qquad (18)$$

Where:

h is the coefficient of heat transfer by convection.
A_t is the cross-sectional area of the storage tank.
T_t is the temperature on the outer surface of the tank.
T_a is ambient temperature.

To calculate the coefficient of heat transfer by convection, equation (19) is used:

$$h = \frac{N_u \times K}{D} \qquad (19)$$

Where:

N_u is the Nusselt number.
K is the coefficient of thermal conductivity of air.
D is the outside diameter of the storage tank.

Equation (20) is used to calculate the radiation losses in the tank:

$$Q_{rad} = \varepsilon \sigma A_t(T_t^4 - T_a^4) \qquad (20)$$

Where:

ε is the emissivity of the tank's surface.
σ is the Stefan Boltzman coefficient.
A_t is the cross-sectional area of the storage tank.

2.3.2. Characterization of solar heater of vacuum tubes with heat pipes.

The process of calculating efficiency and losses in the tank is the same as for vacuum tubes; the difference for this type of heater is in the vacuum tube system with heat pipes, where an additional element inter-venes in the exchange that will modify the efficiency value in the system. For this particular case the U_{lr} will now be U_l, which is the coefficient of heat losses by radiation of the tubes.

The calculation of U_l for this type of heater is carried out using the formula proposed by Duffie & Beckman [13], in which they relate the radiation losses from the surface of the receiver tube to the cover tube ($h_{r, r-c}$), radiation losses from the cover tube to the environment ($h_{r, c-a}$) and, in addi-tion, losses between the heat pipe and the receiver tube ($h_{r, tc-r}$) are considered as shown in equation (21):

$$U_l = \left[\frac{A_r}{h_w + h_{r, c-a} \times A_c} + \frac{1}{h_{r, r-c}} + \frac{1}{h_{r, tc-r}} \right]^{-1} \qquad (21)$$

The incorporated term considers the losses between the heat pipe to the receiver tube ($h_{r, tc-r}$) and is calculated with formula (22):

$$h_{r, tc-r} = \frac{\sigma \times 4 \times T^3}{\frac{1-\varepsilon_1}{\varepsilon_1} + 1 \frac{(1-\varepsilon_2)A_1}{\varepsilon_2 A_2}} \qquad (22)$$

Where:

ε_1 is the emissivity of copper.
ε_2 is the emissivity of the glass tube.
A_1 is the area of the heat pipe.
A_2 is the area of the glass tube.
σ is the Stefan Boltzman coefficient.
T is the temperature of the receiver.

2.3.3. Practical determination of the efficiency of the vacuum tube collector and the vacuum tube collector with heat pipes.

For the two types of heaters installed, the following variables are monitored:

- Room temperature [°C]

- Water temperature in the storage tank [°C]

- Temperature of water that enters from the supply network [°C]

- Water volume [liters]

The values measured throughout a year are used to calculate the efficiency of the heater using formula 23:

$$\eta_s = \frac{\dot{m} \times C_p \times (T_s - T_t)}{Q_{inc}} \qquad (23)$$

Where:

$\dot{m}$ is the mass flow of water that circulates through the heater [kg/s].
C_p is the specific heat of water [J/kg·K].
T_s is the water outlet temperature [°C].
T_i is the water intake temperature [°C].
Q_{inc} is useful energy coming from the sun [W/m^2].

Finally, the measured data are compared with the calculated data and the correction is made in the theoretical analysis.

2.4. Feasibility of implementation of solar systems to obtain SHW and determination of reduction of environmental pollution

At this point, the feasibility of implementing systems to obtain SHW will be defined considering the amount of solar energy measured during the years 2014 and 2015 for the parishes of the canton of Cuenca.

For the analysis, data on measured solar radiation are used to calculated the energy that the two types of heaters are able to provide to obtain SHW based on radiation, to then be compared with the energy demand determined in the field work. The percentage of contribution that these systems could generate and the decrease that could occur in emanations of CO_2 with their implementation is also calculated.

In addition, the amount of energy that should be generated with complementary conventional sources to guarantee a constant supply of hot water in the residences is determined.

3. Results and discussion

In the first stage, equation (1) is applied to determine the sample.

By replacing the values, the size of the sample is 531 households.

The applied survey shows that 82% of households in the canton of Cuenca use SHW and 18% do not. (Figure 6)
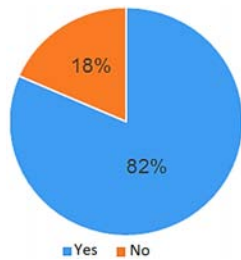
Figura 6. SHW in homes in the canton of Cuenca.

Those who do not use SHW consider that it is a costly implementation, while potential environmental pollution was not considered as an important factor at all (Figure 7).
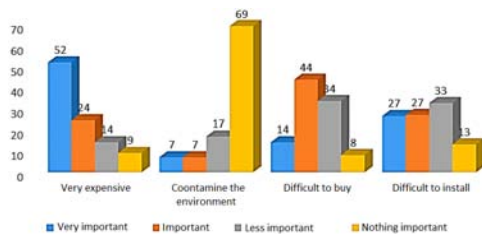
Figura 7. Reasons why a Cuenca household does not have SHW.

In Cuenca, the number of inhabitants per household is between 3 and 6, as shown in Figure 8; the trend of the curve is to the right and is maintained for the urban and rural areas, so the value of five members per household considered is a valid alternative for the analysis.
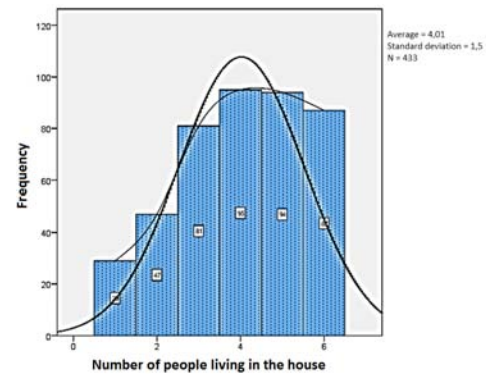
Figura 8. Number of inhabitants per household in the canton of Cuenca.

With regard to the systems used to obtain domestic hot water, the LPG heating system predominates (Figure 9).

SHW is used mainly in showers, sinks and kitchen sinks, and the frequency of use for the five members in sinks and kitchen sinks is between 30 to 45 min daily, and for the shower it is between 30 and 60 minutes (Figure 10).
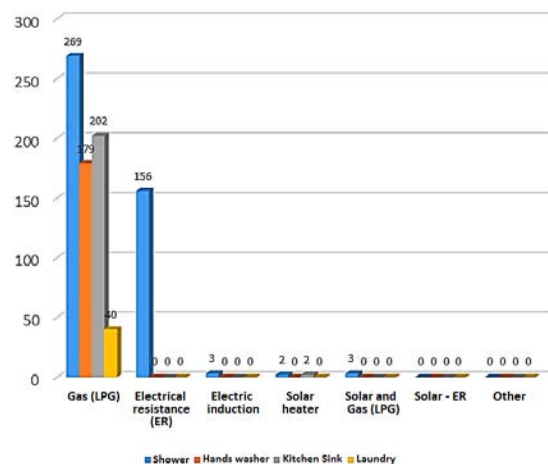
Figura 9. Systems used to obtain SHW.
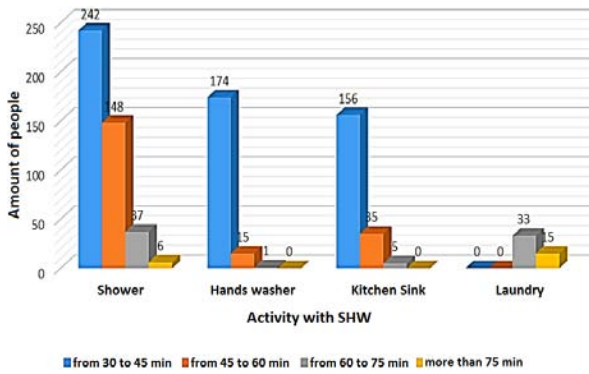
Figura 10. Type of activity with SHW and time spent

The systems currently used to obtain SHW are effi-cient since the population qualifies them as good and very good (Figure 11).
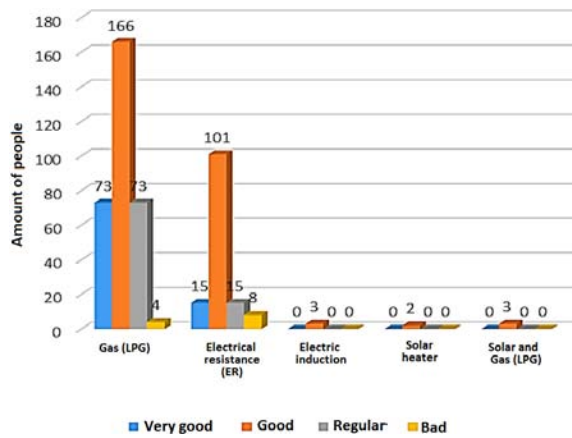
Figura 11. Rating of the SHW system.

When it comes to selecting the system, what is most important is the cost of the system and what is less important is the pollution it may generate (Figure 12).
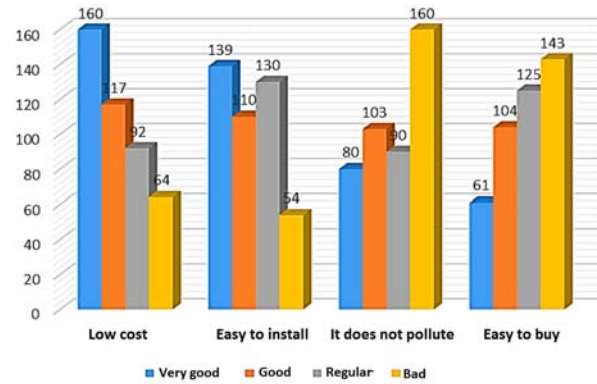
Figura 12. Importance of parameters when choosing a system to obtain SHW.

The average value of SHW consumption is deter-mined with question 4. To accomplish this, the average values of the sum of the times of use for shower, sink and kitchen sink are calculated. The value correspond-ing to laundry is neglected since the percentage of us-ers in this activity is minimal.

With the aforementioned, SHW consumption is de-termined, multiplying the total time used by the mem-bers of the household by an average consumption of 0.006 m^3/min [14], and by a coincidence factor since all the members bathe every day, or use SHW in the sink or in the kitchen sink. These values have been identified considering the habits of the inhabitants of the canton of Cuenca. The results obtained can be seen in Table 4.

Tabla 4. Calculation of effective SHW consumption per 5-member household in the canton of Cuenca

Activity	Average daily time (min)	Match factor	Efective daily time (min)	Flow in pipe (m^3/min)	Effective consumption (m^3/day)
Shower	44	0,5	22	0,006	0,13
Hands washer	30	0,4	12	0,006	0,07
Kitchen sink	20	0,4	8	0,006	0,05
				Total	**0,25**

To calculate the monthly energy demand, we use equation (2). The value corresponding to Tuso is 60°C, while for Tred it is an average of 8°C, this value is assumed since there is a variation between 6 and 10°C in urban and rural areas; the value of V$_{ACS}$ is 0.25 m^3/day, if the values of the parameters are known, the expression is replaced by considering the days of each month and the monthly and annual value of energy required to produce SHW is determined; the calculated values are shown in Table 5.

Once the value of monthly and annual energy de-mand required to obtain SHW for a family of 5 mem-bers is obtained, CO$_2$ production is calculated by multiplying the obtained value by the emission in-dex which, in the case of generic LPG, is 0.234 kg of CO$_2$ eq/kWh [7], resulting in a value of 2141.20 kg of CO$_2$ eq. per year in an average family of 5 members in the canton of Cuenca, as presented in Table 5.

Tabla 5. Monthly and annual energy demand to produce SHW in a household of 5 members in the Cuenca canton and production thereof CO_2

Month	Days	Consumtion (m^3/day)	Consumption total (m^3) monthly	Tred $(°C)$	Tuse $(°C)$	ΔT $(°C)$	D_{ACS} (MJ) per month	D_{ACS} (kWh) per month	kg eq of CO_2
January	31	0,25	7,81	8	60	52	1700,86	472,46	181,9
February	28	0,25	7,06	8	60	52	1536,26	426,74	164,29
March	31	0,25	7,81	8	60	52	1700,86	472,46	181,9
April	30	0,25	7,56	8	60	52	1645,99	457,22	176,03
May	31	0,25	7,81	8	60	52	1700,86	472,46	181,9
June	30	0,25	7,56	8	60	52	1645,99	457,22	176,03
July	31	0,25	7,81	8	60	52	1700,86	472,46	181,9
August	31	0,25	7,81	8	60	52	1700,86	472,46	181,9
September	30	0,25	7,56	8	60	52	1645,99	457,22	176,03
October	31	0,25	7,81	8	60	52	1700,86	472,46	181,9
November	30	0,25	7,56	8	60	52	1645,99	457,22	176,03
December	31	0,25	7,81	8	60	52	1700,86	472,46	181,9
						Demand per year	20026,25	5562,85	2141,7

Considering the previous data and with 114 553 5-member households, the contribution to pollution is of 245 338 160 kg eq of CO_2 or 245338 of tn $CO_2$2 eq.

With respect to monitoring, processing and analysis of global solar radiation, the process takes into account radiation data measured by a group of 16 meteorological stations installed in the canton of Cuenca according to Table 6.

Complementation of missing data is performed using an Angström – Page correlation for the data of the stations as shown in Table 7.

The complemented tables are obtained; as an example, Table 8 is presented for the station at the rural parish of Chaucha.

Tabla 7. Weather stations with missing data

Weather station	Year	Month	Days with missing data
CTS	2014	january	1-9
	2014	march	19-24
Chaucha	2014	november	27-30
	2014	december	9-15
Cumbe	2014	january	1-8
Irquis	2014	january	1-3
Santa Ana	2014	january	1-3
Turi	2014	january	1-7
UPS	2014	january	1-7

Tabla 6. Weather station data

Weather station	Coordinates	Elevation (m s. n. m.)
Quingeo	729057; 9664602	2893
Molleturo	679708; 9692232	3530
Baños	712899; 9672817	3062
CTS	720504; 9677509	2561
UPS	723584; 9680788	2556
Tixán	723017; 9686678	2725
Cumbe	719190; 9656242	3179
Sayausí	715974; 9681200	2727
Nulti	729704; 9682466	2601
San Joaquín	714405; 9680807	2764
Llacao	730418; 9685180	2542
Santa Ana	730085; 9672006	2651
Chaucha	672859; 9678690	1929
Turi	721103; 9674971	2768
Sinincay	722340; 9685283	2696
Victoria del Portete	713645; 9659192	2665

Tabla 8. Missing radiation data complemented in the month of december 2014 at the Chaucha station

Hour/Day	december 14								
	8	9	10	11	12	13	14	15	16
01H00	0	0	0	0	0	0	0	0	0
02H00	0	0	0	0	0	0	0	0	0
03H00	0	0	0	0	0	0	0	0	0
04H00	0	0	0	0	0	0	0	0	0
05H00	0	0	0	0	0	0	0	0	0
06H00	0	0	0	0	0	0	0	0	0
07H00	13	7	13	13	24	9	14	3	5
08H00	59	72	67	81	112	89	72	64	76
09H00	123	255	267	495	292	217	151	305	279
10H00	569	309	500	739	331	504	191	633	465
11H00	955	355	719	941	570	719	387	1071	902
12H00	1123	569	940	1085	923	783	555	1054	1187
13H00	1114	453	922	1129	798	536	651	1063	1022
14H00	975	224	670	1128	1004	664	419	325	686
15H00	1059	67	226	432	399	394	790	69	216
16H00	173	57	96	89	383	389	241	78	86
17H00	50	85	31	90	184	177	68	51	57
18H00	11	47	6	54	8	71	62	53	73
19H00	1	4	2	4	1	7	6	5	9
20H00	0	0	0	0	0	0	0	0	0
21H00	0	0	0	0	0	0	0	0	0
22H00	0	0	0	0	0	0	0	0	0
23H00	0	0	0	0	0	0	0	0	0
24H00	0	0	0	0	0	0	0	0	0

With the supplemented data, the total daily, monthly and annual radiation is calculated for each station (Figure 12, example from Chaucha station).
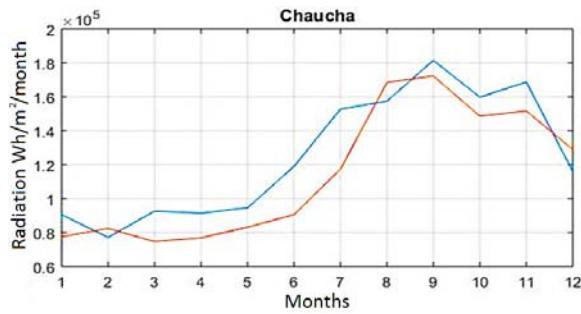
Figura 13. Global Solar Radiation – Chaucha sector

With the averages of all the data measured in the 16 stations, the average global solar radiation curve for the canton of Cuenca is obtained as shown in Figure 14.
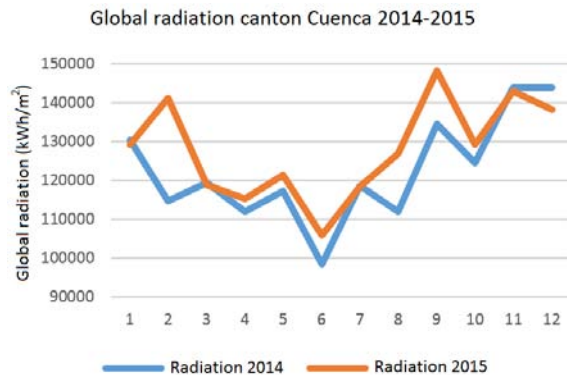

Figura 14. Global Radiation - Cuenca canton 2014-2015

The installed heaters have the following characteristics (Figure 15):

Figura 15. Characteristics of solar heaters installed

The efficiency of the solar collectors is calculated both theoretically and practically and the values are compared, leading to the conclusion that the average of the percentage difference for the heater of simple evacuated vacuum tubes is 5% and that of vacuum tubes with tubes of heat is 2%; (Figure 16) with these values the analysis is corrected and the real efficiency of the collectors is determined, the results being 74% for vacuum tube and 80% for of vacuum tubes with heat pipes.
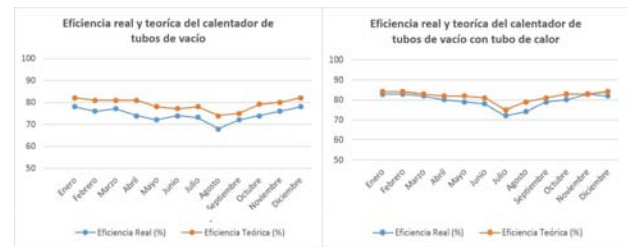
Figura 16. Real and theoretical efficiency of solar heaters

Energy of loss and useful energy that will be used to obtain SHW is compared with the energy demand to establish the missing amount which must be covered with auxiliary systems for each type of heater (Tables 9, 10). The calculation contemplates 9 effective daily hours of sunshine.

Tabla 9. Energy analysis for the vacuum tube heater

Station	Average irradiance kWh/m²		Incident energy kWh		Lost energy kWh		Useful energy kWh		Demand energy kWh		Missing energy kWh		Missing energy kg (GLP)	
	2014	2015	2014	2015	2014	2015	2014,00	2015,00	2014	2015	2014	2015	2014	2015
Baños	1359,11	1349,73	2729,67	2710,82	709,71	704,81	2019,96	2006,00	5562,85	5562,85	3542,89	3556,85	280,32	281,42
Chaucha	1454,31	1372,09	2920,86	2755,73	759,42	716,49	2161,43	2039,24	5562,85	5562,85	3401,42	3523,61	269,12	278,79
CTS	1527,98	1551,79	3068,82	3116,64	797,89	810,33	2270,93	2306,31	5562,85	5562,85	3291,92	3256,54	260,46	257,66
Cumbe	1457,39	1525,81	2927,04	3064,46	761,03	796,76	2166,01	2267,70	5562,85	5562,85	3396,84	3295,15	268,76	260,72
Irquis	1466,93	1509,14	2946,20	3030,99	766,01	788,06	2180,19	2242,93	5562,85	5562,85	3382,66	3319,92	267,64	262,67
Llacao	1609,21	1665,49	3231,97	3345,01	840,31	869,70	2391,66	2475,31	5562,85	5562,85	3171,19	3087,54	250,91	244,29
Molleturo	1823,05	1968,17	3661,44	3952,91	951,97	1027,76	2709,47	2925,15	5562,85	5562,85	2853,38	2637,70	225,76	208,70
Nulti	1691,23	1781,70	3396,70	3578,40	883,14	930,38	2513,56	2648,01	5562,85	5562,85	3049,29	2914,84	241,26	230,62
Quingeo	1472,95	1570,64	2958,31	3154,51	769,16	820,17	2189,15	2334,34	5562,85	5562,85	3373,70	3228,51	266,93	255,44
San Joaquín	1414,30	1364,51	2840,51	2740,51	738,53	712,53	2101,98	2027,98	5562,85	5562,85	3460,87	3534,87	273,83	279,68
Santa Ana	1431,65	1482,57	2875,36	2977,62	747,59	774,18	2127,76	2203,44	5562,85	5562,85	3435,09	3359,41	271,79	265,80
Sayausí	1435,70	1440,54	2883,49	2893,20	749,71	752,23	2133,78	2140,97	5562,85	5562,85	3429,07	3421,88	271,31	270,74
Sinincay	1523,17	1552,78	3059,17	3118,64	795,38	810,85	2263,79	2307,79	5562,85	5562,85	3299,06	3255,06	261,02	257,54
Tixán	1462,79	1472,53	2937,90	2957,45	763,85	768,94	2174,04	2188,51	5562,85	5562,85	3388,81	3374,34	268,13	266,98
Turi	1441,54	1515,15	2895,23	3043,06	752,76	791,20	2142,47	2251,86	5562,85	5562,85	3420,38	3310,99	270,62	261,97
UPS	1640,31	1679,48	3294,43	3373,09	856,55	877,00	2437,88	2496,09	5562,85	5562,85	3124,97	3066,76	247,25	242,64
										Average values	3313,85	3259,00	262,19	257,85
											3286,42		260,02	

Tabla 10. Energy analysis for the vacuum tube heater with heat pipes

Station	Average irradiance kWh/m^2		Incident energy kWh		Lost energy kWh		Useful energy kWh		Demand energy kWh		Missing energy kWh		Missing energy kg (GLP)	
	2014	2015	2014	2015	2014	2015	2014,00	2015,00	2014	2015	2014	2015	2014	2015
Baños	1359,11	1349,73	2729,67	2710,82	545,93	542,16	2183,74	2168,65	5562,85	5562,85	3379,11	3394,20	267,36	268,55
Chaucha	1454,31	1372,09	2920,86	2755,73	584,17	551,15	2336,69	2204,58	5562,85	5562,85	3226,16	3358,27	255,26	265,71
CTS	1527,98	1551,79	3068,82	3116,64	613,76	623,33	2455,06	2493,31	5562,85	5562,85	3107,79	3069,54	245,89	242,86
Cumbe	1457,39	1525,81	2927,04	3064,46	585,41	612,89	2341,64	2451,57	5562,85	5562,85	3221,21	3111,28	254,87	246,17
Irquis	1466,93	1509,14	2946,20	3030,99	589,24	606,20	2356,96	2424,79	5562,85	5562,85	3205,89	3138,06	253,65	248,29
Llacao	1609,21	1665,49	3231,97	3345,01	646,39	669,00	2585,58	2676,01	5562,85	5562,85	2977,27	2886,84	235,56	228,41
Molleturo	1823,05	1968,17	3661,44	3952,91	732,29	790,58	2929,15	3162,33	5562,85	5562,85	2633,70	2400,52	208,38	189,93
Nulti	1691,23	1781,70	3396,70	3578,40	679,34	715,68	2717,36	2862,72	5562,85	5562,85	2845,49	2700,13	225,14	213,64
Quingeo	1472,95	1570,64	2958,31	3154,51	591,66	630,90	2366,65	2523,61	5562,85	5562,85	3196,20	3039,24	252,89	240,47
San Joaquín	1414,30	1364,51	2840,51	2740,51	568,10	548,10	2272,41	2192,41	5562,85	5562,85	3290,44	3370,44	260,34	266,67
Santa Ana	1431,65	1482,57	2875,36	2977,62	575,07	595,52	2300,29	2382,09	5562,85	5562,85	3262,56	3180,76	258,14	251,66
Sayausí	1435,70	1440,54	2883,49	2893,20	576,70	578,64	2306,79	2314,56	5562,85	5562,85	3256,06	3248,29	257,62	257,01
Sinincay	1523,17	1552,78	3059,17	3118,64	611,83	623,73	2447,34	2494,91	5562,85	5562,85	3115,51	3067,94	246,50	242,74
Tixán	1462,79	1472,53	2937,90	2957,45	587,58	591,49	2350,32	2365,96	5562,85	5562,85	3212,53	3196,89	254,18	252,94
Turi	1441,54	1515,15	2895,23	3043,06	579,05	608,61	2316,18	2434,45	5562,85	5562,85	3246,67	3128,40	256,88	247,52
UPS	1640,31	1679,48	3294,43	3373,09	658,89	674,62	2635,54	2698,47	5562,85	5562,85	2927,31	2864,38	231,61	226,63
Valores promedio											3131,49	3072,20	247,77	243,07
											3101,85		**245,42**	

With the established values, it is determined that the solar heater of vacuum tubes shows an average coverage with solar energy of 40.92%, and the heater of vacuum tubes with heat pipe 44.23%, this implies an average reduction, in the first case, of 100 397.17 tn CO_2 eq and in the second case 108 537.24 tn CO_2 eq, taking into account that using LPG-based heaters implies the generation of 245 337.84 tn CO_2 eq per year (Figure 17).

The values of coverage and reduction of pollution will vary slightly depending on the area in which they are located, which are assigned to the measurements of the 16 installed meteorological stations [15].
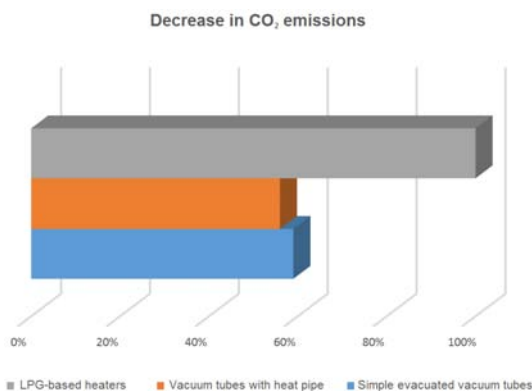
Figura 17. Decrease in CO_2 emissions through obtaining SHW with hybrid heaters with solar technology in contrast to LPG-based heaters

4. Conclusions

To obtain SHW in the canton of Cuenca, its inhabitants mainly use LPG-based systems, causing an approximate contamination of 245,337 tn CO_2 eq.

The amount of hot water used for the different activities, corresponding to 50 l per person per day,

is excessive compared to the 30 l per day used in Spain [16, 17] in accordance with the ordinances imposed in that country.

The average radiation in the canton of Cuenca is between 1359 kWh/m^2 and 1968 kWh/m^2 depending on the geographical conditions of each sector. Using solar heaters of vacuum tubes can generate an energy contribution to obtain SHW ranging from 40.92% to 44.23%.

To guarantee a constant supply of SHW the heaters must be hybrid, that is, they must work with solar energy and have an auxiliary system that can be based on LPG or electrical resistance.

If the implementation of hybrid systems with solar technology is carried out, a reduction in contamination of CO_2 of around 44% is obtained, this implies stopping the emanation to the environment of 108 537.24 tn CO_2 eq per year.

Referencias

[1] B. Veritas, *Manual para la formación en medio ambiente*, S. LEX NOVA, Ed., 2008, advances in Material & Processing Technologies Conference. [Online]. Available: https://goo.gl/vLX6Hy

[2] Eurobserv'er. (2017) Solar thermal and concentrated solar power barometer 2017. [Online]. Available: https://goo.gl/2XFMc8

[3] F. Entrena, *Determinación del potecial solar UF0212*, ic editorial, Ed., 2013. [Online]. Available: https://goo.gl/9PsoEw

[4] R. Hernández Sampieri, C. Fernández Collado, and P. Baptista Lucio, *Metodología de la Investigación*, 5th ed., M. G. Hill, Ed., 2010. [Online]. Available: https://goo.gl/1zETzt

[5] G. Ríos Jiménez. (2016) Métodos para calcular la población futura. [Online]. Available: https://goo.gl/WCH7wy

[6] INEC. (2010) Resultados del censo 2010. [Online]. Available: https://goo.gl/1BC66V

[7] G. de Aragón. (1967) Cálculo de emisiones. [Online]. Available: https://goo.gl/yPfTVh

[8] UPS - INER. (2013) Métodos para el control de calidad y compementación de datos faltantes en parámetros meteorológicos relacionados con la utilización de energías renovables. [Online]. Available: https://goo.gl/1JLb9m

[9] I. Korkut, M. Kasap, I. Ciftci, and U. Seker, *Cultivos energéticos alternativos*, 2009, ch. Determinación de emplazamientos adecuados para estaciones meteorológicas en la provincia de Imbabura utilizando sistemas de información geográficos, pp. 75–87. [Online]. Available: https://goo.gl/a8b2ZB

[10] J. Martínez Aguirre and J. Asitimbay Chávez, "Caracterización y análisis estadístico de la radiación solar directa para aplicaciones de media y alta temperatura en áreas circundantes al ocp," Master's thesis, Universidad de las Fuerzas Armadas, 2015. [Online]. Available: https://goo.gl/X4RgVK

[11] J. Jiménez Patiño, H. Llivichuzca Chacha, and J. Calle Sigüencia, "Diseño, implementación y monitoreo de calentadores híbridos con energía solar-glp y energía solar-calentadores eléctricos para la obtención de agua caliente sanitaria." Tesis de grado, Universidad Politécnica Salesiana, Ecuador, 2014. [Online]. Available: https://goo.gl/4kV4w8

[12] Sitiosolar. (2014) Los colectores solares de tubo de vacío. Hybrid evolutionary systems for manufacturing processes. [Online]. Available: https://goo.gl/EnpH8n

[13] J. A. Duffie and W. A. Beckman, *Solar Engineering of Thermal Processes*, I. John Wiley & Sons, Ed., 2013. [Online]. Available: https://goo.gl/rjjMtJ

[14] Afta-asociation. Dimensionado de instalaciones. [Online]. Available: https://goo.gl/pnQpzi

[15] O. Delgado, "Plan de ordenamiento y desarrollo territorial del cantón Cuenca," in *Memorias del II Congreso Binacional de Investigación, Ciencia y Tecnología de las Universidades*, 2013, pp. 721–729. [Online]. Available: https://goo.gl/S3WixM

[16] D. Fuentes Cantero, "Instalación de colectores solares para suministro de acs en valencia." Proyecto de Fin de Carrera, Universidad Carlos III de Madrid, España, 2009. [Online]. Available: https://goo.gl/UTh93M

[17] ATECYR - IDAE, *Guía técnica Agua Caliente Sanitaria Central*, Instituto para la Diversificación y Ahorro de la Energía Std., 2015. [Online]. Available: https://goo.gl/HCKYtz

Quantification of opacity in diesel electronic engines using diesel and biodiesel

Cuantificación de la opacidad en motores electrónicos diésel usando diésel y biodiésel

Carlos Mafla Yépez[1,*], Rommel Imbaquingo Navarrete[1], Jorge Melo Obando[1],

Ignacio Benavides Cevallos[1], Erik Hernández Rueda[1]

Abstract

The present study has the purpose of determining the levels of opacity with the use of diesel as biodiesel based on castor oil at 15% (B15). For the determination of the opacity an electronic diesel engine test bench was used, the opacity measurements were made using a duly calibrated opacimeter. The Opacimeter consists of a probe which is installed at the end of the exhaust pipe, which captures the gases and yields values for each test, considering the types of fossil or biofuel fuels and engine speed, subjecting several RPMs that go from 1200 to 3000 for each fuel. At the end of the tests, the opacimeter allowed to obtain values that indicate the difference in opacity and to make a comparative analysis of the use of diesel and biodiesel. At the same time, an average opacity of the tests was obtained for each type of fuel, this value being the same that will be compared with the national standard concerning this study. From the tests carried out, a 96% reduction in the opacity of the engine could be evidenced with the use of B15 biodiesel from Higuerilla oil compared to diesel.

Keywords: biodiesel, B15, fossil diesel, castor oil, opacity, RPM.

Resumen

El presente estudio tiene la finalidad de determinar los niveles de opacidad con el uso de diésel fósil como de biodiésel a base de higuerilla al 15 % (B15). Para la determinación de la opacidad se utilizó un banco de pruebas de motores diésel electrónico, se realizó las mediciones de opacidad usando un opacímetro debidamente calibrado. El opacímetro consta de una sonda la cual se le instala en el extremo del tubo de escape, captando los gases y arrojando valores propios por cada prueba, considerando los tipos de combustibles fósil o biocombustible y el régimen del motor, sometiendo a varias revoluciones por minuto que van de 1200 a 3000 por cada combustible. Al concluir las pruebas el opacímetro permitió obtener una opacidad de 11,1 % con diésel fósil y 0,386 con biodiésel B15 obteniendo una reducción del 96 % de opacidad, a la vez se obtuvo un promedio de opacidad de las pruebas por cada tipo de combustible siendo este valor el que se comparará con las normas nacionales e internacionales concernientes a este estudio. Con estos resultados se contribuye a la mejor conservación del ambiente ya que se emana menor cantidad de hollín, de igual manera se disminuye las enfermedades respiratorias y de corazón de las personas según la organización mundial de la salud.

Palabras clave: biodiésel, B15, diésel fósil, higuerilla, opacidad, RPM.

[1,*]Research group in internal combustion engines with biofuel (BICER), Universidad Técnica del Norte, Ibarra – Ecuador. Author for correspondence ✉: cnmafla@utn.edu.ec, http://orcid.org/0000-0003-3704-8676
https://orcid.org/0000-0001-7140-3374, https://orcid.org/0000-0003-0546-6988
https://orcid.org/0000-0003-3332-8523, https://orcid.org/0000-0003-1969-9619

1. Introduction

Greenhouse gas emissions (GH) (NO_x, CO_2, CO, HC) are respon-sible for causing global warming, deteriorating the environment and the health of human beings [1]. According to the World Environment Organization, the automotive industry is the cause of 15% of environmental pollution worldwide. Something very important and that should not be overlooked when using fossil fuels is their potential to generate polluting emissions, among which are carbon dioxide (CO_2), the main responsible for the greenhouse effect; Carbon monoxide (CO), which has lethal effects on man; nitrogen oxides (NO_x) and unburned or partially burned hydrocarbons (HC), main photochemical smog formers in the presence of light; sulphurous emissions (SO_x), which cause acid rain, sulphates, and particulate matter, caus-ing respiratory diseases and cancer [2].

In addition, it is known that the automotive fleet with gaso-line and diesel engines is increasing, the latter being responsible for the emission of soot particles into the environment.

Soot, ash and dust are relatively heavy particles that are depos-ited on the ground and the air cleans them quickly. But near their source of origin they are often a health hazard, since they can cause chronic respiratory diseases such as emphysema and cancer [3].

The percentage of opacity is the unit of measurement that determines the degree of opacity of the exhaust emissions of a diesel mobile source. In Ecuador, this unit is determined by the Ecuadorian Standardization Institute through the NTE INEN 2 202:2000 technical standard, which states the maximum opacity limits of emissions for mobile sources with diesel engines as follows: 50% opacity for models from the year 2000 back, and 60% opacity for models from the year 2000 onward [4].

For this reason the scientific community is in a tireless ef-fort to find new sources of clean and renewable energy, which helps to reduce emissions to the atmosphere and therefore reduce the diseases produced in humans.

This is how biodiesel rose as an alternative to fossil diesel, as it is a renewable liquid biofuel that is composed of monoalkyl esters of long-chain fatty acids derived from renewable lipids such as vegetable oils that are mixed, in different percentages, with gasoil [5]. It is also a carbon neutral alternative fuel that must be taken into account as a mechanism to reduce emissions of polluting gases that occur in combustion [6].

Currently, there are several technologies for Biodiesel production. Vegetable oils have properties that allow for the manipulation of their density and viscosity, which is why these oils are suitable for the production of biodiesel [7].

Biodiesel has some very interesting characteristics: No major changes are needed in the engine, it is bio-degradable and innocuous for the environment, it generates employment in rural areas, it diversifies energy sources [8].

Through the use of pure or mixed biodiesel, fantastic re-sults have been achieved. The use of this biofuel has signifi-cantly reduced the potential for destruction of the ozone layer by up to 50%. Sulfate and sulfure oxide emissions are eliminated with pure biodiesel. These are the main components of acid rain and are linked to the formation of particles mainly by the content of sulfur and the content of heavy aromatic components [9]. The use of biodiesel in diesel engines causes a signifi-cant reduction in total unburned hydrocarbons, of carbon monoxide and particles in suspension; the emissions of nitrogen oxides are similar or slightly increased [10].

With regard to diesel engines, biodiesel, given the tech-nical, strategic and environmental advantages it offers, is the best alternative to partially or totally replace petroleum diesel fuel [11].

By using biodiesel it is possible to reduce CO and CO_2 emissions resulting from combustion due to the fact that a biodiesel molecule contains between 12 and 18 carbons, and a diesel molecule can contain up to 20 carbons [12].

The properties of biodiesel have a great influence on the emissions of soot to the environment, for this reason the quality of the B15 castor oil biodiesel obtained are: Its high cetane number, 50.5, and its high viscosity, $5.02 mm_2/s$ [11]. On the other hand, castor oil biodiesel has points of cloud and fluidity that give it advantages for use at low temperatures.

The opacity of fumes is an indirect measure of the soot content of the particulate material generated during combus-tion and exhaust. Biodiesel in its chemical structure provides extra oxygen to combustion, so it is expected to facilitate the oxidation of the particles and therefore a decrease in smoke opacity occurs as its concentration increases in the mixtures [13].

1.1. Biodiesel production

Biodiesel originates due to a chemical reaction, such as transesterification, where the glycerol present in the oils is supplied by an alcohol, such as methanol, generally used in the produc-tion of recycled vegetable oils, and in mixtures with ethanol in new oils in the presence of a catalyst.

Potassium hydroxide (KOH) or sodium hydroxide (NaOH) can be used as catalysts. When using KOH, the glycerin result-ing from the process is much less toxic than when using NaOH. Additionally, potassium hydroxide dissolves much better in methanol. For the process to be as efficient as possible, the catalysts must have a purity of at least 96% for NaOH and around 92-85% in KOH; it is quite difficult to find the latter with a higher purity.

Transesterification consists in the reaction between a tri-glyceride (composed of a glycerol molecule esterified by three molecules of fatty acids) contained in castor oil and alcohol (methanol or ethanol), originating glycerin and esters derived from fatty acids. When using methanol, the biodiesel will be composed of methyl esters. The catalyst is dissolved in light alcohol (methanol), then it enters the reactor, along with the crude oil extracted from castor, where they will remain at a minimum temperature of 45.4 °C and maximum of 55 °C, at a rate of 3000 rpm, around 3 hours, giving rise to the transesteri-fication process. Subsequently the glycerin will be separated, which will go through a washing process, which is to add 26% of water in volume of oil.

Finally, the process of water evaporation is carried out, at temperatures of around 100 °C, to then mix it with fossil diesel in B15 proportion and use it in compression engines.

By using biodiesel, it is possible to reduce the emissions of carbon monoxide and carbon dioxide present in combustion, since one molecule of biodiesel contains between 12 and 18 carbons, and one diesel molecule of fossil origin can contain up to 20 carbons [14].

1.2. Properties of B15 castor oil biodiesel

The physicochemical properties of biodiesel B15 were deter-mined in the petroleum laboratories of the Central University of Quito with positive results. Table 1 shows the most relevant:

Table 1. Physicochemical properties of B15

Determination	Result
Density API A 60 F	544,62
Falshpoint* °C	72,1
Sulfur* % P	0,0148
Calculated cetane index	51

One of the main characteristics of diesel fuel is cetane, this indicates the quality of the fuel. As can be seen, it has a value of 51, thus achieving a better expansion and burning of the gases that are generated in the combustion and therefore less environmental pollution. These parameters are found in research projects of the Automotive Engineering Major at Universidad Técnica del Norte.

Due to the great benefits that the use of biodiesel has shown, the purpose of this article is to demonstrate the decrease in opacity with the use of B15 castor oil biodiesel.

2. Materials and methods

The present study is based on an experimental quantitative study of transversal descriptive type.

First of all, of a quan-titative order in obtaining results of percentages of opacity in each test, considering the type of fuel and the engine regime, as well as in the comparative analysis of results versus the tables of limit values of opacity for diesel engines adhering to the INEN 2 207: 2002 standard.

Of experimental type: In obtaining biodiesel from the castor plant and in the opacity measurements made in the vehicle's exhaust system.

Of descriptive type in the analysis of the comparative results, of realization of tests, and in the description of the study itself.

Cross type since it was done in a specific time frame, en-abling us to obtain the information immediately and also corre-late results obtained from the different tests and the values imposed by the current national standard and to determine the benefits of both fuels in the environment.

In order to determine and analyze the opacity of exhaust gases for diesel engines, a Braen Bee opacimeter model OPA 100 [15] was used, owned by the Universidad Técnica del Norte in the city of Ibarra, calibrated to current Ecuadorian regula-tions, as well as an experimental test workbench for diesel en-gines. In this case, tests were carried out on a Mazda diesel engine model BT-50 year 2013, 4 cylinders, power of 157.30 HP at 3500 RPM and torque 363 Nm at 1800 RPM, Direct electronic CRD-i injection system. It is worth noting that the engine was in standard conditions for the respective tests.

In terms of fuel, B15 castor oil biodiesel (15% biodiesel and 85% fossil diesel) and pure fossil diesel was used, and the opacity obtained by each fuel was compared.

Ten tests were carried out for each type of fuel and the previously mentioned RPM prior to a respective cleaning of the fuel injection system in order to obtain optimal and more accurate results.

The opacity measurements were made at the normal op-erating temperature of 80 °C. Once this condition was fulfilled, the opacimeter was heated, this being one of its automatic functions. Then a verification test of the opacimeter was performed to discard possible leaks on what was designated as car zero. Finally, the probe was intro-duced to the opening of the exhaust pipe and tests are carried out with both biofuel and fossil fuel, each of them carried out at various engine speeds: 1200, 1500, 2000, 2500, 3000 RPM.

Next, Table 2 shows the percentages of opacity obtained using fossil diesel, as indicated above, with tests at several RPM, taking into account the most common operating condi-tions of the engine where it can be seen that at higher revolu-tions the opacity is greater due to higher fuel consumption.

Table 2. Diesel fossil opacity tests

RPM	OPA 1	OPA 2	OPA 3	OPA 4	OPA 5	OPA 6	OPA 7	PRO. OPA
1200	9,8	9	10	8,7	9	10	9,9	**9,5**
1500	10,9	9,7	10,8	9,7	9,7	10,1	10,7	**10,2**
2000	11,7	10,8	11,1	10,8	10,5	11,8	11,1	**11,1**
2500	12,9	11,3	11,9	11,5	11,6	12,3	11,9	**11,9**
3000	13,5	12,8	12,6	12,7	12,5	12,7	12,6	**12,8**

Table 3 shows the results of opacity using B15 biodiesel. The same methodology was replicated to perform these tests, lower percentages of opacity were obtained. Likewise, higher revolutions resulted in greater opacity.

Table 3. B15 opacity tests

RPM	OPA 1	OPA 2	OPA 3	OPA 4	OPA 5	OPA 6	OPA 7	PRO. OPA
1200	0,3	0,2	0,2	0,1	0,1	0,2	0,2	**0,19**
1500	0,3	0,3	0,2	0,1	0,15	0,2	0,3	**0,22**
2000	0,4	0,4	0,4	0,1	0,2	0,2	0,4	**0,3**
2500	0,6	0,7	0,8	0,1	0,2	0,3	0,6	**0,47**
3000	0,6	1,1	1	0,55	0,5	0,5	1	**0,75**

According to the INEN 2 207: 2002 standard, Table 4 shows the emission opacity limits for diesel vehicles (free accel-eration tests).

Table 4. Opacity percentage [4]

Year and model	% opacity
2000 and later	50
1999 and earlier	60

The international standards with which we worked for this study are the EURO standards which state: Vehicles with super-charged diesel engines registered for the first time before 01/07/2008: 30% opacity, taking into account that this law indicates the EURO 3 that is in effect in Ecuador.

3. Results and discussion

Figure 1 shows opacity results using diesel fossil fuel, resulting in an average opacity of 11.1%. With these results, the engine would be approved without problems according to national and international standards.

Taking into account that the tests are performed on an electronic engine and that low levels of opacity are obtained due to its operating characteristics, the opacity percentages are analyzed at 1200 RPM, resulting in 9.5% opacity, and 12.8% opacity at 3000 RPM. The average opacity value is 11.1%. Comparing all the data, the opacity law for fossil diesel is acquired in equation (1).

$$Diésel\ fósil_{opa} = 0.0018(RPM) + 7.4619 \qquad (1)$$

Where:

Opa: Opacity.
RPM: Engine revolutions.
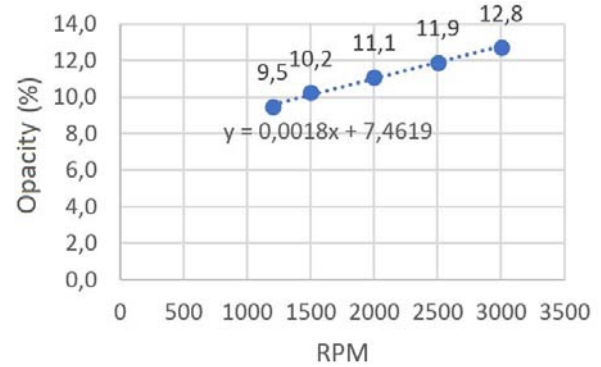
Figure 1. Fossil diesel opacity percentage

Opacity tests using B15 biodiesel were conducted in the same engine and with the same conditions as the previous tests. Before performing the tests, the whole feeding system was purged to ensure the results obtained.

Figure 2 shows the opacity results in 7 tests, at different engine RPM where an opacity of 0.19% was found at 1200 RPM and 0.75% opacity was obtained at 3000 RPM, with an average opacity value of 0.38%, this result being optimal for the engine. Similarly, the law to calculate opacity with the use of B15 biodiesel is shown in equation (2).

$$B15_{opa} = 0.0706e^{0.0008RPM} \qquad (2)$$

Donde:

B15: Biodiesel mixture.
Opa: Opacity.
RPM: Engine revolutions per minute.
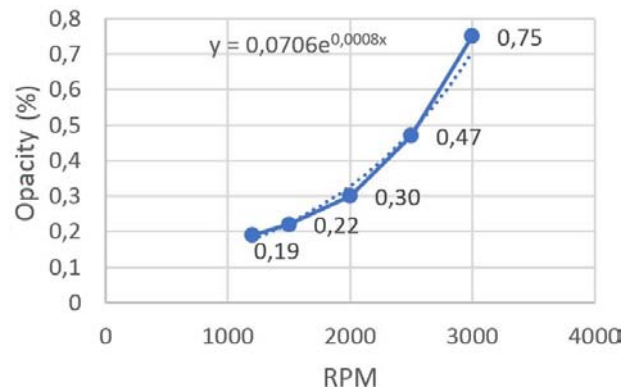
Figure 2. B15 opacity percentage

Figure 2 shows the opacity percentage according to engine RPM. It shows an increase in the opacity percentage, this is because at higher RPM there is greater

fuel consumption and therefore a greater amount of unburned fuel originating higher amounts of soot. The Ecuadorian INEN 2 207: 2007 standard states that the opacity limit is 50% for vehicles with diesel engines. Analyz-ing the results, it is concluded that the percentages of opacity decrease in considerable values using biodiesel at 15%.

Comparing the graphs for each type of fuel, B15 and fos-sil diesel, a significant difference of opacity values is evident. An analysis of the diesel trend line shows that, as the engine RPM increases, the percentage of opacity is proportional, with an increase of Opacity at each RPM higher to the use of B15, which increases the percentage of opacity in the same way, the difference being observable in the trend line, where in the same RPM the increase in opacity is lower. An average increase in opacity with fossil diesel of 0.9% per 500 RPM increase is observable, while at the same conditions the opacity with biodiesel B15 increases an average of 0.17%, decreasing 96% of the engine's soot emissions.

Analyzing the national regulations and taking into ac-count the characteristics of the engine, it can be concluded that the engine approves the percentage of opacity with the two fuels without faults; fossil diesel and biodiesel with B15 mix-ture, where the opacity value is 11.1% and 0.38% respectively. The data shows a 96% opacity reduction with the use of B15 biodiesel. Taking into account international EURO standards, which states that vehicles must not exceed an opacity percentage of 30%, the obtained data would be approved by EURO standards, emphasizing that the tests were carried out in an electronic diesel engine test bench Mazda BT-50 in perfect conditions both regarding its mechanical and electronic elements.

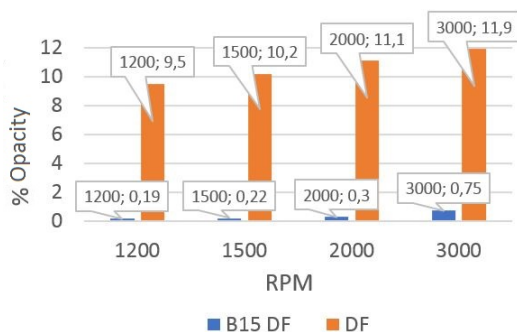Figure 3 shows the comparative data of the opacity per-centage with fossil fuel and B15 biofuel.

Figure 3. Comparative graphs for fossil diesel and B15 biodiesel

4. Conclusions

With the use of B15 castor oil biodiesel, opacity decreases by 96% with respect to the use of fossil diesel, this is due to the increase in the temperature in the combustion chamber and the better oxidation of the mixture.

With the equations obtained in this study, opacity can be known more quickly with the use of the two fuels, considering the use of motors with the same characteristics as the study.

Using biodiesel can mitigated carcinogenic diseases in the lungs in a large percentage, as stated by the WHO, which points to the smallest particles of soot as a cause of this problem.

The engine model used for the study is in optimal conditions. For this reason its values with fossil diesel and biodiesel are low, in street vehicles these percentages can vary in small amounts.

References

[1] J. Hernández Gaitán, G. Zambrano Ruano, and C. Rossi, "Emisión de gases en vehículos experimentales diesel-biodiesel," *Revista de la Universidad del Valle de guatemala*, no. 27, pp. 64–67, 2014. [Online]. Available: https://goo.gl/AfA1vR

[2] A. A. Agudelo, J. Agudelo, and P. Benjumea, "Diagnóstico exergético del proceso de combustión en un motor diésel," *Revista Facultad de Ingeniería Universidad de Antioquia*, no. 45, pp. 41–53, 09 2008. [Online]. Available: https://goo.gl/AbLZ2z

[3] Z. Z. Yu and L. Jing, "Effects of exhaust post-treatment technology on diesel engine emissions," in *Proceedings 2011 International Conference on Transportation, Mechanical, and Electrical Engineering (TMEE)*, Dec 2011, pp. 1804–1807. [Online]. Available: https://doi.org/10.1109/TMEE.2011.6199564

[4] INEN, *Gestión ambiental. Aire. Vehículos automotores. determinación de la opacidad de emisiones de escape de motores de diésel mediante la prueba estática. Método de aceleración libre*, Instituto Ecuatoriano de Normalización Std., 2010. [Online]. Available: https://goo.gl/211cW7

[5] F. Marcos Martín, J. Almazán Gárate, and C. Palomino Monzón, "Biodiésel de algas," *Energética XXI*, no. 74, pp. 100–104, 2008. [Online]. Available: https://goo.gl/UFhkYS

[6] S. Imtenan, M. Varman, H. Masjuki, M. Kalam, H. Sajjad, M. Arbab, and I. R. Fattah, "Impact of low temperature combustion attaining strategies on diesel engine emissions for diesel and biodiesels: A review," *Energy Conversion and Management*, vol. 80, Supplement C, pp. 329–356, 2014. [Online]. Available: https://doi.org/10.1016/j.enconman.2014.01.020

[7] C. S. Aalam, C. Saravanan, and M. Kannan, "Experimental investigations on a crdi system assisted diesel engine fuelled with aluminium oxide nanoparticles blended biodiesel," *Alexandria Engineering Journal*, vol. 54, no. 3, pp. 351–358, 2015. [Online]. Available: https://doi.org/10.1016/j.aej.2015.04.009

[8] E. Jiaqiang, P. Minhhieu, D. Zhao, D. Yuanwang, L. DucHieu, Z. Wei, Z. Hao, L. Teng, P. Qingguo, and Z. Zhiqing, "Effect of different technologies on combustion and emissions of the diesel engine fueled with biodiesel: A review," *Renewable and Sustainable Energy Reviews*, vol. 80, Supplement C, pp. 620–647, 2017. [Online]. Available: https://doi.org/10.1016/j.rser.2017.05.250

[9] J. Azjargal, "The comparison of combustion characteristics and performances of diesel engine fueled with biodiesel and diesel blends," in *2014 9th International Forum on Strategic Technology (IFOST)*, Oct 2014, pp. 313–317. [Online]. Available: https://doi.org/10.1109/IFOST.2014.6991129

[10] E. Bernard. (2010) Biodiésel: Los aspectos mecánicos en los vehículos. Centro Nacional de la Producción mss Limpia, Costa Rica. [Online]. Available: https://goo.gl/aRbzGf

[11] A. Benavides, P. Benjumea, and V. Pashova, "El biodiésel de aceite de higuerilla como combustible alternativo para motores diésel," *DYNA*, vol. 74, no. 153, pp. 141–150, 2007. [Online]. Available: https://goo.gl/FrAArX

[12] J. M. Amaris, D. A. Manrique, and J. E. Jaramillo, "Biocombustibles líquidos en Colombia y su impacto en motores de combustión interna," *Fuentes, el reventón energético*, vol. 13, no. 2, pp. 23–34, 2015, hybrid evolutionary systems for manufacturing processes. [Online]. Available: https://doi.org/10.18273/revfue.v13n2-2015003

[13] J. Agudelo, P. Benjumea, and J. Pérez, "Pruebas cortas en ruta en un vehículo tipo microbús con biodiésel de aceite de palma colombiano," *Scientia et Technica*, vol. 1, no. 24, pp. 163–168, 2004. [Online]. Available: http://dx.doi.org/10.22517/23447214.7321

[14] T. Saba, J. Estephane, B. E. Khoury, M. E. Khoury, M. Khazma, H. E. Zakhem, and S. Aouad, "Biodiesel production from refined sunflower vegetable oil over koh/zsm5 catalysts," *Renewable Energy*, vol. 90, Supplement C, pp. 301–306, 2016. [Online]. Available: https://doi.org/10.1016/j.renene.2016.01.009

[15] Globaltech. (2016) Opacímetro brain bee opa-100. [Online]. Available: https://goo.gl/QPiHA2

Guidelines for publication in Ingenius Journal

1. General Information

INGENIUS is a scientific publication of the *Universidad Politécnica Salesiana* of Ecuador, published since January 2007, with a fixed biannual periodicity, specialized in Mechanical Engineering, Electrical Engineering, Electronics, Computer Science and its integration in what is now known as Mechatronics; these lines of action strengthen areas such as automation, control, robotics, among others..

It is a scientific journal, which uses the peer-review system, under double-blind review methodology, according to the publication standards of the Institute of Electrical and Electronics Engineers (IEEE). Compliance with this system allows authors to guarantee an objective, impartial and transparent review process, which facilitates the publication of their inclusion in reference databases, repositories and international indexing.

INGENIUS is indexed in the directory and selective catalog of the Regional Online Information System for Scientific Journals of Latin America, the Caribbean, Spain and Portugal (Latindex), in the Directory of Journals of Open Access DOAJ, In the Information Matrix for the Analysis of Journals, MIAR, In the Ibero-American Network of Innovation and Scientific Knowledge, REDIB and in repositories, libraries and specialized catalogs of Latin America.

The journal is published in a double version: printed (ISSN: 1390-650X) and digital (e-ISSN: 1390-860X), in Spanish, each work being identified with a DOI (Digital Object Identifier System. The articles sent to INGENIUS magazine must comply with the following criteria:

2. Scope and policy

2.1. Theme

Original contributions in Mechanical Engineering, Electrical and Electronic Engineering, Computer Science and its integration in what is now known as Mechatronics, as well as related areas: Automation, Control, Domotics, Robotics in their different fields of action and all those related disciplines with the same central theme.

All the work carried out by national or foreign researchers may be published once they meet the required scientific quality criteria.

2.2. Contributions

INGENIUS Journal preferably publishes articles related to empirical research, and also reports of technological development, proposals for models and innovations, products for the elaboration of graduate and postgraduate thesis that contribute to the field of science and technology, as well as select revisions of literature. (state-of-the-art).

- **Research:** 5,000 to 6,500 words of text, including title, abstracts, descriptors, charts and references.
- **Reports:** 5,000 to 6,500 words of text, including title, abstracts, charts and references.
- **Reviews:** 6,000 to 7,000 words of text, including charts and references. Current, selective and justified references, would be specially valued from among 40 works

The INGENIUS Journal publishes original and unpublished works written in Spanish and English, they may not have been published

through any printed or electronic media, nor be in the process of arbitration or publication.

Every article will be subjected to a rigorous arbitration process; the evaluation of the article will be made according to criteria of originality, relevance, relevance, contributions, scientific rigor and compliance with established editorial guidelines.

Being an arbitrated publication, the Editorial Board approves its publication based on the concept of specialized pairs. The reception of a document does not imply commitment of publication.

It is essential to present a letter of presentation and grant of rights which can be downloaded from: < urlhttps://goo.gl/ZNkMRD>.

Contributions must be exclusively sent and through the OJS (Open Journal System) `<https://goo.gl/JF7dWT>`. In which all authors must previously register as a user. For any consultation of the procedure you should contact:

<revistaingenius@ups.edu.ec>,
<jcalle@ups.edu.ec> ó
<mquinde@ups.edu.ec>.

3. Presentation and structure of the manuscripts

For those works that are empirical investigations, the manuscripts will follow the IMRDC structure (Introduction, Materials and Methods, Results and Discussion and Conclusions), being optional the Notes and Supports. Those papers that, on the contrary, deal with reports, studies, proposals and reviews may be more flexible in their epigraphs, particularly in material and methods, analysis, results, discussion and conclusions. In all typologies of works, references are mandatory.

Articles may be written on Microsoft Word (.doc or .docx) or LATEX(.tex). The template to

be used can be downloaded from the journal's website, a, `<https://goo.gl/gtCg6m>`, while for LATEX in `<https://goo.gl/hrHzzQ>`, it is necessary that the file be anonymised in Properties of File, so that the author(s) ID is not displayed.

Figures, Graphs and/or Illustrations, as well as Charts shall be numbered sequentially including an explanatory description for each. The equations included in the article must also be numbered; the figures, charts and equations must be cited in the text.

Use space after point, commas and question marks.

Use "enter" at the end of each paragraph and title heading. Do not use .ᵉⁿter.ᵃnywhere else, let the word processor program automatically break the lines.

Do not center headings or subheadings as they should be aligned to the left.

Charts must be created in the same program used for the document body, but must be stored in a separate file. Use tabs, not spaces, to create columns. Remember that the final size of printed pages will be 21 x 28 cm, so the tables must be designed to fit the final print space.

3.1. Structure of the manuscripts

3.1.1. Presentation and cover letter

1. **Título (español) / Title (inglés):** Concise but informative, in Spanish on the front line and in English on the second, when the article is written in Spanish and vice versa if it is written in English.

2. **Authors and affiliations:** Full name and surname of each author, organized by order of priority and their institutional affiliation with reference to the end of the first sheet, where it must include: Dependency to which belongs within the

institution, Institution to which he/she belongs, country, ORCID. A maximum of 5 authors will be accepted, although there may be exceptions justified by the complexity and extent of the topic.

3. **Abstract (Spanish) / Abstract (English):** It will have a maximum extension of 230 words, first in Spanish and then in English. : 1) Justification of the topic; 2) Objectives; 3) Methodology and sample; 4) Main results; 5) Main conclusions.

4. **Keywords (Spanish) / Keywords (English):** 6 descriptors must be presented for each language version directly related to the subject of the work. The use of the key words set out in UNESCO's Thesaurus will be positively valued.

5. **Presentation (Cover Letter):** A statement that the manuscript is an original contribution, not submission or evaluation process in another journal, with the confirmation of the signatory authors, acceptance (if applicable) of formal changes in the manuscript according to the guidelines and partial assignment of rights to the publisher, according to the format established in: <https://goo.gl/ZNkMRD>

3.1.2. Manuscript

1. **Título (español) / Title (inglés):** Concise but informative, in Spanish on the front line and in English on the second, when the article is written in Spanish and vice versa if it is written in English.

2. **Authors and affiliations:** Full name and surname of each author, organized by order of priority and their institutional affiliation with reference to the end of the first sheet, where it must include: Dependency to which belongs within the institution, Institution to which he/she belongs, country, ORCID. A maximum of 5 authors will be accepted, although

there may be exceptions justified by the complexity and extent of the topic.

3. **Abstract (Spanish) / Abstract (English):** It will have a maximum extension of 230 words, first in Spanish and then in English. : 1) Justification of the topic; 2) Objectives; 3) Methodology and sample; 4) Main results; 5) Main conclusions.

4. **Keywords (Spanish) / Keywords (English):** 6 descriptors must be presented for each language version directly related to the subject of the work. The use of the key words set out in UNESCO's Thesaurus will be positively valued.

5. **Introduction:** It should include the problem statement, context of the problem, justification, rationale and purpose of the study, using bibliographical citations, as well as the most significant and current literature on the topic at national and international level.

6. **Material and methods:** It must be written so that the reader can easily understand the development of the research. If applicable, it will describe the methodology, the sample and the form of sampling, as well as the type of statistical analysis used. If it is an original methodology, it is necessary to explain the reasons that led to its use and to describe its possible limitations.

7. **Analysis and results:** It will try to highlight the most important observations, describing, without making value judgments, the material and methods used. They will appear in a logical sequence in the text and the essential charts and figures avoiding the duplication of data.

8. **Discussion and Conclusions:** It will summarize the most important findings, relating the observations themselves to relevant studies, indicating contributions

and limitations, without adding data already mentioned in other sections. It should also include deductions and lines for future research.

9. **Supports and acknowledgments (optional):** The Council Science Editors recommends the author (s) to specify the source of funding for the research. Priority will be given to projects supported by national and international competitive projects.

10. **The notes (optional):** will go, only if necessary, at the end of the article (before the references). They must be manually annotated, since the system of footnotes or the end of Word is not recognized by the layout systems. The numbers of notes are placed in superscript, both in the text and in the final note. The numbers of notes are placed in superscript, both in the text and in the final note. No notes are allowed that collect simple bibliographic citations (without comments), as these should go in the references.

11. **References:** Bibliographical citations should be reviewed in the form of references to the text. Under no circumstances should references mentioned in the text not be included. Their number should be sufficient to contextualize the theoretical framework with current and important criteria. They will be presented sequentially in order of appearance, as appropriate following the format of the IEEE.

3.2. Guidelines for Bibliographical references

Journal articles:

[1] J. Riess, J. J. Abbas, "Adaptive control of cyclic movements as muscles fatigue using functional neuromuscular stimulation". IEEE Trans. Neural Syst. Rehabil. Eng vol. 9, pp.326–330, 2001. [Onine]. Available: https://doi.org/10.1109/7333.948462

Books:

[1] G. O. Young, "Synthetic structure of industrial plastics" in Plastics, 2nd ed., vol. 3, J. Peters, Ed. New York: McGraw–Hill, 1964, pp. 15–64.

Technical reports:

[1] M. A. Brusberg and E. N. Clark, "Installation, operation, and data evaluation of an oblique–incidence ionosphere sounder system," in "Radio Propagation Characteristics of the Washington–Honolulu Path," Stanford Res. Inst., Stanford, CA, Contract NOBSR–87615, Final Rep., Feb. 1995, vol. 1

Articles presented in confeences (unpubished):

[1] Vázquez, Rolando, Presentación curso "Realidad Virtual". National Instruments. Colombia, 2009.

Articles of memories of Conferences (Published):

[1] L. I. Ruiz, A. García, J. García, G. Taboada. "Criterios para la optimización de sistemas eléctricos en refinerías de la industria petrolera: influencia y análisis en el equipo eléctrico," IEEE CONCAPAN XXVIII, Guatemala 2008.

Thesis:

[1] L.M. Moreno, "Computación paralela y entornos heterogéneos," Tesis doctoral, Dep. Estadística, Investigación Operativa y Computación, Universidad de La Laguna, La Laguna, 2005.

Guidelines:

[1] IEEE Guide for Application of Power Apparatus Bushings, IEEE Standard C57.19.100–1995, Aug. 1995.

Patents:

[1] J. P. Wilkinson, "Nonlinear resonant circuit devices," U.S. Patent 3 624 125, July 16, 1990.

Manuals:

[1] Motorola Semiconductor Data Manual, Motorola Semiconductor Products Inc., Phoenix, AZ, 1989.

Internet resources:

[1] E. H. Miller, "A note on reflector arrays" [Online]. Available. https://goo.gl/4cJkCF

3.3. Epigraphs, Figures and Charts

The epigraphs of the body of the article will be numbered in Arabic. They should go without a full box of capital letters, neither underlined nor bold. The numbering must be a maximum of three levels: 1. / 1.1. / 1.1.1. At the end of each numbered epigraph will be given an enter to continue with the corresponding paragraph.

The charts must be included in the text according to order of appearance, numbered in Arabic and subtitled with the description of the content, the subtitle should go at the top of the table justified to the left.

Figures can be linear drawings, maps or black and white halftone or color photographs in 300 dpi resolution. Do not combine photographs and line drawings in the same figure.

Design the figures so that they fit eventually to the final size of the journal 21 x 28 cm. Make sure inscriptions or details, as well as lines, are of appropriate size and thickness so that they are not illegible when they are reduced to their final size (numbers, letters and symbols must be reduced to at least 2.5 mm in height After the illustrations have been reduced to fit the printed page). Ideally, the linear illustrations should be prepared at about a quarter of their final publication size.

Different elements in the same figure should be spelled a, b, c, etc.

Photographs should be recorded with high contrast and high resolution. Remember that photographs frequently lose contrast in the printing process. Line drawings and maps should be prepared in black.

The text of the figures and maps must be written in easily legible letters.

If the figures have been previously used, it is the responsibility of the author to obtain the corresponding permission to avoid subsequent problems related to copyright.

Each figure must be submitted in a separate file, either as bitmap (.jpg, .bmp, .gif, or .png) or as vector graphics (.ps, .eps, .pdf).

4. Submission process

The manuscript must be sent through the OJS system of the journal, <`https://goo.gl/JF7dWT`>,the manuscript should be uploaded as an original file in .pdf without author data and anonymized according to the above; In complementary files the complete manuscript must be loaded in .doc or .docx (Word file), that is to say with the data of the author (s) and its institutional ascription; Also the numbered figures should be uploaded in independent files according to the corresponding in the manuscript (as bitmap .jpg, .bmp, .gif, or .png or as vector graphics .ps, .eps, .pdf). It is also obligatory to upload the cover letter and grant of rights as an additional file.

All authors must enter the required information on the OJS platform and only one of the authors will be responsible for correspondence.

Once the contribution has been sent the system will automatically send the author for correspondence a confirmation email of receipt of the contribution.

5. Editorial process

Once the manuscript has been received in OJS, a first check by the editorial team of the following points:

- The topic is in accordance with the criteria of the journal.
- Must have the IMRDC structure.
- Must be in the INGENIUS format.
- Must use the IEEE citation format.
- All references should be cited in the text of the manuscript as well as charts, figures and equations.
- The manuscript is original; for this, software is used to determine plagiarism.

The assessment described above can take up to 4 weeks.

If any of the above is not complete or there is inconsistency, an email will be sent to the author to make the requested corrections.

The author will make the corrections and resend the contribution through an email in response to the notification and will also upload the corrected manuscript into OJS supplementary files.

The editorial team will verify that the requested corrections have been incorporated, if it complies, the manuscript will start the second part of the process that may be followed by the author through OJS, otherwise the author will be notified and the manuscript will be archived.

The second phase of the process consists of the evaluation under the methodology of double-blind review, which includes national and foreign experts considering the following steps:

- The editor assigns two or more reviewers for the article.

- After reviewing the article, the reviewers will submit the evaluation report with one of the following results.
  - Publishable
  - Publishable with suggested changes
  - Publishable with mandatory changes
  - Non publishable
- The editor once received the evaluation by the reviewers will analyze the results and determine if the article is accepted or denied.
- If the article is accepted, the author will be notified to make corrections if required and the corresponding editorial process will be continued.
- If the article is denied, the author will be notified and the manuscript will be archived.
- In the two previous cases the result of the evaluation of the reviewers and their respective recommendations will be sent.

The second phase of the process lasts at least 4 weeks, after which they will be notified to the author giving instructions to continue with the process.

6. Publication

The INGENIUS Journal publishes two issues per year, on January 1st and July 1st, so it is important to consider the dates for sending the articles and their corresponding publication. Articles received until October will be considered for the January publication and those received until April for the July publication.

Exchange

Exchange with other periodicals is accepted.

Address:

Secretaría Técnica de Comunicación

Universidad Politécnica Salesiana

Turuhuayco 3-69 y Calle Vieja

Postal code 2074

Cuenca, Ecuador

Phone: (+593 7) 205 00 00 Ext. 1182

Fax: (+593 7) 408 89 58

Email: rpublicas@ups.edu.ec

www.ups.edu.ec

Cuenca – Ecuador

Printed

Centro Gráfico Salesiano: Antonio Vega Muñoz 10-68 y General Torres.

Phone: (+593 7) 283 17 45

Cuenca – Ecuador

Email: centrograficosalesiano@lns.com.ec